Finanziato dall'Unione europea
NextGenerationEU

Ministero dell'Università e della Ricerca

Italiadomani
PIANO NAZIONALE DI RIPRESA E RESILIENZA

Dipartimento di Fisica e Astronomia
UNIVERSITÀ DEGLI STUDI DI PADOVA

Magnetars

Dipartimento di Fisica e Astronomia
UNIVERSITÀ DEGLI STUDI DI PADOVA

Frontiers in X-ray polarimetry Academy

2025

FIXP

Neutron stars: general notions

- Neutron stars (NSs) are relics of massive stars ($M_{\rm prog} \approx 8 - 25\ M_\odot$)
- Masses $M_{\rm NS} \approx 1 - 2\ M_\odot$
- Radii $R_{\rm NS} \approx 10 - 15\ \rm km$

$\rho_{\rm m} \approx 10^{14} - 10^{15}\ \rm g/cm^3$

- Mostly made of neutrons ($8\ n$ every p^+/e^-) sustained by the pressure of degenerate neutrons
- Fast rotators and powerful magnets

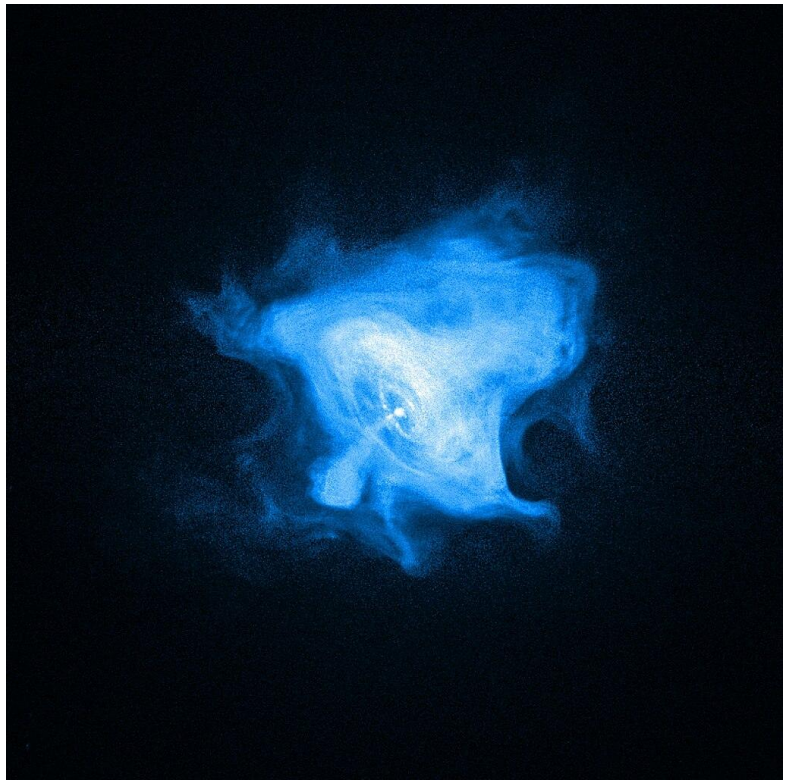

Magneto-rotational evolution

- A rotating dipole field emits EM radiation at the expenses of the rotational energy

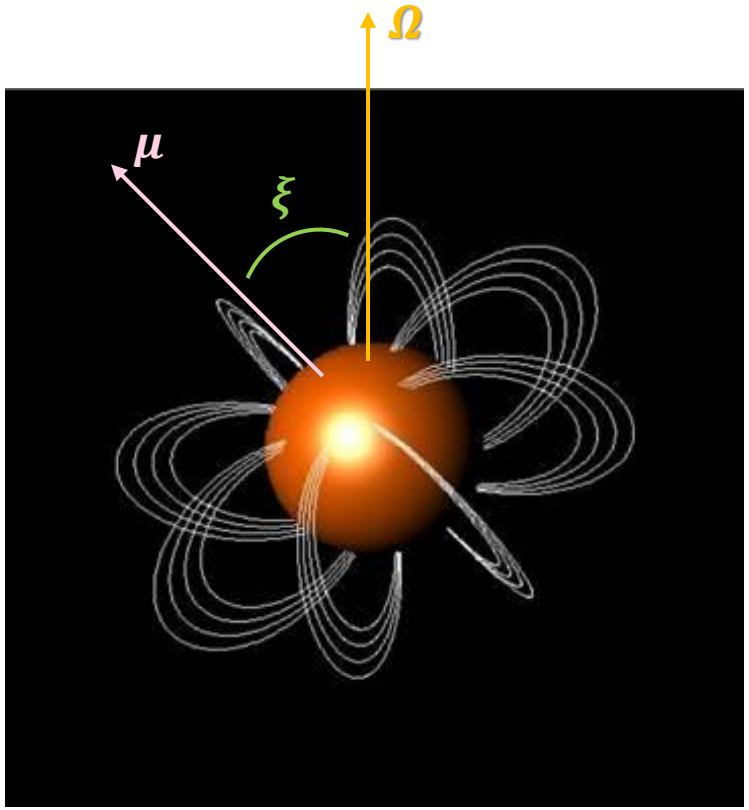

Larmor formula

$$-\frac{2}{3c^3}\left(\frac{\partial^2\mu}{\partial t^2}\right)^2 = I\Omega\dot{\Omega}$$

Magnetic dipole moment

Rotation frequency ($\Omega = 2\pi/P$)

Magneto-rotational evolution

- A rotating dipole field emits EM radiation at the expenses of the rotational energy

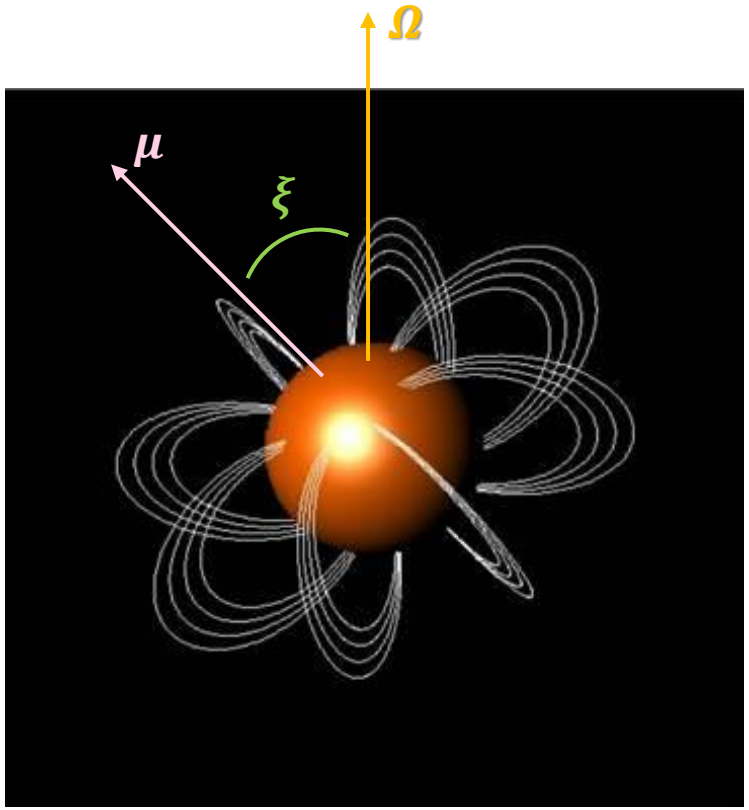

Solving for B

$$B \approx 3.2 \times 10^{19} \sqrt{P\dot{P}}\ \mathrm{G}$$

⚠ This holds for:

- purely dipolar magnetic field
- all the rotation energy is converted into EM emission

$P\dot{P}$ diagram

- Classification of NSs according to their P and $\dot{P}$

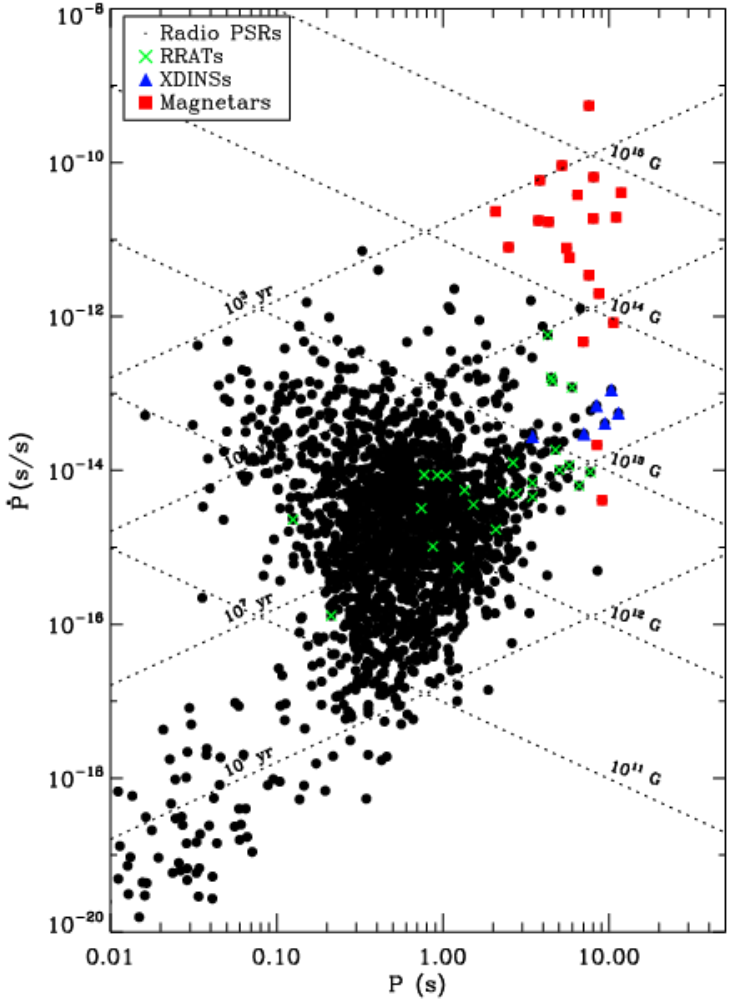

$P\dot{P}$ diagram

- Classification of NSs according to their P and $\dot{P}$

Rotation-Powered Pulsars (RPPs)

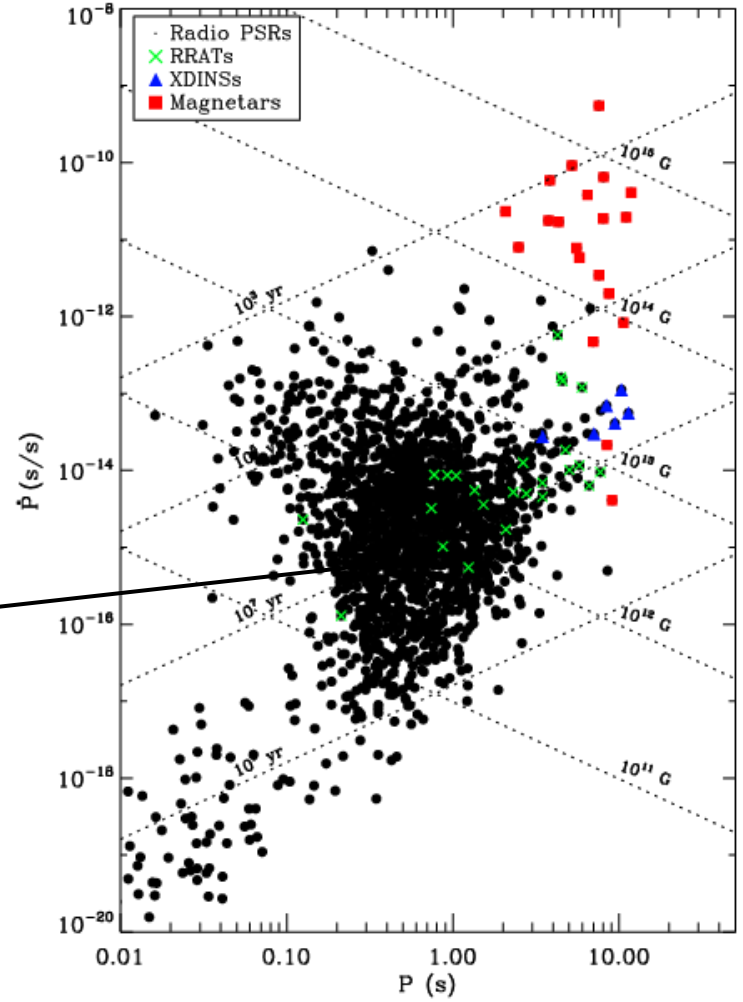

$P\dot{P}$ diagram

- Classification of NSs according to their P and $\dot{P}$

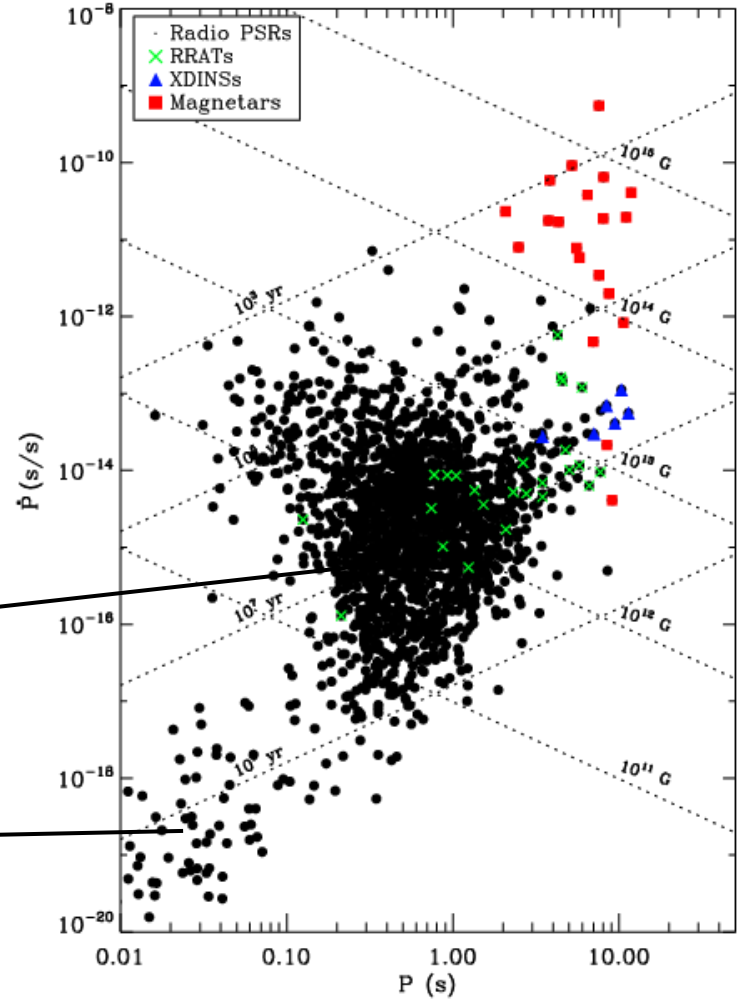

Rotation-Powered Pulsars (RPPs)

(Accreting) millisecond pulsars

$P\dot{P}$ diagram

- Classification of NSs according to their P and $\dot{P}$

Rotating Radio Transients (RRaTs)

Rotation-Powered Pulsars (RPPs)

(Accreting) millisecond pulsars

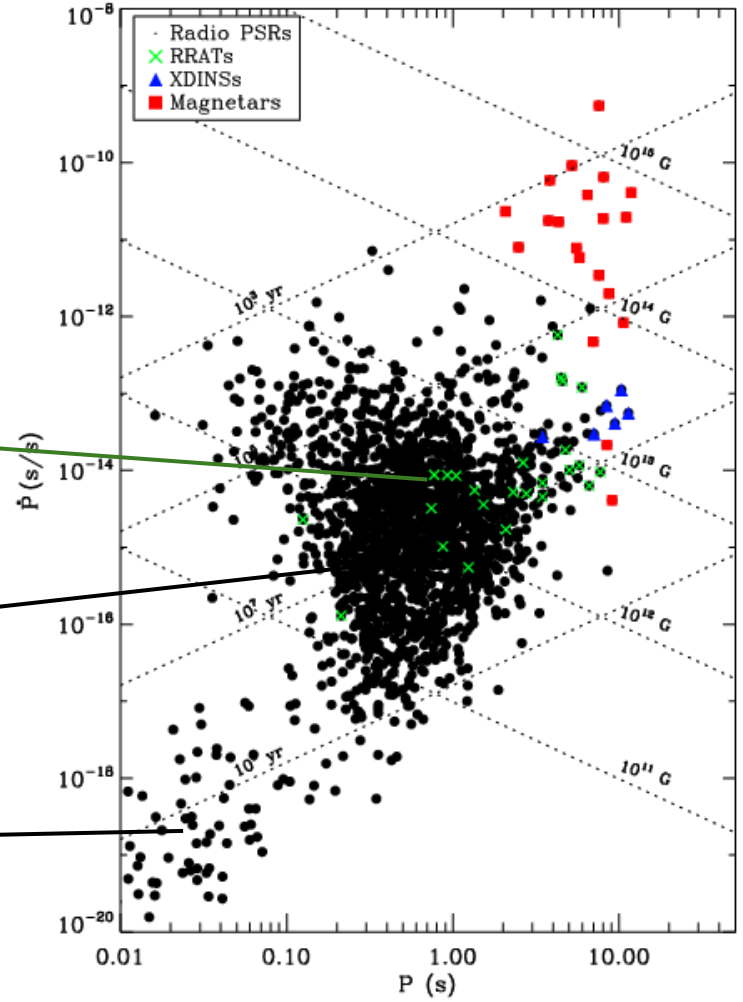

$P\dot{P}$ diagram

- Classification of NSs according to their P and $\dot{P}$

X-ray Dim Isolated NSs (XDINSs)

Rotating Radio Transients (RRaTs)

Rotation-Powered Pulsars (RPPs)

(Accreting) millisecond pulsars

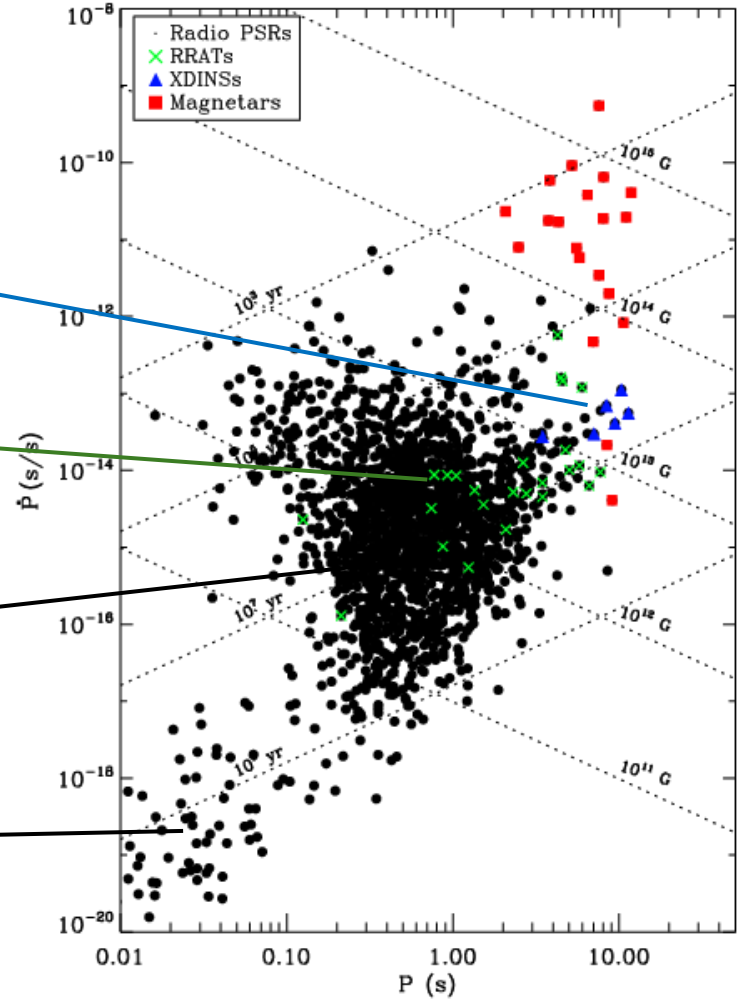

$P\dot{P}$ diagram

- Classification of NSs according to their P and $\dot{P}$

X-ray Dim Isolated NSs (XDINSs)

Rotating Radio Transients (RRaTs)

AXPs and SGRs

Rotation-Powered Pulsars (RPPs)

(Accreting) millisecond pulsars

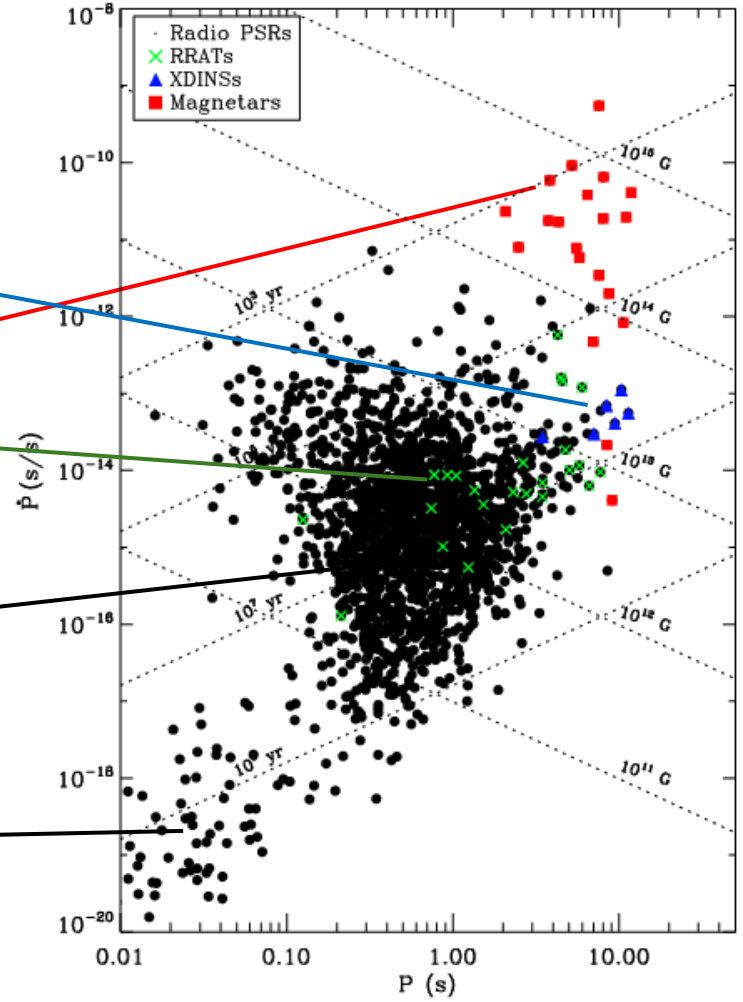

Anomalous X-ray pulsars (AXPs)

- Class of isolated NSs (no accretion)
- X-ray luminosity (usually) in excess of the rotational energy loss rate ($L_X > I\Omega\dot{\Omega}$)

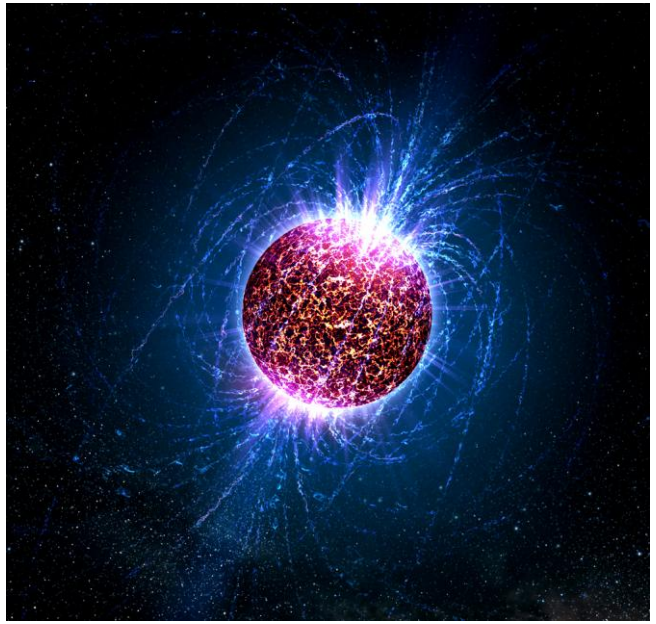

Anomalous X-ray pulsars (AXPs)

- Class of isolated NSs (no accretion)
- X-ray luminosity (usually) in excess of the rotational energy loss rate ($L_X > I\Omega\dot{\Omega}$)
- Large spin periods and spin-down rates lead to ultra-strong magnetic fields

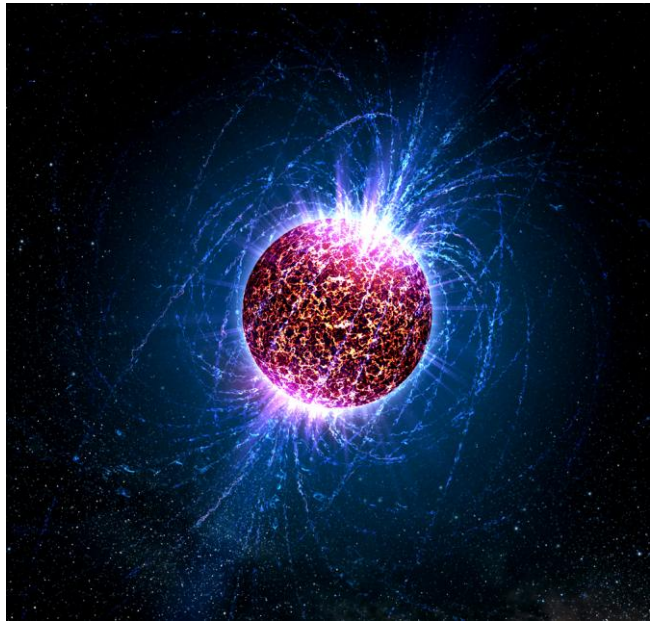

$$P \approx 2 - 12\ \mathrm{s}$$
$$\dot{P} \approx 10^{-13} - 10^{-9}\ \mathrm{s/s} \quad \Rightarrow \quad B_{\mathrm{sd}} \approx 10^{14} - 10^{15}\ \mathrm{G}$$

Soft-gamma repeaters (SGRs)

- Sudden emission of a huge amount of X-ray energy (up to 10^{47} erg/s)
- Initially confused with GRBs (but then observed to repeat)
- Pulsations detected in the event after-glow (⇒ NSs)

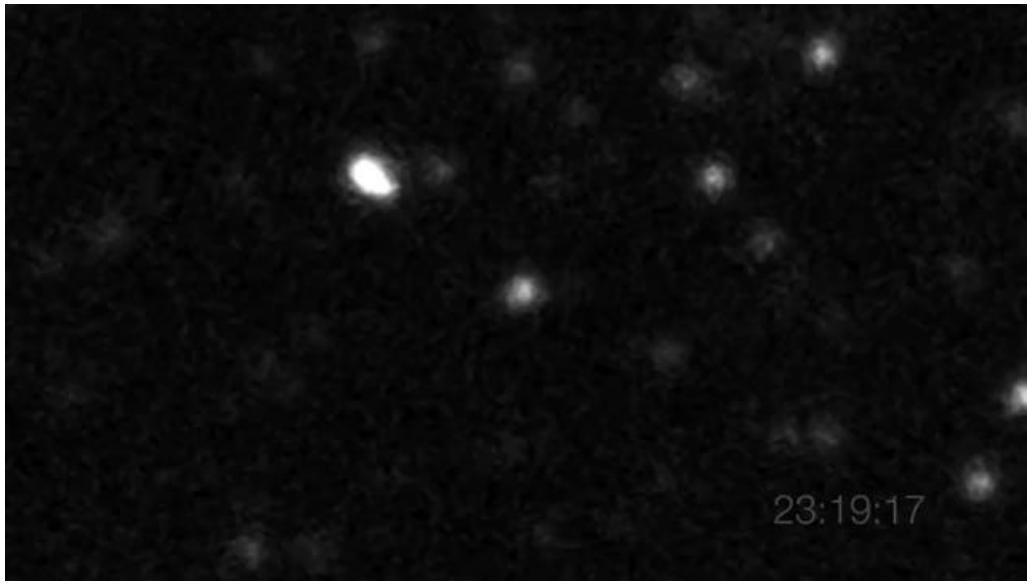

A.J. Castro-Tirado/IAC80/ESO

- P and $\dot{P}$ compatible with AXPs (so $B \approx 10^{14-15}$ G) and isolated as well
- Both AXPs and SGRs identified as **magnetars**

Magnetars – Persistent emission

- Magnetars are divided in persistent and transient sources
- Soft X-ray persistent spectra ($0.5 - 10$ keV) are usually fitted by a BB+PL decomposition (or BB+BB, especially for transients)
- Additional PL components are observed at higher energies ($\gtrsim 20$ keV)
- Transient sources are often identified as they enter in a outburst phase (flux enhancement by a factor $\approx 100 - 1000$ in typically 1 yr)

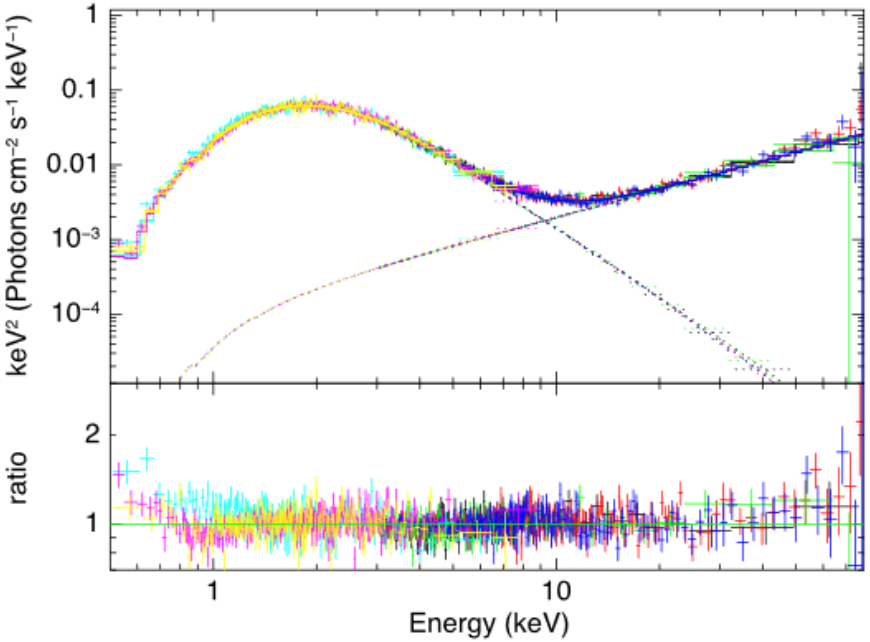

Tendulkar et al. (2015)

Magnetars – Bursting activity

- Short bursts
  - $\Delta t \approx 0.01 - 1\ \mathrm{s}$
  - $L_{\mathrm{X}} = 10^{36} - 10^{41}\ \mathrm{erg/s}$

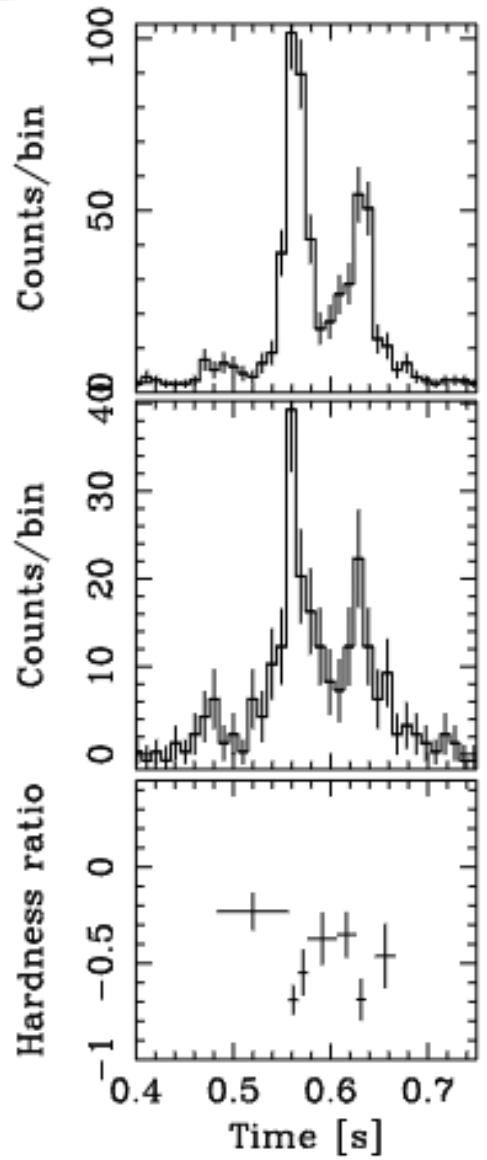

Gotz et al. (2004)

Magnetars – Bursting activity

- Short bursts
  - $\Delta t \approx 0.01 - 1\ \mathrm{s}$
  - $L_{\mathrm{X}} = 10^{36} - 10^{41}\ \mathrm{erg/s}$
- Intermediate flares
  - $\Delta t \approx 1 - 10\ \mathrm{s}$
  - $L_{\mathrm{X}} \approx 10^{41} - 10^{43}\ \mathrm{erg/s}$

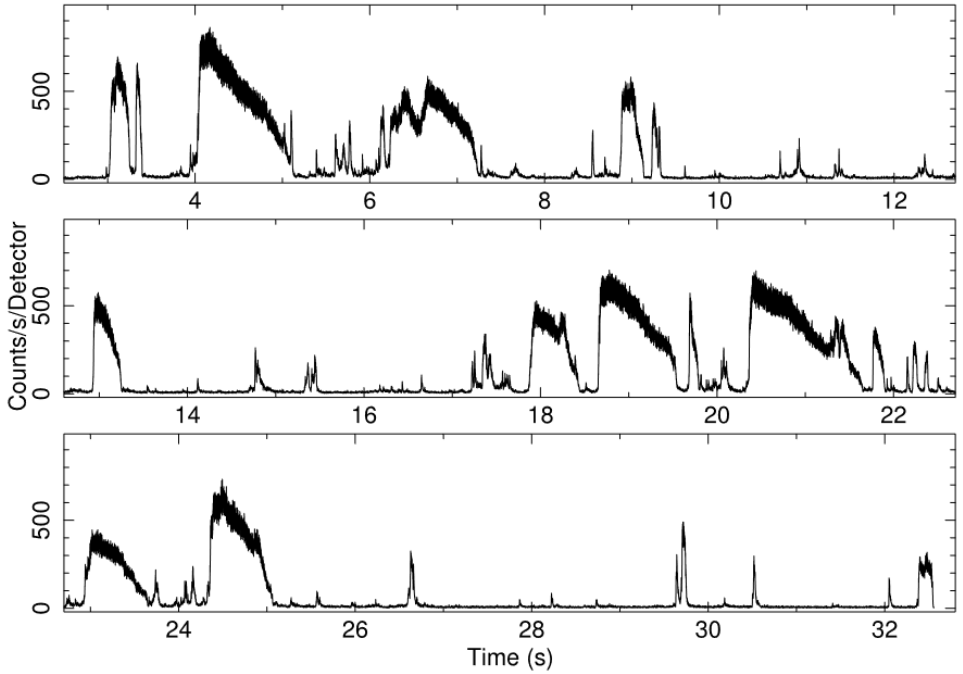

Israel et al. (2008)

Magnetars – Bursting activity

- Short bursts
  - $\Delta t \approx 0.01 - 1$ s
  - $L_{\mathrm{X}} = 10^{36} - 10^{41}$ erg/s
- Intermediate flares
  - $\Delta t \approx 1 - 10$ s
  - $L_{\mathrm{X}} \approx 10^{41} - 10^{43}$ erg/s
- Giant flares
  - $\Delta t \approx 10^{2}$ s
  - $L_{\mathrm{X}} \approx 10^{44} - 10^{47}$ erg/s

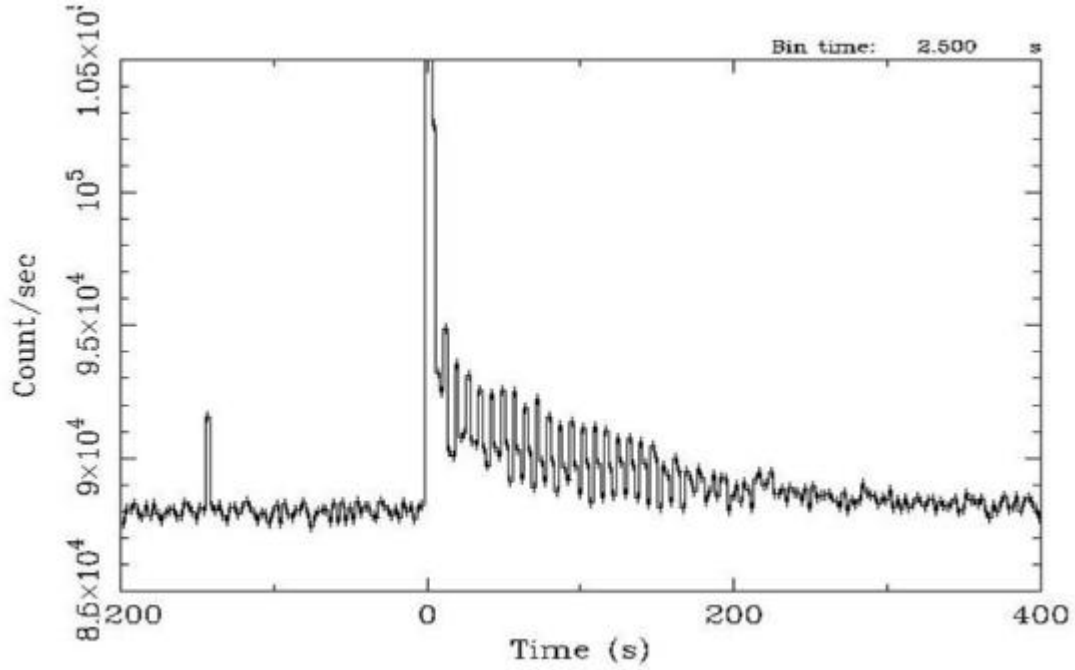

Mereghetti et al. (2005)

Twisted-magnetosphere

- Strong internal field (up to 10^{16} G) with a toroidal component at least of the same order

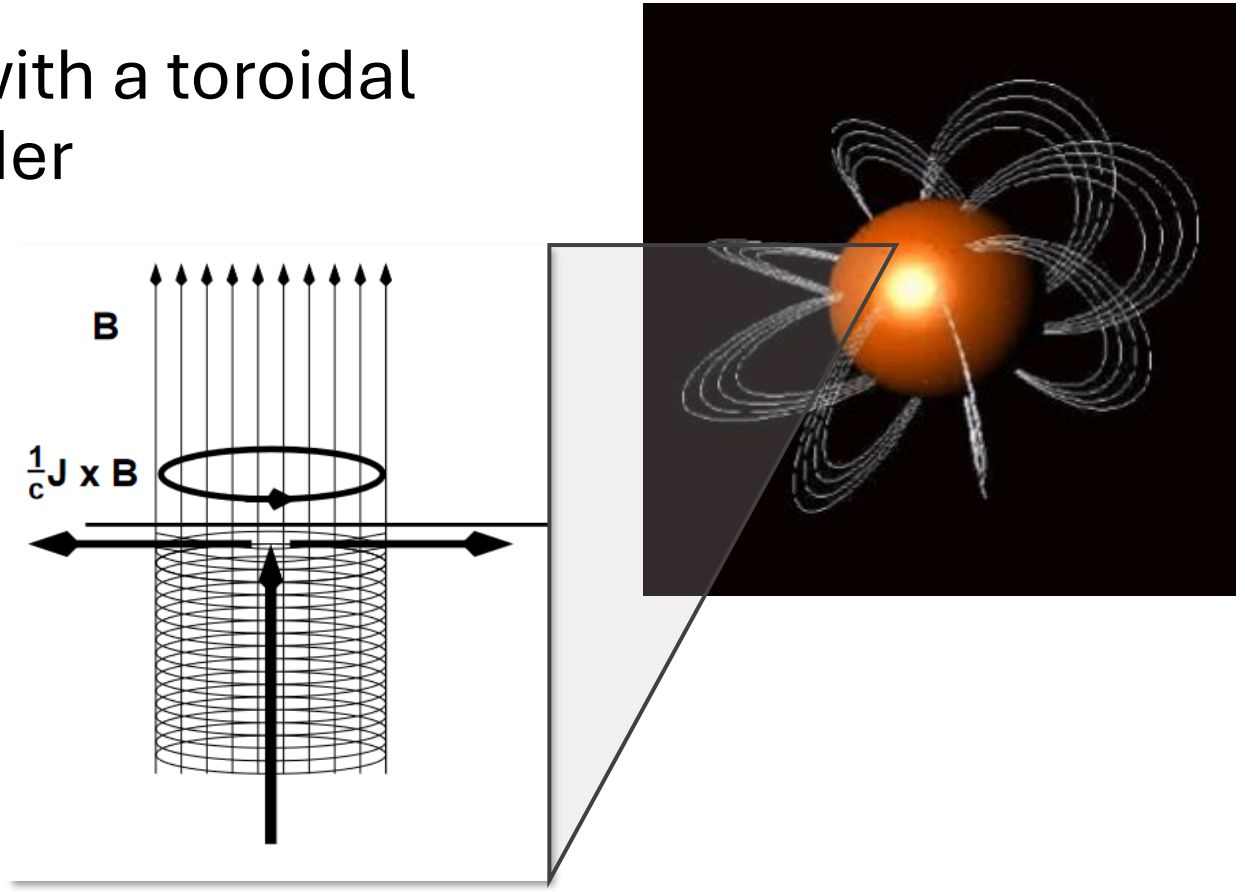

Thompson et al. (2002)

Twisted-magnetosphere

- Strong internal field (up to 10^{16} G) with a toroidal component at least of the same order
- Once the magnetic stress exceeds the crust mechanical yield, helicity is transferred outside

$$\boldsymbol{B} = [B_r, B_\theta . B_\phi] = \frac{B_\mathrm{p}}{2}\left(\frac{R_\mathrm{NS}}{r}\right)^3 [2\cos\theta\,, \sin\theta\,, 0]$$

dipole

$$\boldsymbol{B} = \frac{B_\mathrm{p}}{2}\left(\frac{R_\mathrm{NS}}{r}\right)^{2+p}\left[-\frac{df}{d\cos\theta}, \frac{pf}{\sin\theta}, \sqrt{\frac{pC(p)}{p+1}}\frac{f^{1+1/p}}{\sin\theta}\right]$$

twisted dipole

$$0 < p \leq 1$$

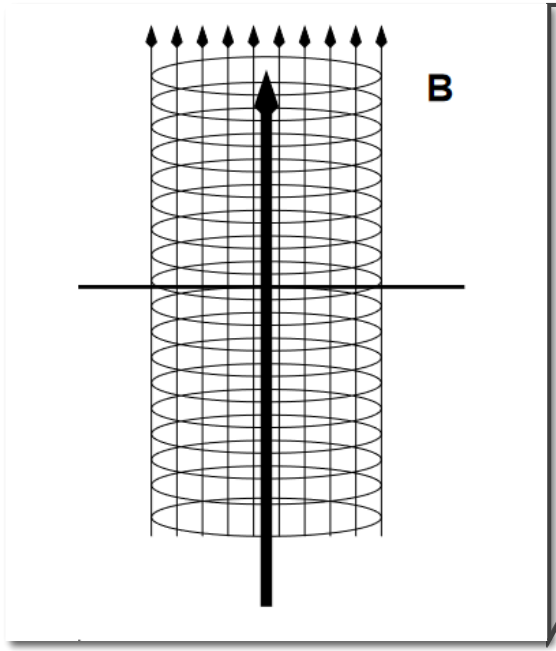

Thompson et al. (2002)

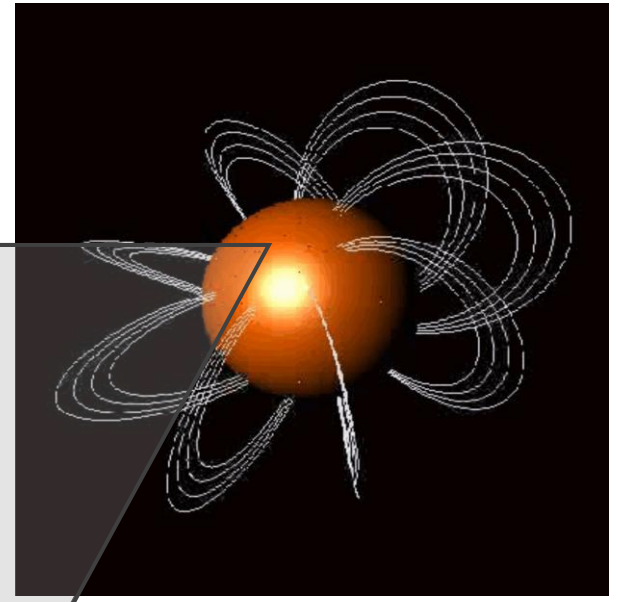

Global twist

Magnetospheric currents

$$\nabla \times \boldsymbol{B}_{\mathrm{dip}} = \mu_0 \boldsymbol{j} \qquad \nabla \times \boldsymbol{B}_{\mathrm{twist}} = \mu_0 \boldsymbol{j}$$

$$\| \qquad \Downarrow \qquad \nparallel \qquad \Downarrow$$

$$0 \quad \text{no currents} \qquad 0 \quad \text{currents}$$

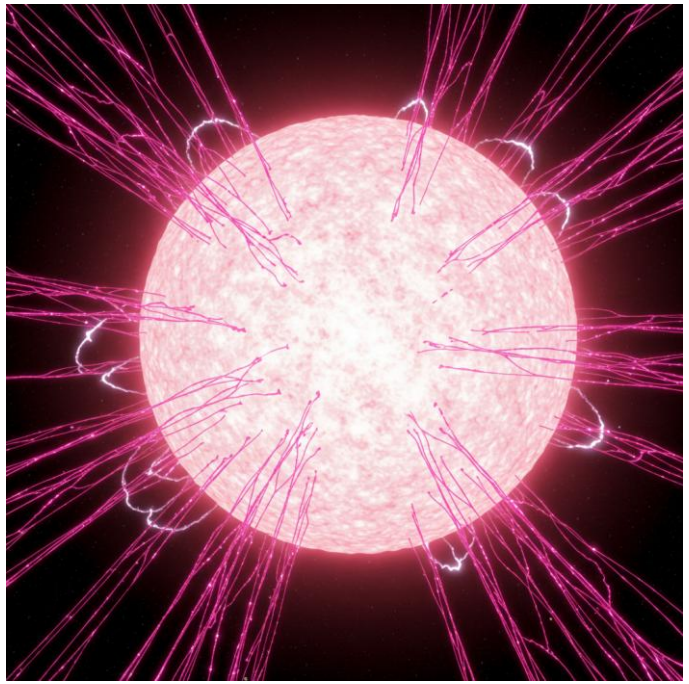

- Magnetosphere is populated by charged particles, with density

$$n_e \sim \frac{B}{r\beta}\left(\frac{B_\phi}{B_\theta}\right)$$

not enough for photons to interact efficiently

Magnetospheric currents

$$\nabla \times \boldsymbol{B}_{\mathrm{dip}} = \mu_0 \boldsymbol{j}$$

$$\| \qquad \Downarrow$$

$$0 \quad \text{no currents}$$

$$\nabla \times \boldsymbol{B}_{\mathrm{twist}} = \mu_0 \boldsymbol{j}$$

$$\nparallel \qquad \Downarrow$$

$$0 \quad \text{currents}$$

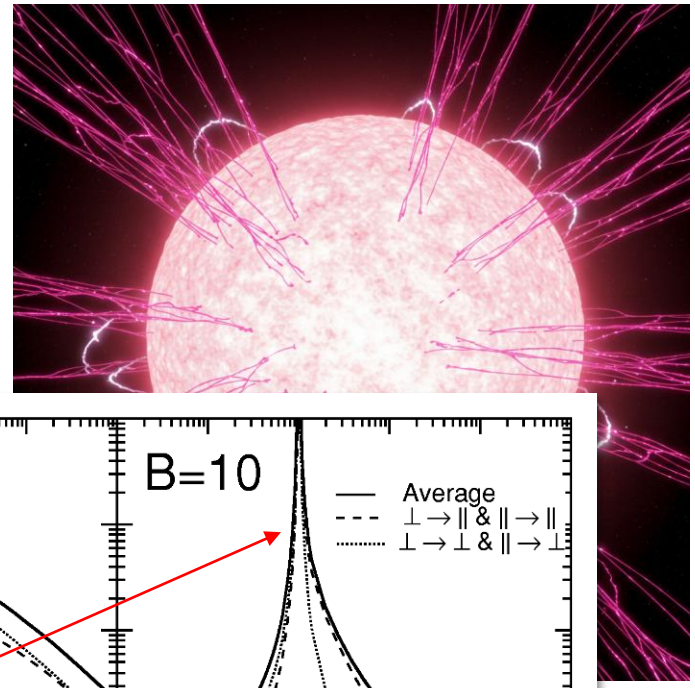

- Magnetosphere is populated by charge
  with density

$$n_e \sim \frac{B}{r\beta}\left(\frac{B_\phi}{B_\theta}\right)$$

not enoug t effic

Scattering cross sections peak at the cyclotron energy

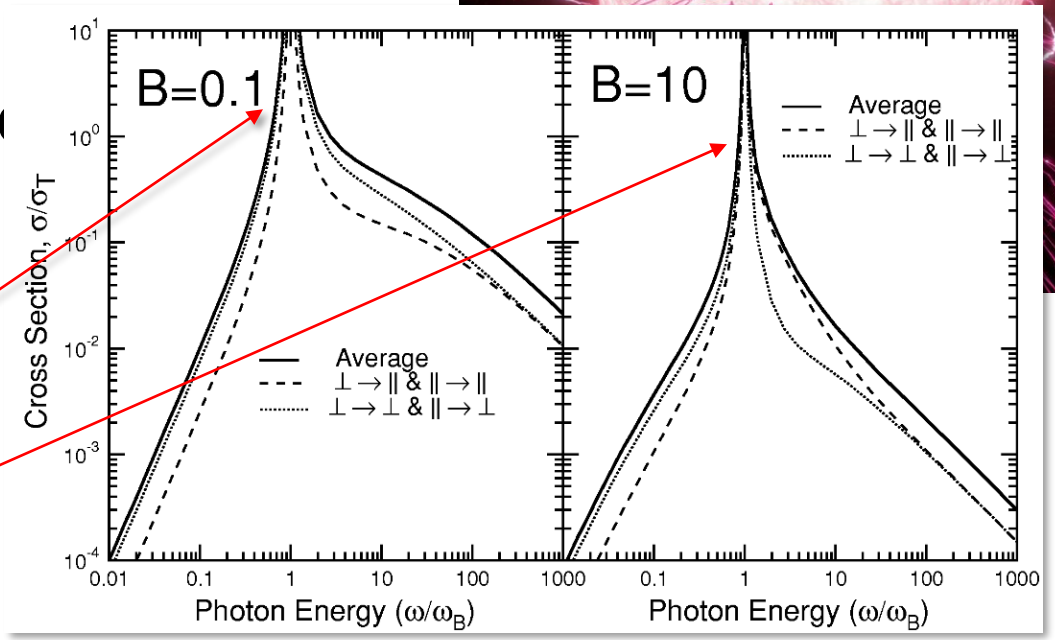

Magnetar model achievements

- RCS of thermal photons onto magnetospheric particles generates PL tails at soft X-ray energies

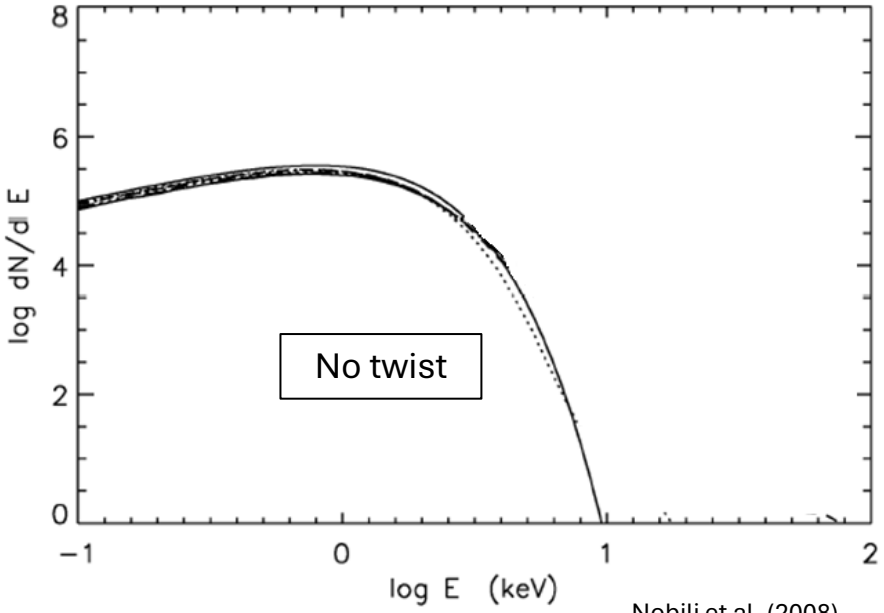

Nobili et al. (2008)

Magnetar model achievements

- RCS of thermal photons onto magnetospheric particles generates PL tails at soft X-ray energies

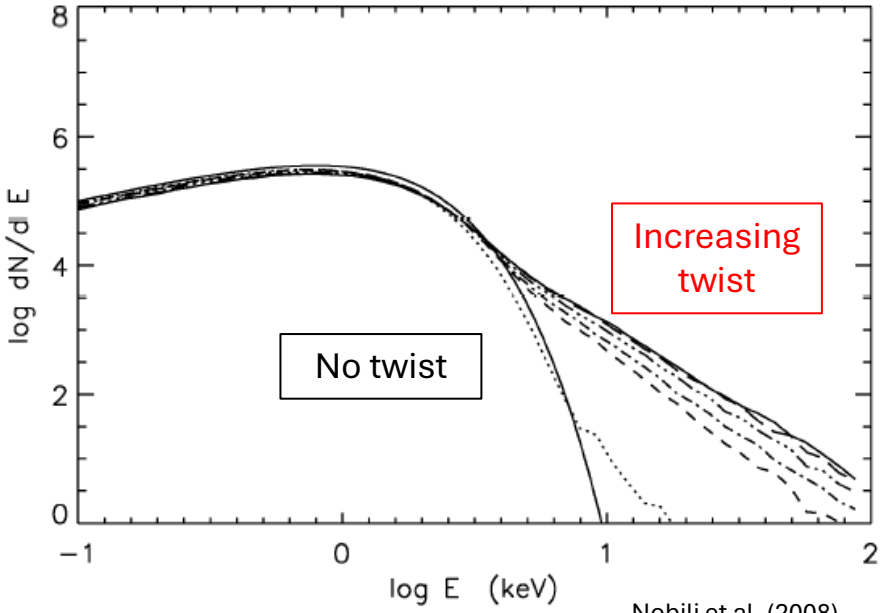

Nobili et al. (2008)

Magnetar model achievements

- RCS of thermal photons onto magnetospheric particles generates PL tails at soft X-ray energies

- Internal magnetic stresses deform the crust inducing the injection of e^+e^- fireballs enclosed within the closed field lines (at the base of bursts/ flare emission)

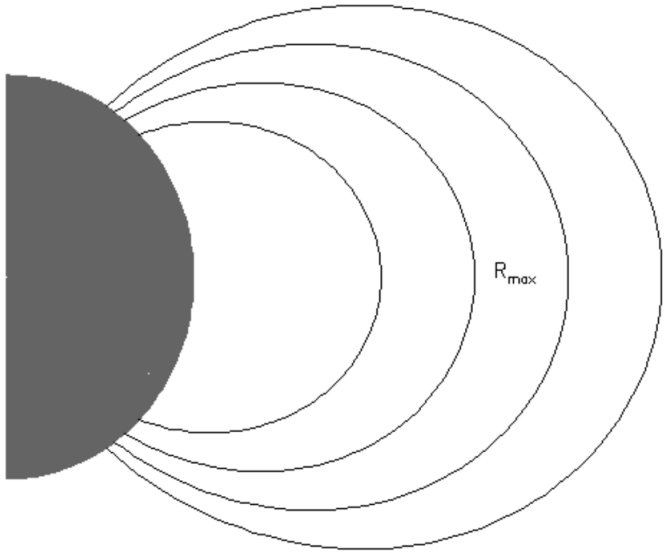

Alternative models

- The P-$\dot{P}$ estimate of the magnetic field holds for:
  - dipolar fields (magnetar field topology not dipolar)
  - emission energy all supplied by rotation (need for another source of energy)

- Magnetar phenomenology very different from other NSs
  - strongly-magnetized ($\approx 10^9$ G) white dwarfs?
  - disrupting events (for SGR flares)?

May polarimetry provide new constraints?

Polarization in strong magnetic fields

- The polarization state of photons can be studied solving the wave equation

$$\boldsymbol{\nabla} \times (\bar{\boldsymbol{\mu}} \cdot \boldsymbol{\nabla} \times \boldsymbol{E}) = \frac{\omega^2}{c^2} \boldsymbol{\epsilon} \cdot \boldsymbol{E}$$

magnetic permeability tensor (inverse)

dielectric tensor

Polarization in strong magnetic fields

- The polarization state of photons can be studied solving the wave equation

$$\boldsymbol{\nabla} \times (\bar{\boldsymbol{\mu}} \cdot \boldsymbol{\nabla} \times \boldsymbol{E}) = \frac{\omega^2}{c^2} \boldsymbol{\epsilon} \cdot \boldsymbol{E}$$

- $\boldsymbol{\epsilon}$ and $\bar{\boldsymbol{\mu}}$ contain plasma interaction terms

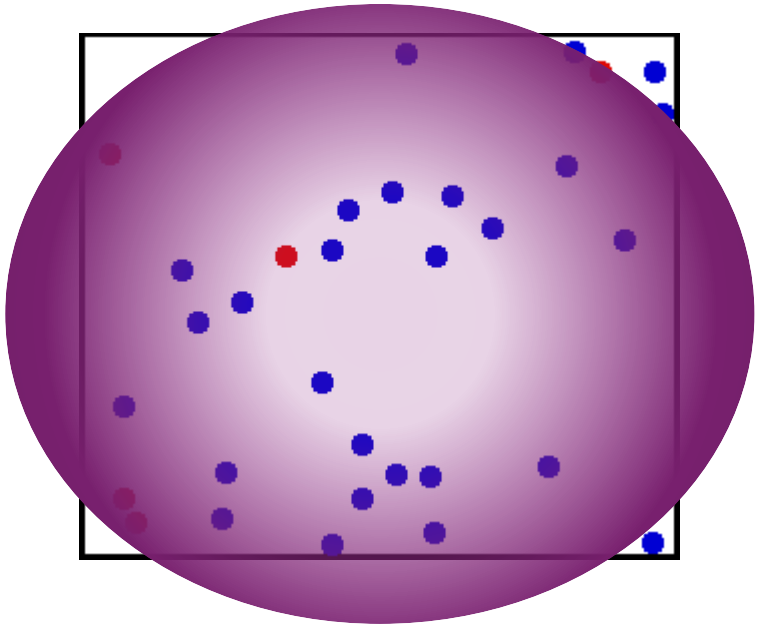

magnetized plasma

In strong $\boldsymbol{B}$ fields the charge motion is quantized

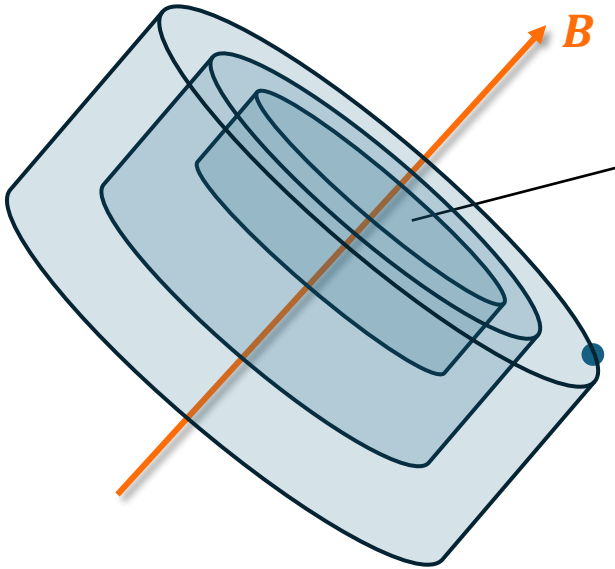

1st Landau level energy

$$\hbar\omega_{\mathrm{B}} = \frac{\hbar e B_{\mathrm{Q}}}{m_{\mathrm{e}} c} = m_e c^2$$

$$\Downarrow$$

$$B_{\mathrm{Q}} = \frac{m_e^2 c^3}{\hbar e} = 4.414 \times 10^{13}\ \mathrm{G}$$

Polarization in strong magnetic fields

- The polarization state of photons can be studied solving the wave equation

$$\boldsymbol{\nabla} \times (\bar{\boldsymbol{\mu}} \cdot \boldsymbol{\nabla} \times \boldsymbol{E}) = \frac{\omega^2}{c^2} \boldsymbol{\epsilon} \cdot \boldsymbol{E}$$

- $\boldsymbol{\epsilon}$ and $\bar{\boldsymbol{\mu}}$ contain plasma interaction terms and vacuum terms

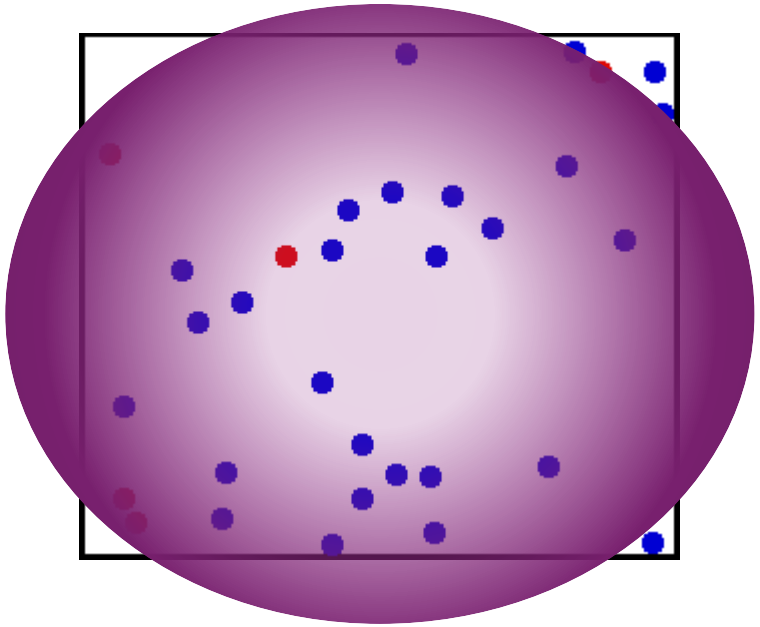

magnetized plasma

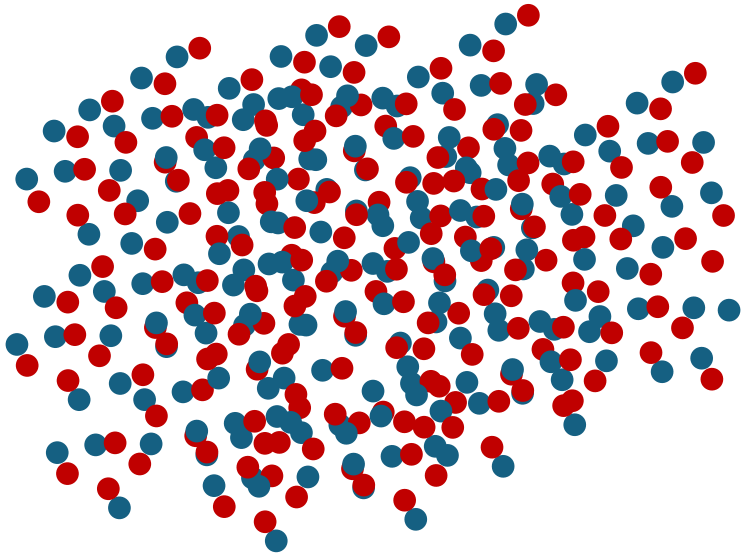

vacuum birefringence

Polarization in strong magnetic fields

- The polarization state of photons can be studied solving the wave equation

$$\boldsymbol{\nabla} \times (\bar{\boldsymbol{\mu}} \cdot \boldsymbol{\nabla} \times \boldsymbol{E}) = \frac{\omega^2}{c^2} \boldsymbol{\epsilon} \cdot \boldsymbol{E}$$

- $\boldsymbol{\epsilon}$ and $\bar{\boldsymbol{\mu}}$ contain plasma interaction terms and vacuum terms

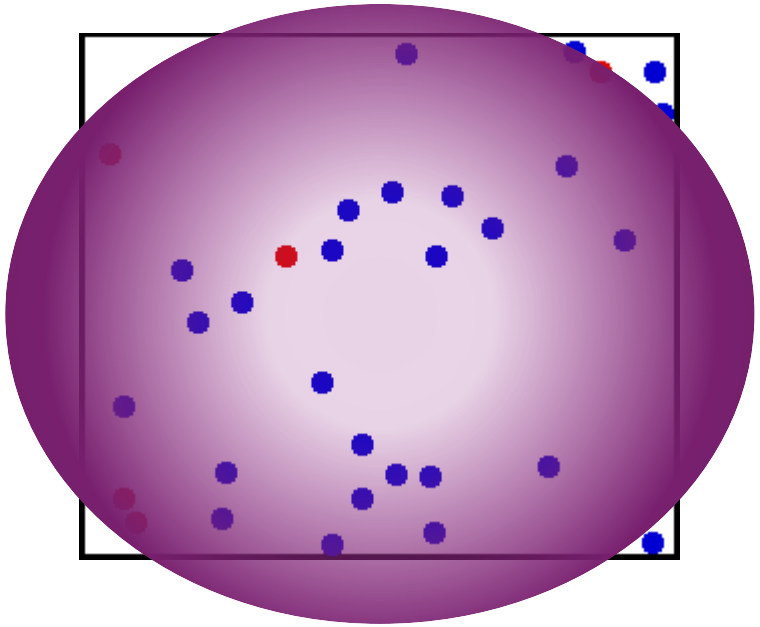

magnetized plasma

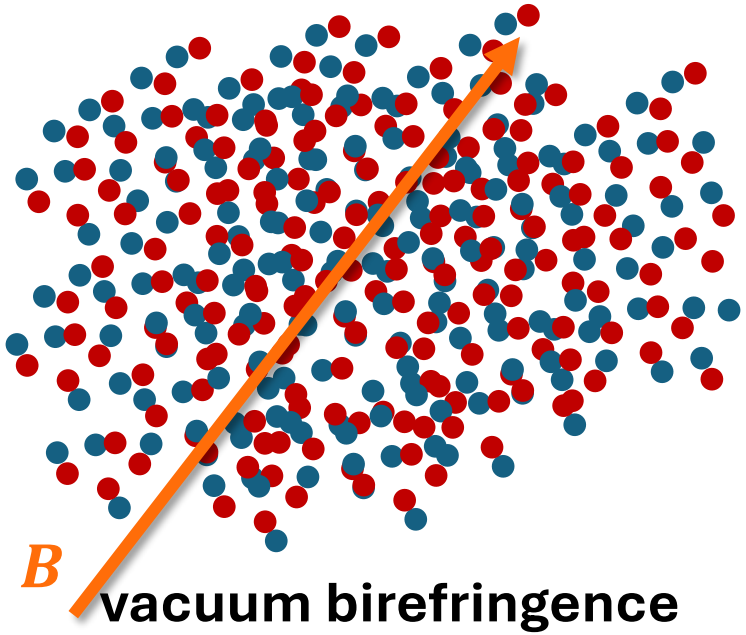

vacuum birefringence

Polarization in strong magnetic fields

- The polarization state of photons can be studied solving the wave equation

$$\boldsymbol{\nabla} \times (\bar{\boldsymbol{\mu}} \cdot \boldsymbol{\nabla} \times \boldsymbol{E}) = \frac{\omega^2}{c^2} \boldsymbol{\epsilon} \cdot \boldsymbol{E}$$

- $\boldsymbol{\epsilon}$ and $\bar{\boldsymbol{\mu}}$ contain plasma interaction terms and vacuum terms

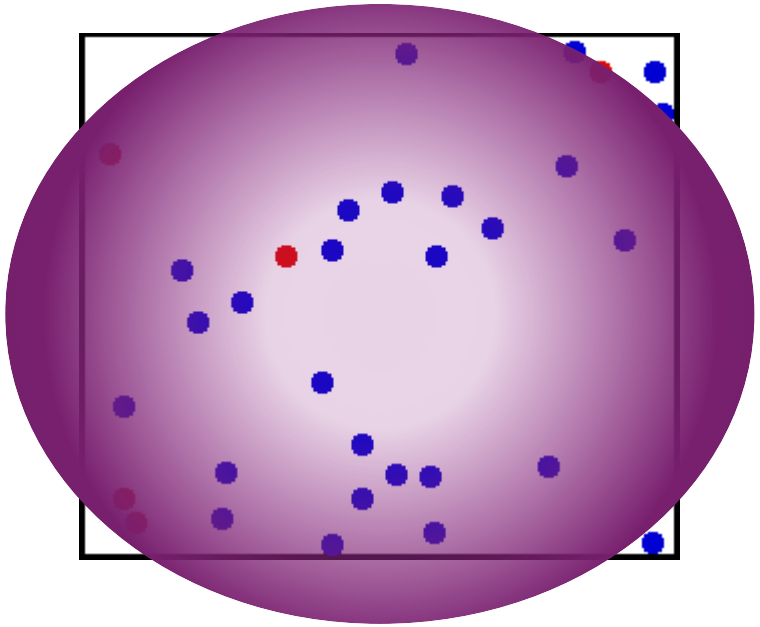

magnetized plasma

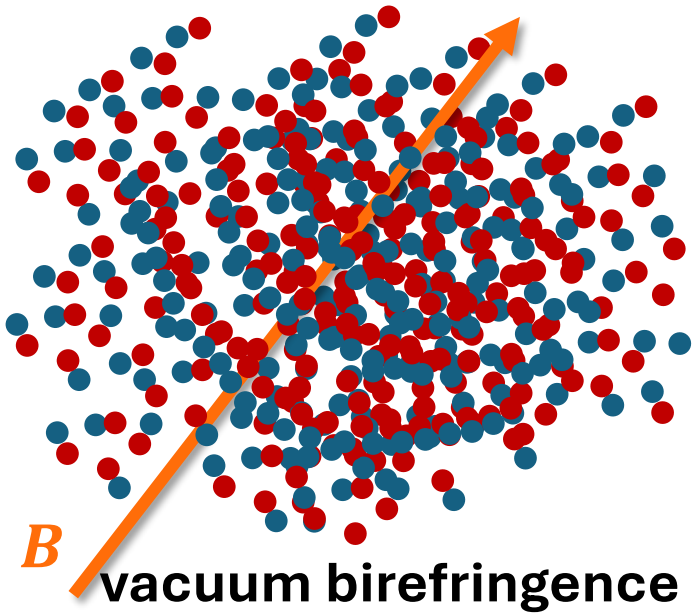

vacuum birefringence

Normal polarization modes

- When vacuum terms dominate in $\boldsymbol{\epsilon}$, photons turn out to be polarized linearly and only in two normal modes

$$\widehat{\boldsymbol{E}} = \begin{pmatrix} 1 \\ 0 \\ 0 \end{pmatrix} \quad \text{or} \quad \begin{pmatrix} 0 \\ 1 \\ 0 \end{pmatrix}$$

Ordinary mode **Extraordinary mode**

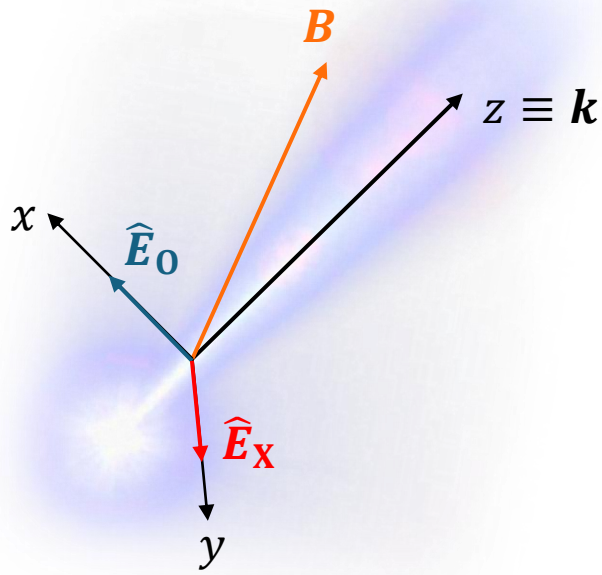

Normal polarization modes

- When vacuum terms dominate in $\boldsymbol{\epsilon}$, photons turn out to be polarized linearly and only in two normal modes

$$\widehat{\boldsymbol{E}} = \begin{pmatrix} 1 \\ 0 \\ 0 \end{pmatrix} \quad \text{or} \quad \begin{pmatrix} 0 \\ 1 \\ 0 \end{pmatrix}$$

Ordinary mode **Extraordinary mode**

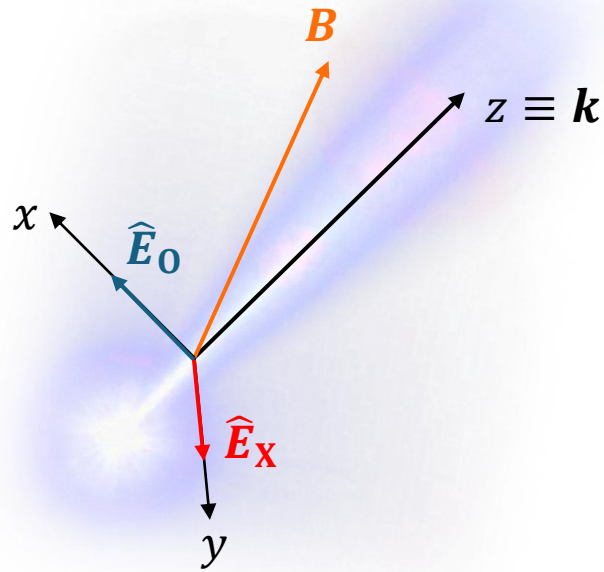

Normal modes in a plasma

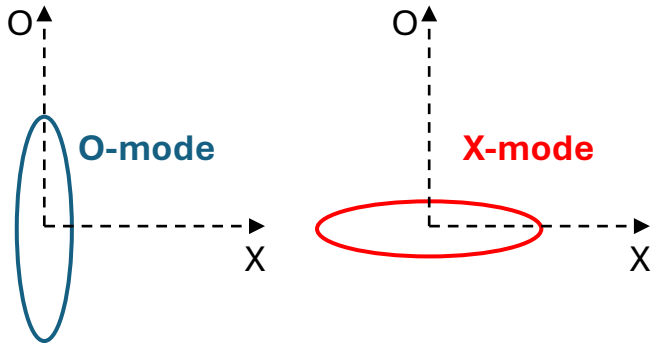

Polarization of photons emerging from plasma

- Radiative processes cross sections in strong magnetic fields

$$\sigma_{\mathrm{OO}} \sim \sigma_{\mathrm{unmag}} \qquad \sigma_{\mathrm{XO}} \sim \left(\frac{B}{B_Q}\right)^{-2} \sigma_{\mathrm{OO}}$$

$$\sigma_{\mathrm{OX}} \sim \left(\frac{B}{B_{\mathrm{Q}}}\right)^{-2} \sigma_{\mathrm{OO}} \qquad \sigma_{\mathrm{XX}} \sim \left(\frac{B}{B_{\mathrm{Q}}}\right)^{-2} \sigma_{\mathrm{OO}}$$

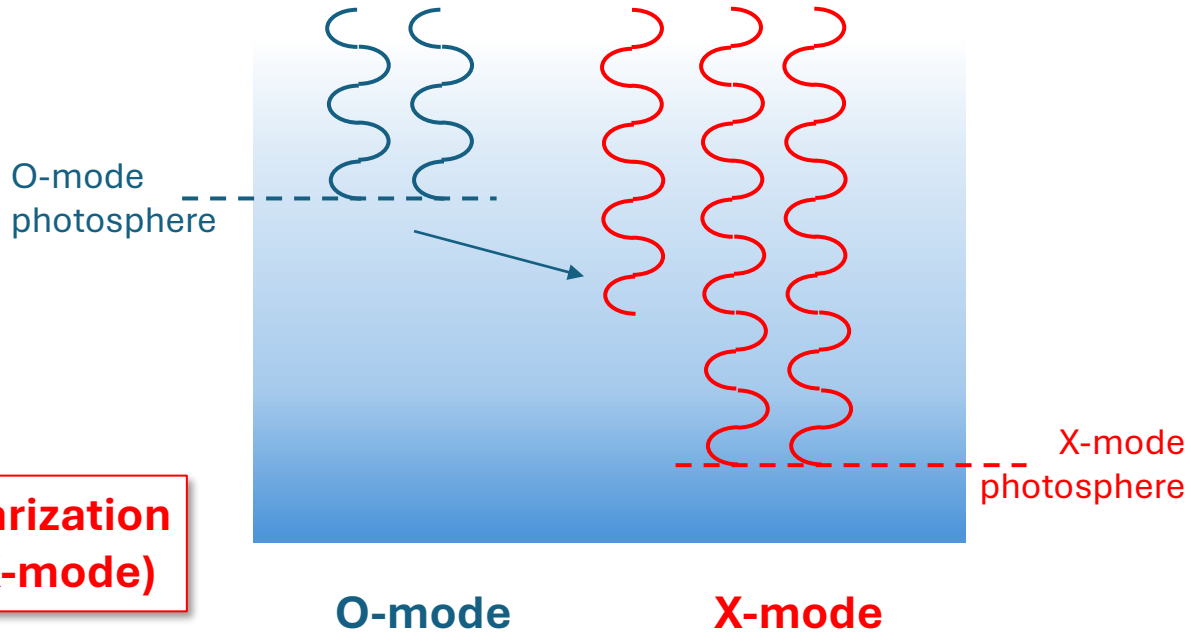

High polarization (in the X-mode)

Vacuum resonance

- Plasma and vacuum polarize photons in opposite ways

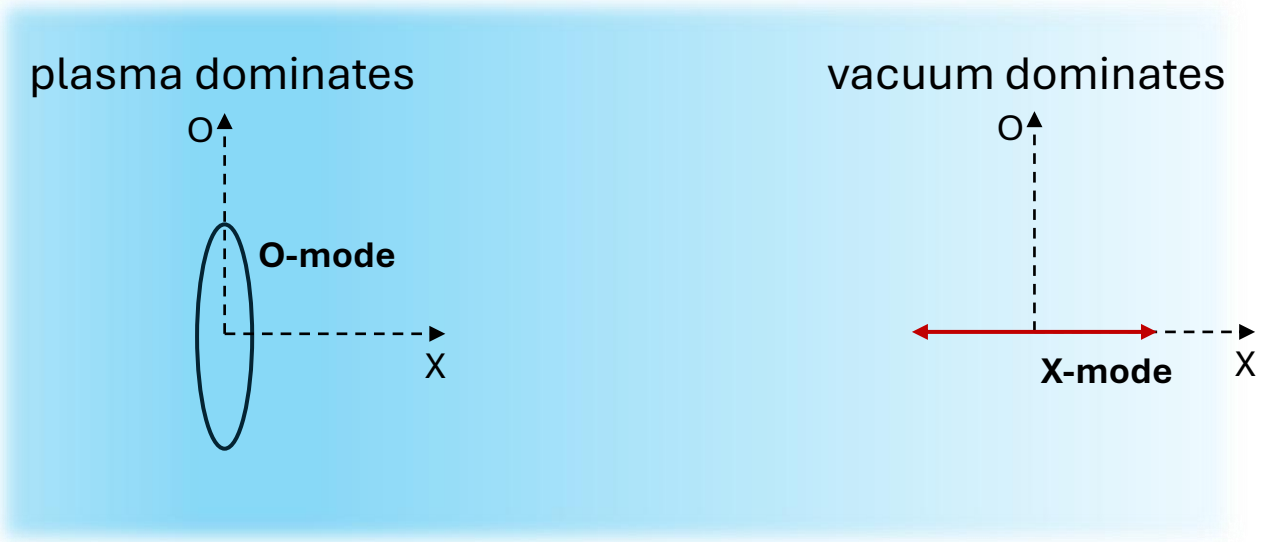

Vacuum resonance

- Plasma and vacuum polarize photons in opposite ways

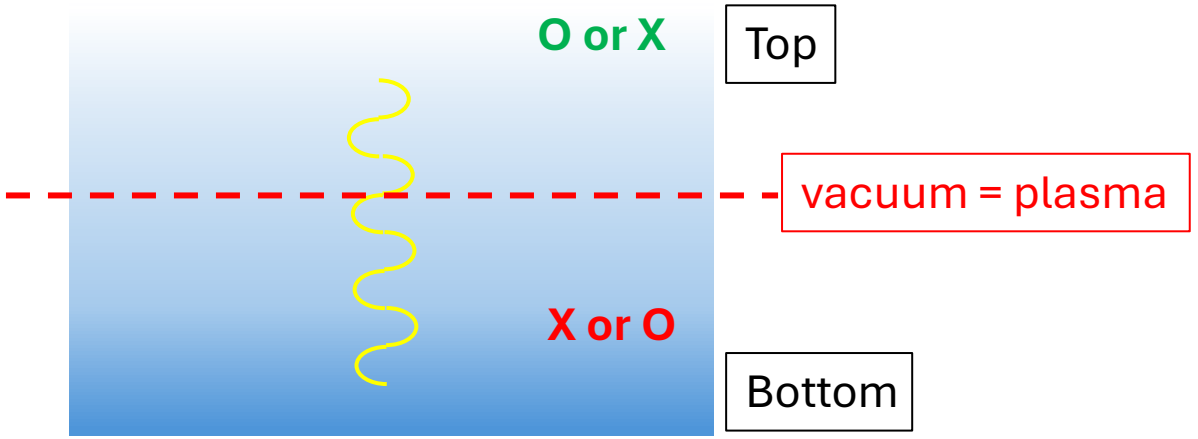

Top

vacuum = plasma

Bottom

Mode conversion

Circular polarization

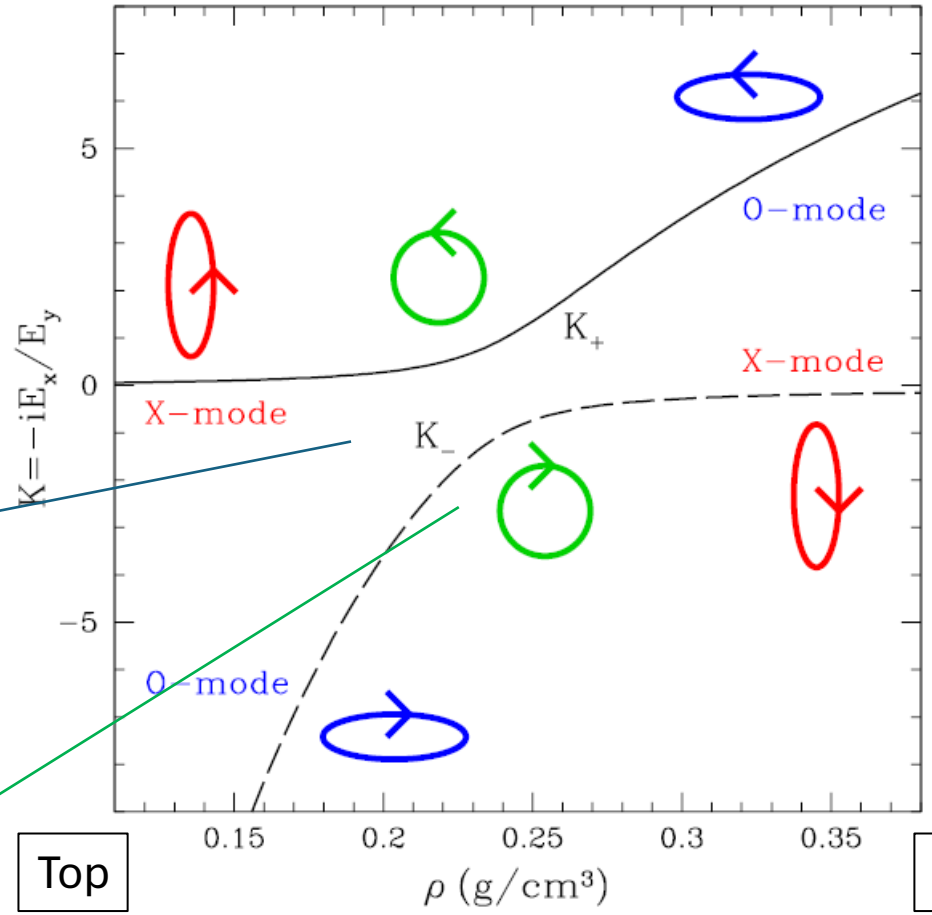

Harding & Lai (2006)

Top

Bottom

Vacuum resonance

- Plasma and vacuum polarize photons in opposite ways
- Mode conversion at the vacuum resonance may modify the polarization pattern of photons emerging from plasma

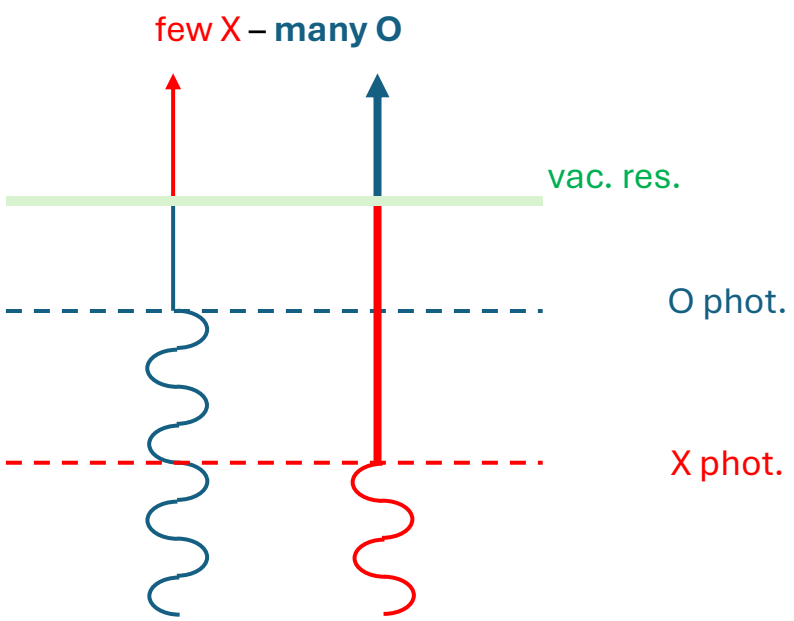

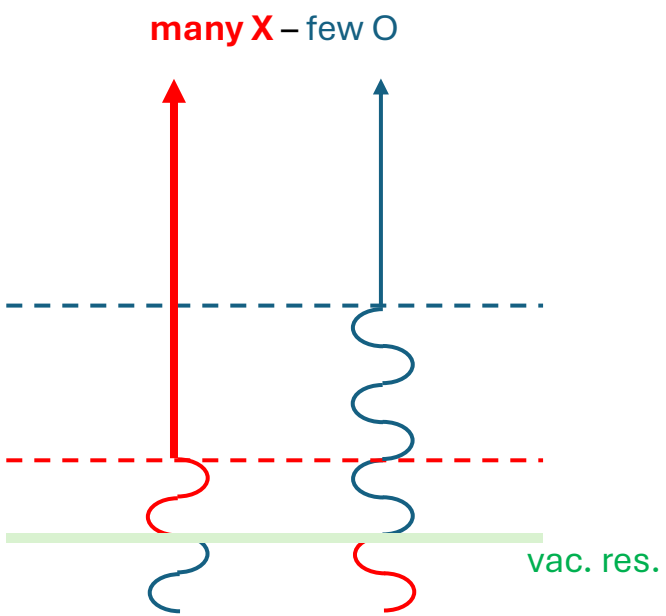

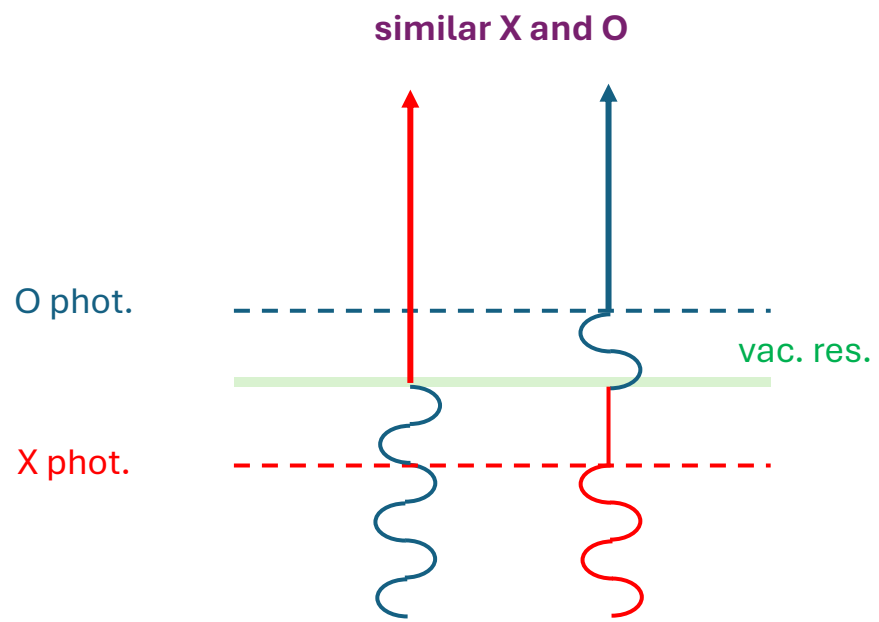

Vacuum resonance

- Plasma and vacuum polarize photons in opposite ways
- Mode conversion at the vacuum resonance may modify the polarization pattern of photons emerging from plasma

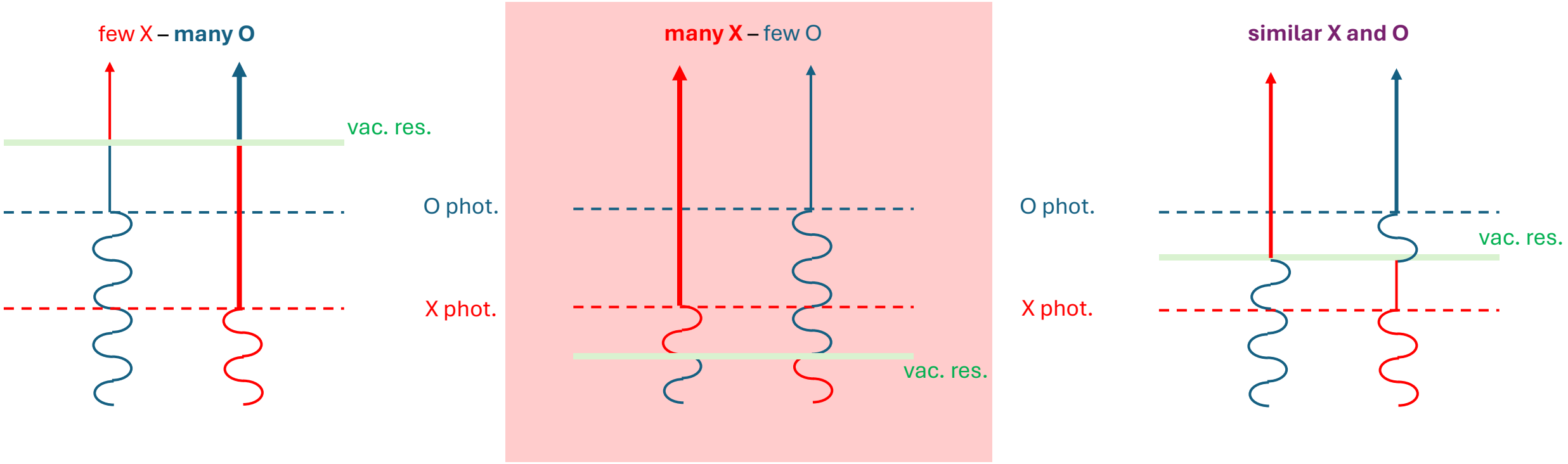

Polarization in the magnetosphere

- Passing through the magnetosphere photons undergo RCS
- At the cyclotron resonance X-mode is still preferred,
- Suppression factor fixed at $1/3$

$$\sigma_{\mathrm{OO}} = \frac{1}{3}\sigma_{\mathrm{OX}} \qquad \sigma_{\mathrm{XX}} = 3\sigma_{\mathrm{XO}}$$

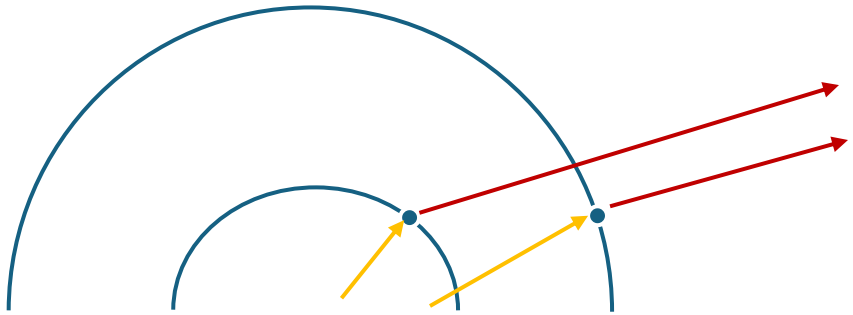

Expected polarization 33% in the X-mode

Transport of polarization at infinity

- Depolarization is expected given the tangled B-field topology close to the surface

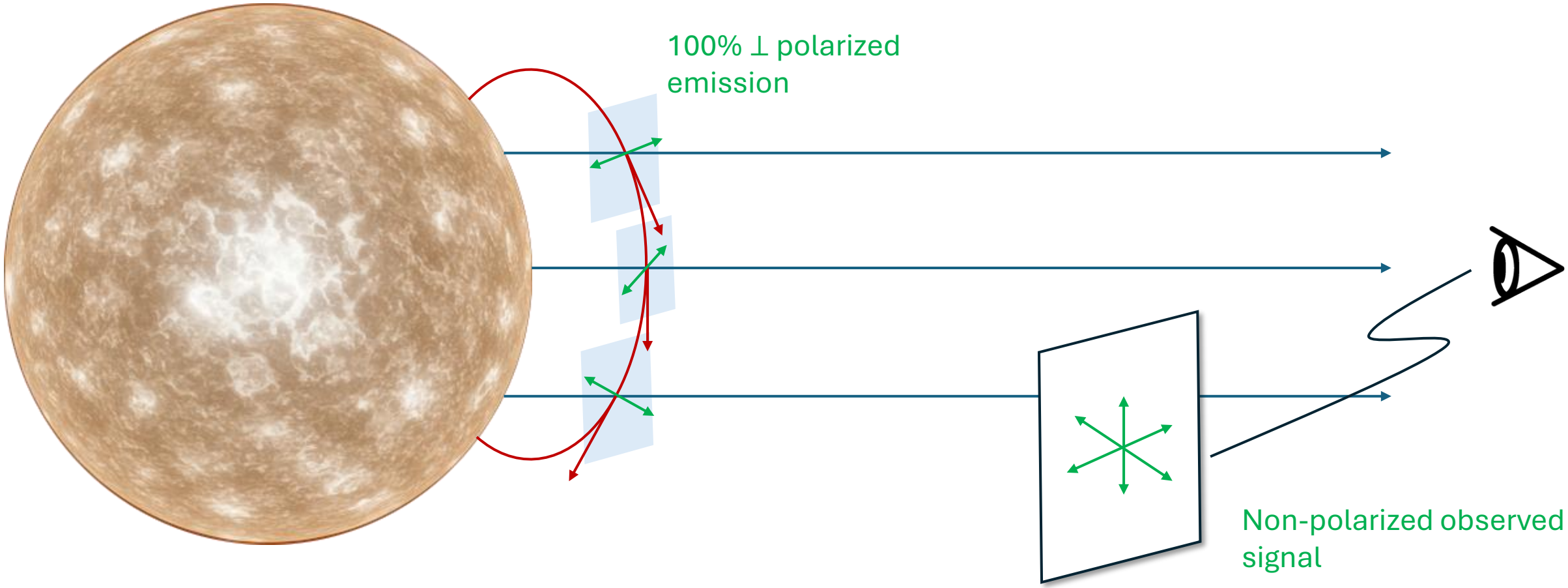

Propagation in the pure magnetized vacuum

- Solving the wave equation accounting for vacuum effects only yields

$$\boldsymbol{\nabla} \times (\bar{\boldsymbol{\mu}} \cdot \boldsymbol{\nabla} \times \boldsymbol{E}) = \frac{\omega^2}{c^2} \boldsymbol{\epsilon} \cdot \boldsymbol{E} \quad \Longrightarrow \quad \frac{2}{k_0 \delta} \frac{dE_x}{dz} = i\left[ME_x + PE_y\right]$$

$$\frac{2}{k_0 \delta} \frac{dE_y}{dz} = i\left[PE_x + NE_y\right]$$

Taverna et al. (2015)

Propagation in the pure magnetized vacuum

- Solving the wave equation accounting for vacuum effects only yields

$$\boldsymbol{\nabla} \times (\bar{\boldsymbol{\mu}} \cdot \boldsymbol{\nabla} \times \boldsymbol{E}) = \frac{\omega^2}{c^2} \boldsymbol{\epsilon} \cdot \boldsymbol{E} \quad \Longrightarrow \quad \frac{2}{k_0 \delta} \frac{dE_x}{dz} = i\left[ME_x + PE_y\right]$$

$$\frac{2}{k_0 \delta} \frac{dE_y}{dz} = i\left[PE_x + NE_y\right]$$

Taverna et al. (2015)

- Evolution of $\boldsymbol{E}$ along the photon trajectory depends on

E-field evolution length:

$$\ell_{\rm E} = \frac{2}{k_0 \delta} \approx 130 \left(\frac{B}{10^{11}\ {\rm G}}\right)^{-2} \left(\frac{\hbar\omega}{1\ {\rm keV}}\right)^{-1} {\rm cm}$$

$$\delta \sim \left(B/B_{\rm Q}\right)^2$$

(Dipolar) B-field evolution length:

$$\ell_{\rm B} = \frac{B}{|\boldsymbol{k} \cdot \boldsymbol{\nabla} B|} \approx \frac{r}{3}$$

- S
- E

ℓ_E

$\ell_E \gg \ell_B$: $\boldsymbol{E}$ direction is frozen

r_{pl} ($\ell_E = \ell_B$)

$\ell_E \ll \ell_B$: $\boldsymbol{E}$ adapts to $\boldsymbol{B}$

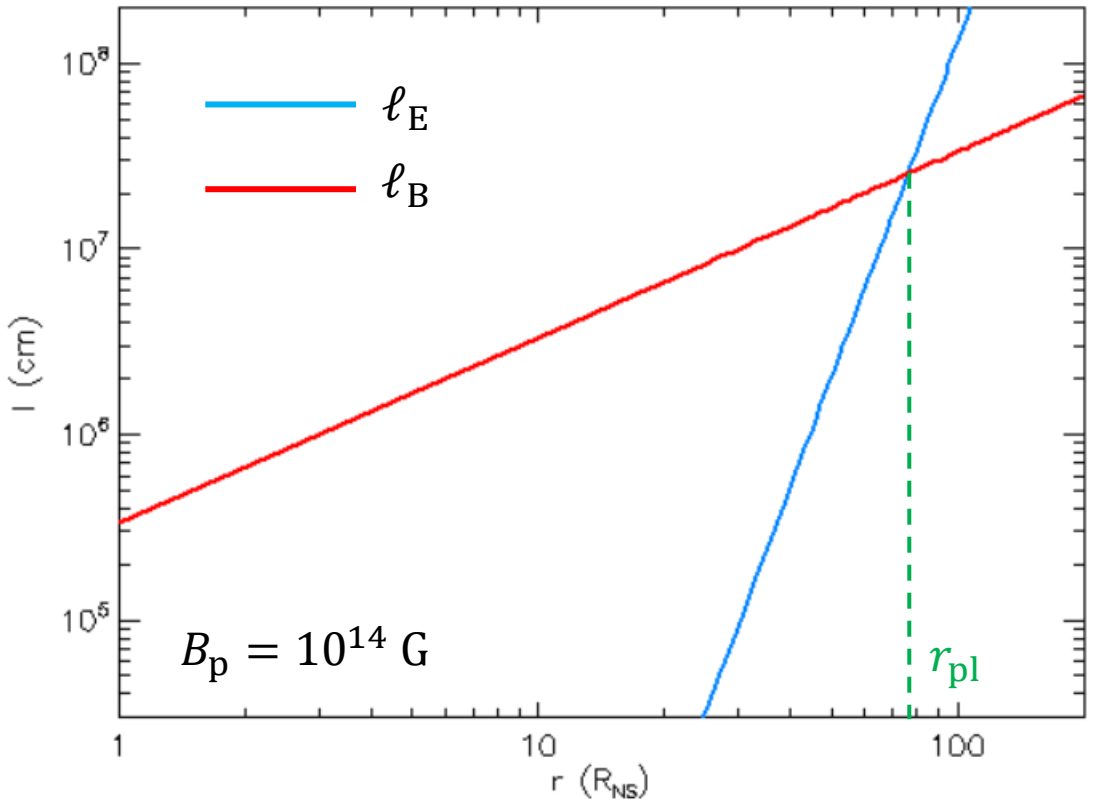

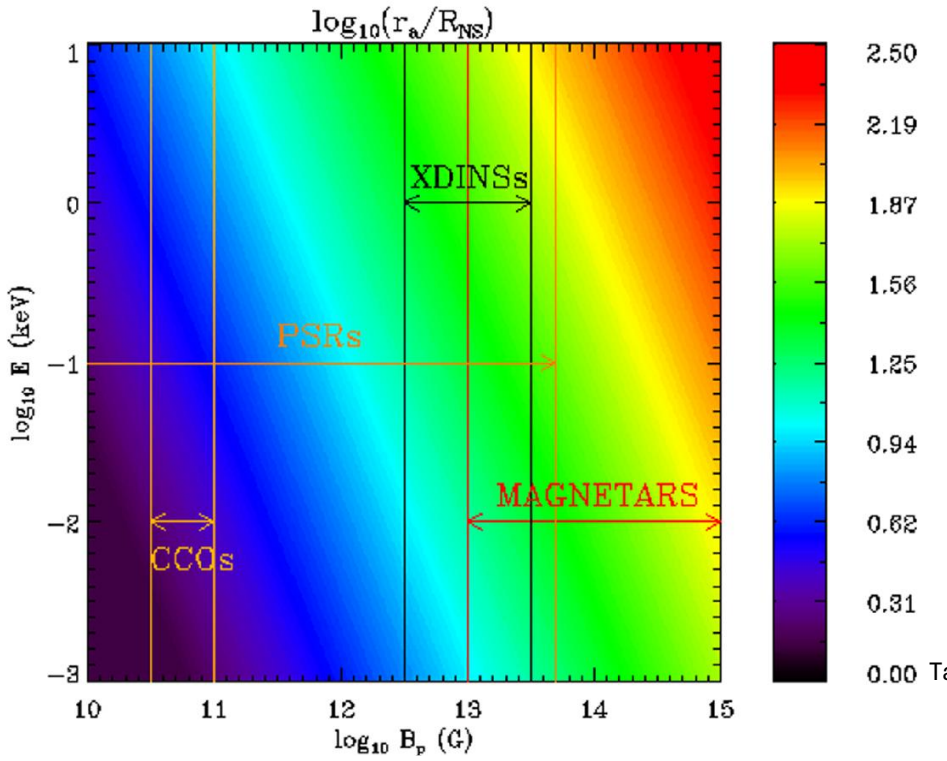

Taverna et al. (2015)

$$r_{\rm pl} \approx 5 \left(\frac{B_{\rm pol}}{10^{11}\ {\rm G}}\right)^{2/5} \left(\frac{\hbar\omega}{1\ {\rm keV}}\right)^{1/5} \left(\frac{R_{\rm NS}}{10\ {\rm km}}\right)^{1/5} R_{\rm NS}$$

Magnetars (with the strongest $\boldsymbol{B}$) have the largest $r_{\rm pl}$

⇓

Best candidates to observe polarization of surface emission (potentially very high)

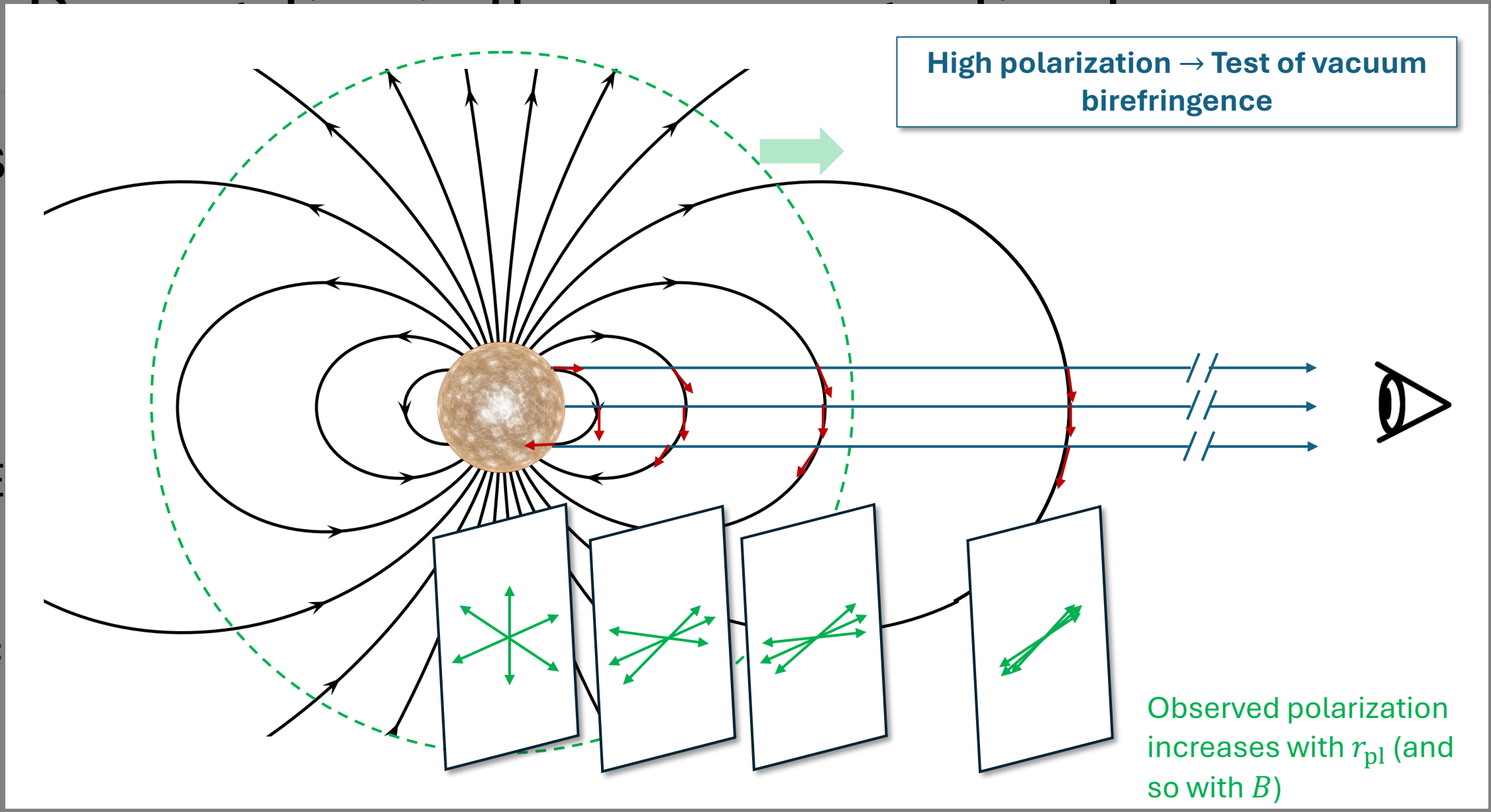
High polarization → Test of vacuum birefringence
Observed polarization increases with $r_{\rm pl}$ (and so with B)

Surface emission models

- NS surface can be covered by a thin, magnetized atmosphere

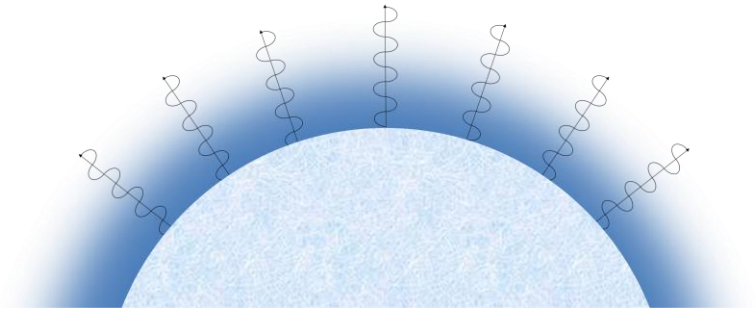

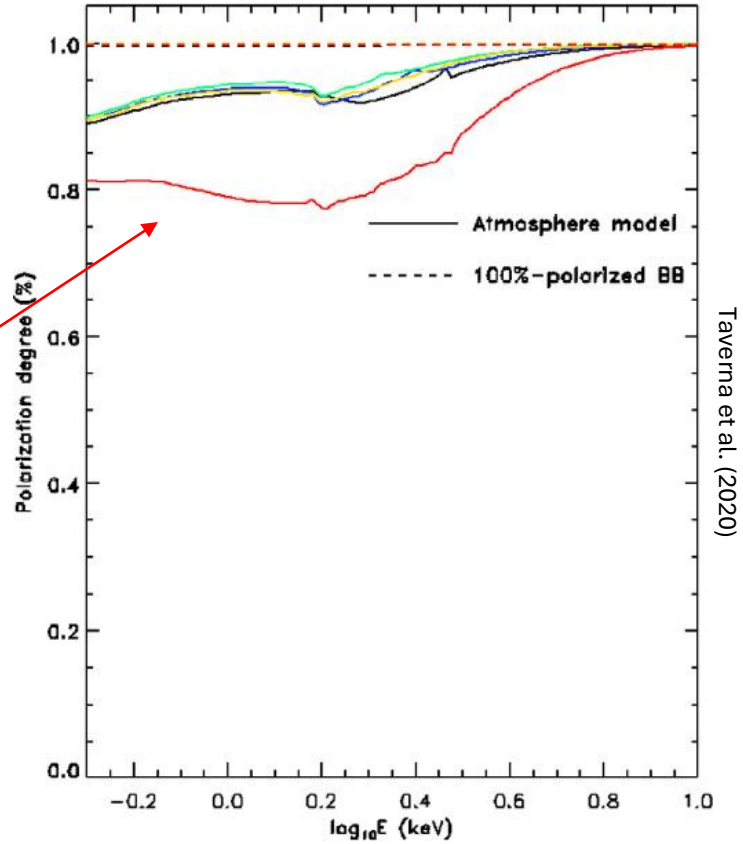

Taverna et al. (2020)

High PD
$\gtrsim 80\%$

Surface emission models

- NS surface can be covered by a thin, magnetized atmosphere
- Atoms under strong B-fields are elongated along the field direction → for sufficiently low T molecular chains are formed (magnetic condensation)
- The condensed atmosphere settles onto the surface and the crust is left exposed

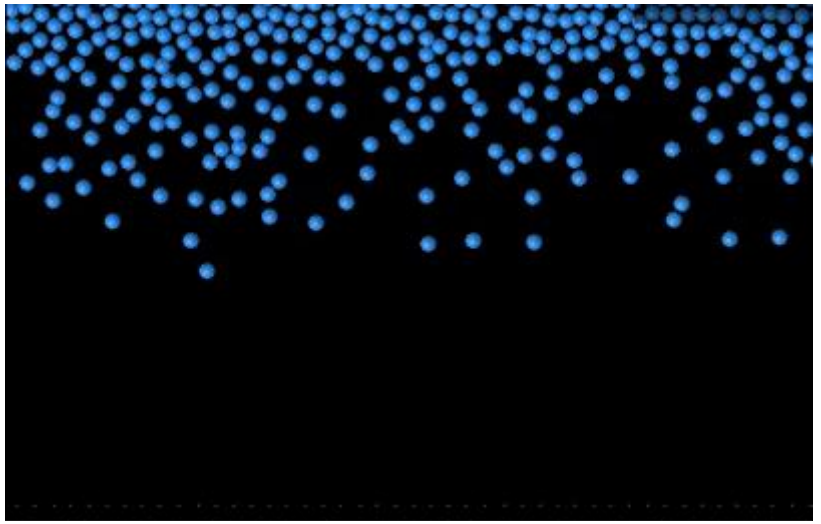

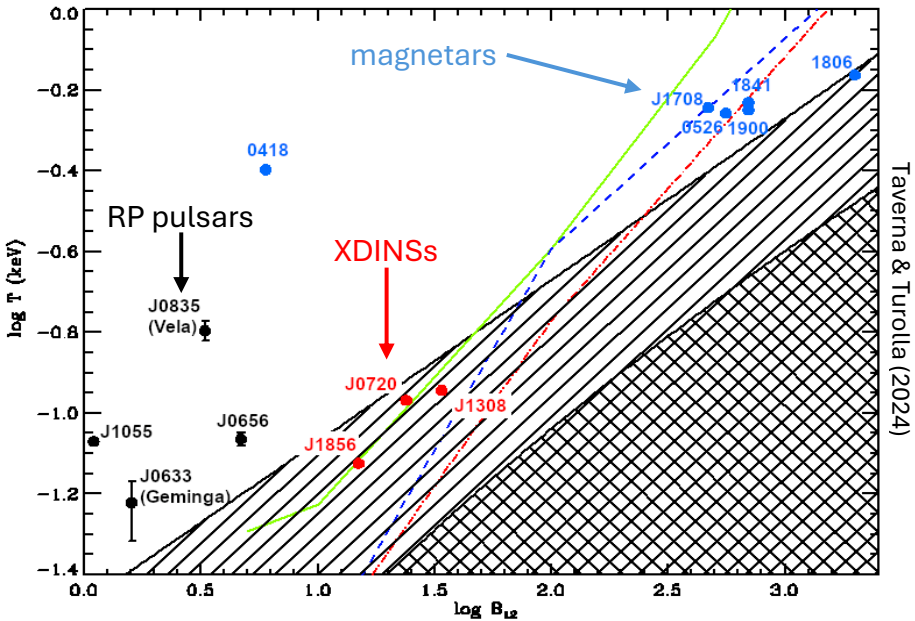

Surface emission models

- NS surface can be covered by a thin, magnetized atmosphere
- Atoms under strong B-fields are elongated along the field direction → for sufficiently low T molecular chains are formed (magnetic condensation)
- The condense datmosphere settles onto the surface and the crust is left exposed
- PD much lower than for atmospheres

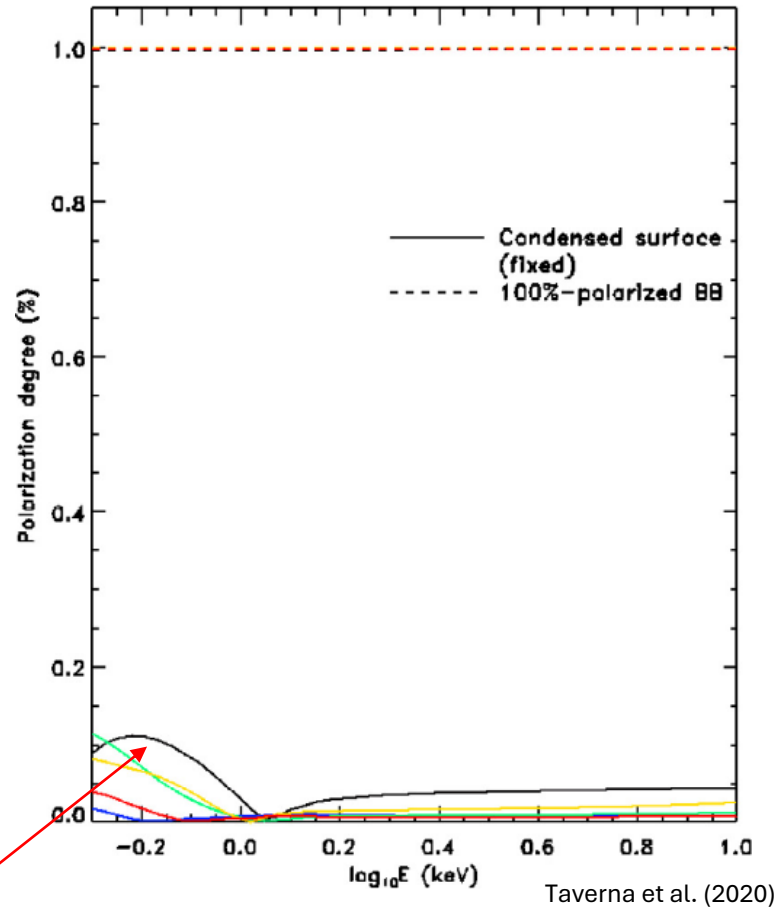

Taverna et al. (2020)

$\mathrm{PD} \lesssim 20\%$

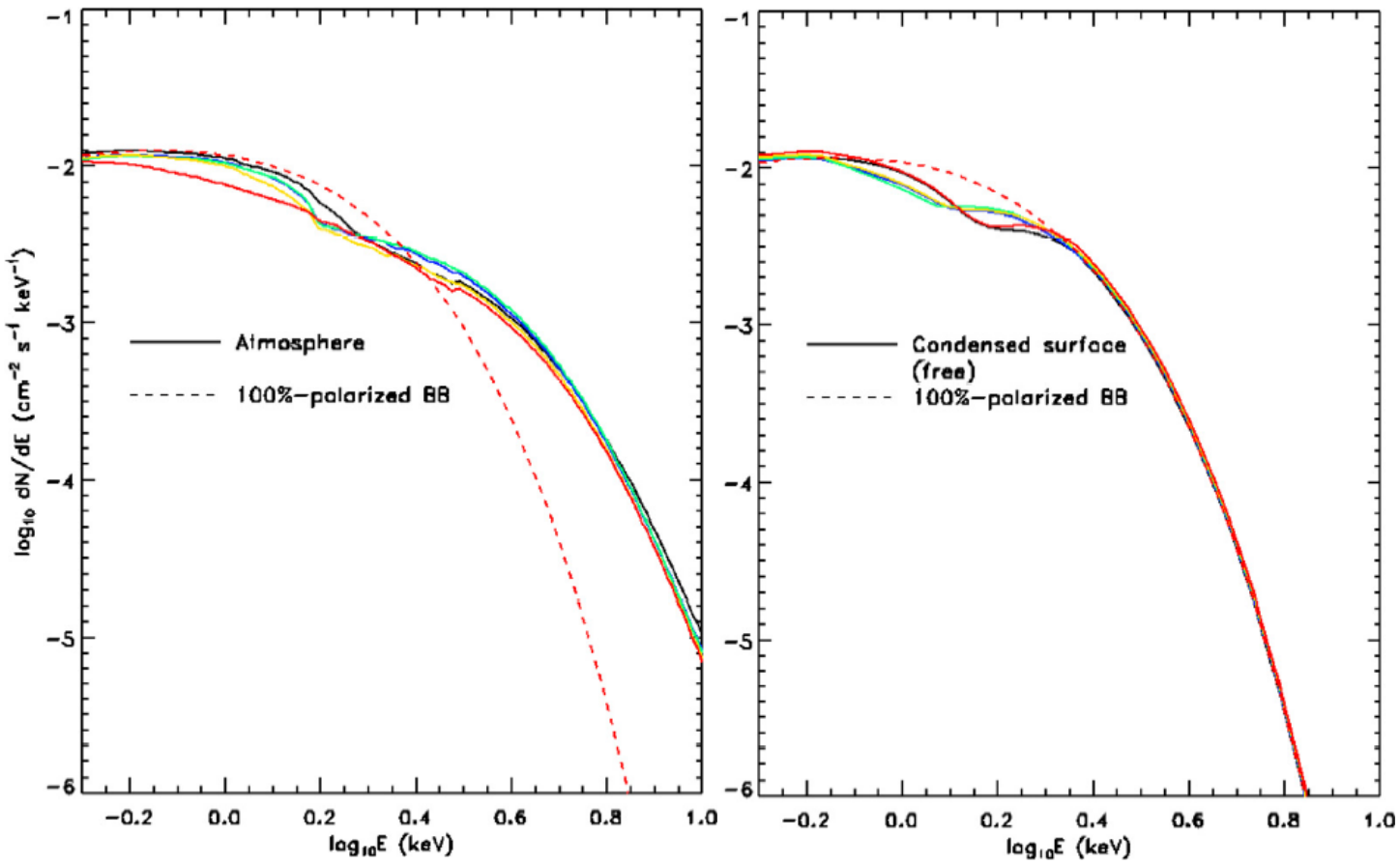

Spectra for atmospheres and condensed-surfaces are similar (BB-like)

Polarization may help in disentangling the surface emission model

Taverna et al. (2020)

Imaging X-ray Polarimetry Explorer (IXPE)

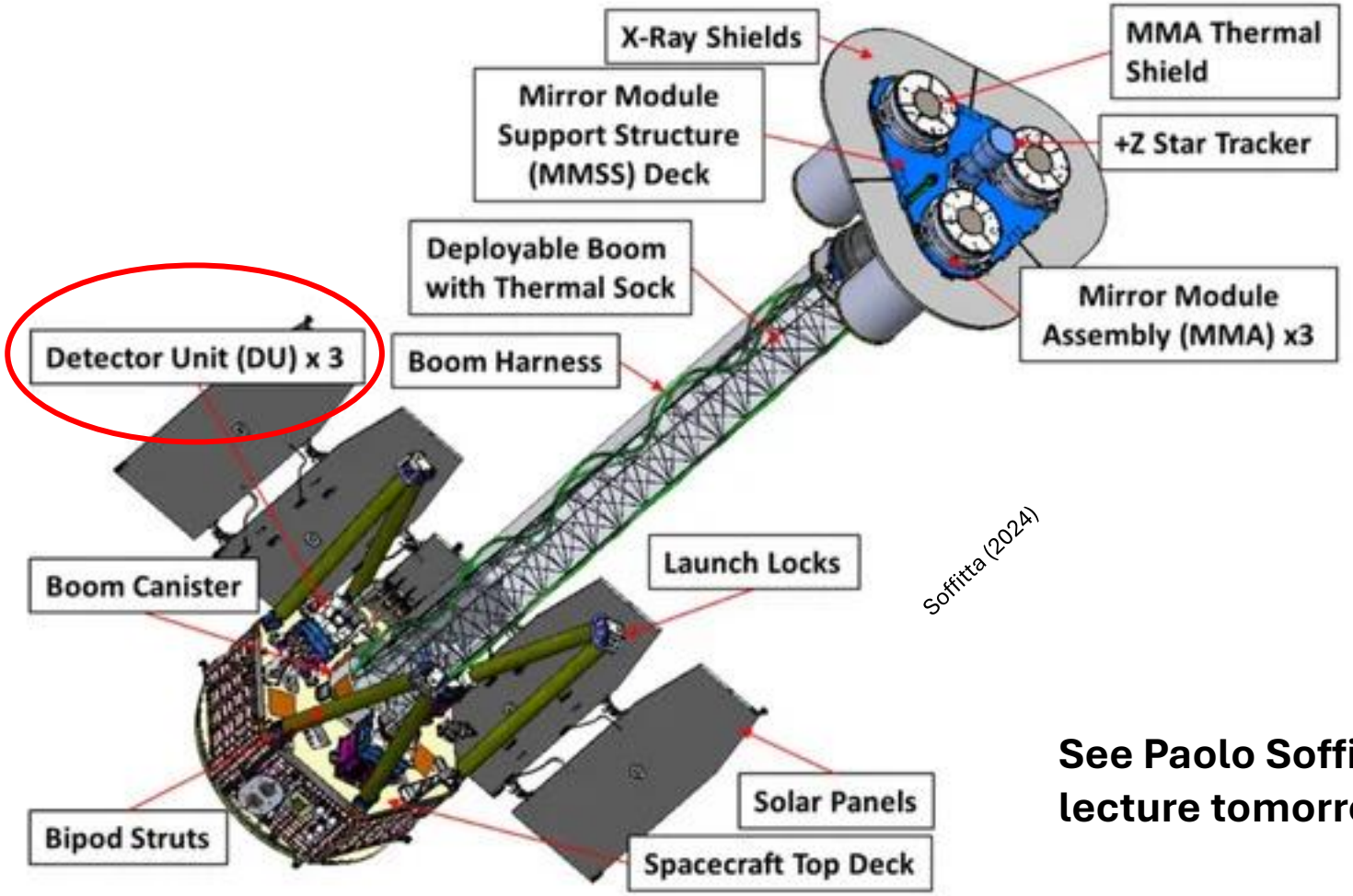

Soffitta (2024)

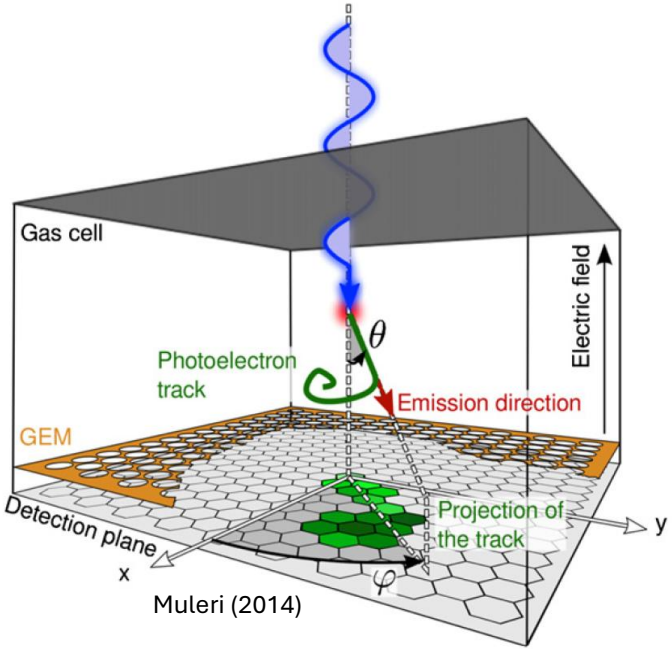

Muleri (2014)

See Paolo Soffitta lecture tomorrow

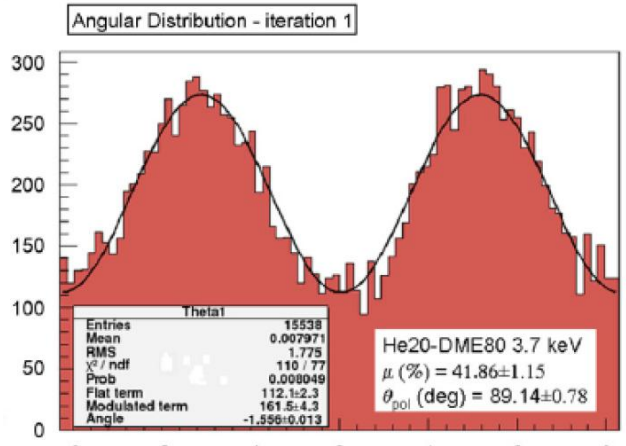

Muleri (2017)

IXPE magnetar targets

- AXP 4U 0142+61
  - $F_{2-10}^{\mathrm{unabs}} \approx 7 \times 10^{-11}$ cgs
  - $B_{\mathrm{P\dot{P}}} \approx 2 \times 10^{14}$ G
  - $t_{\mathrm{exp}} = 840$ ks
- AXP 1RXS J170849.0−4009100
  - $F_{2-10}^{\mathrm{unabs}} \approx 3 \times 10^{-11}$ cgs
  - $B_{\mathrm{P\dot{P}}} \approx 5 \times 10^{14}$ G
  - $t_{\mathrm{exp}} = 837$ ks
- SGR 1806−20
  - $F_{0.5-10}^{\mathrm{unabs}} \approx 1 \times 10^{-11}$ cgs
  - $B_{\mathrm{P\dot{P}}} \approx 7 \times 10^{14}$ G
  - $t_{\mathrm{exp}} = 947$ ks
- AXP 1E 2259+586
  - $F_{2-10}^{\mathrm{unabs}} \approx 1.5 \times 10^{-11}$ cgs
  - $B_{\mathrm{P\dot{P}}} \approx 6 \times 10^{13}$ G
  - $t_{\mathrm{exp}} = 1200$ ks
- AXP 1E 1841−045
  - $F_{2-8}^{\mathrm{unabs}} \approx 2 \times 10^{-11}$ cgs
  - $B_{\mathrm{P\dot{P}}} \approx 7 \times 10^{14}$ G
  - $t_{\mathrm{exp}} = 300$ ks

AXP 4U 0142+61 – Spectral properties

- Spectral decomposition BB+PL (in agreement with the twisted-magnetosphere model)
- Low-energy, thermal photons come from the cooling surface
- High-energy PL tail populated by resonantly up-scattered photons

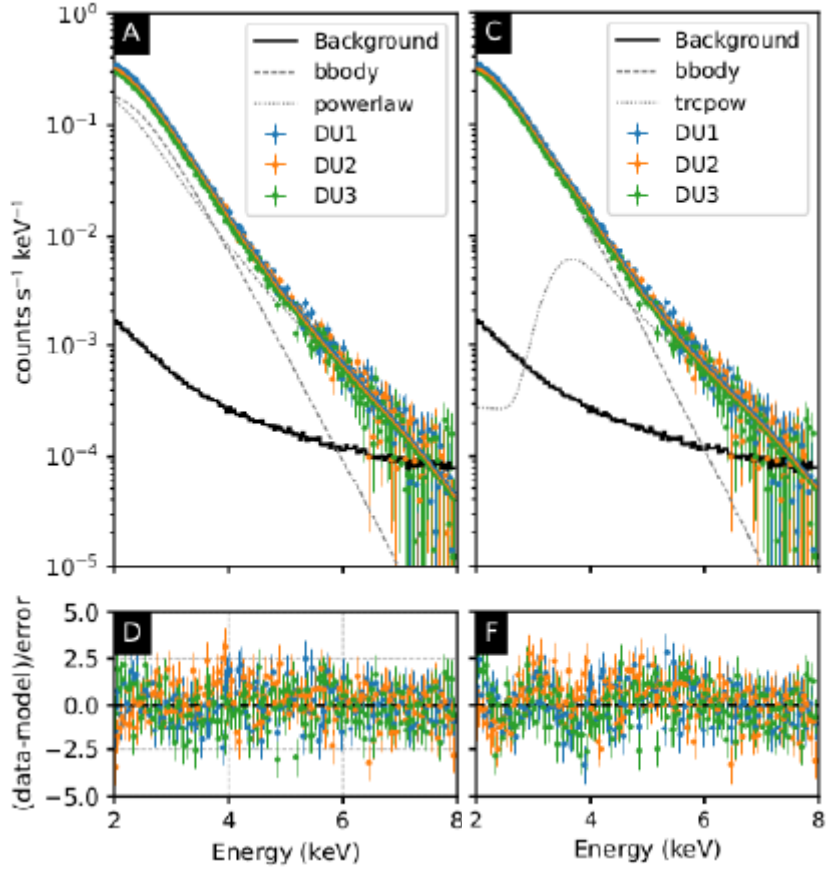

Taverna et al. (2022)

AXP 4U 0142+61 – Polarization

- Phase-integrated, energy-dependent polarization degree and angle

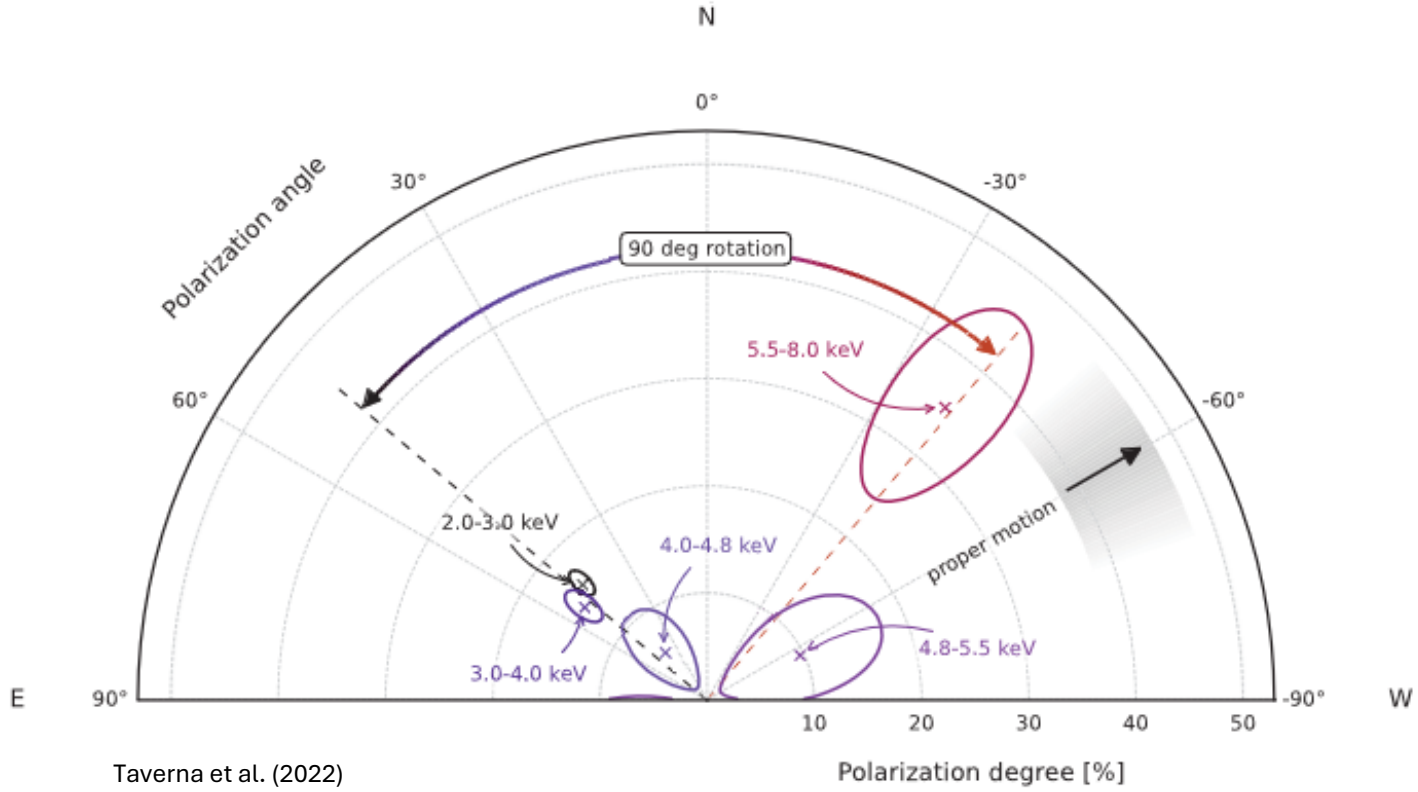

Taverna et al. (2022)

AXP 4U 0142+61 – Polarization

- Phase-integrated, energy-dependent polarization degree and angle

2 normal modes (O and X)

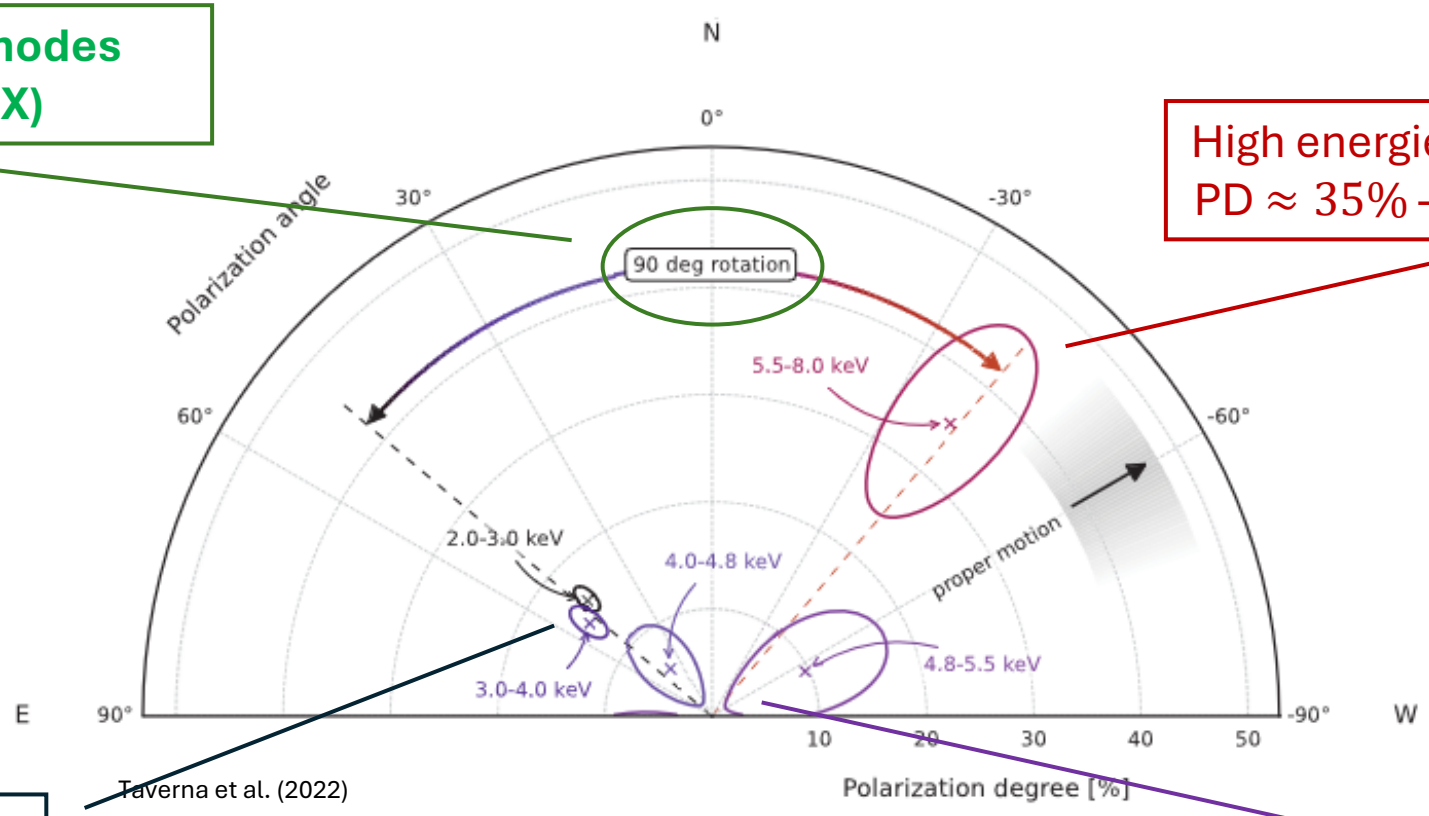

Taverna et al. (2022)

High energies (6–8 keV)
PD ≈ 35% – PA ≈ −40°

Low energies (2–4 keV)
PD ≈ 15% – PA ≈ 50°

4–5 keV
PD ≈ 0

AXP 4U 0142+61 – Polarization

- Phase-integrated, energy-dependent polarization degree and angle
- PD at high energies ($\approx 35\%$) is compatible with magnetar model expectations (33%) for RCS PL tails
- Since RCS photons are polarized mostly in the X-mode → low-energy photons polarized in the O-mode
- Low PD + O-mode photons → condensed surface exposed (emission likely from an equatorial-belt)

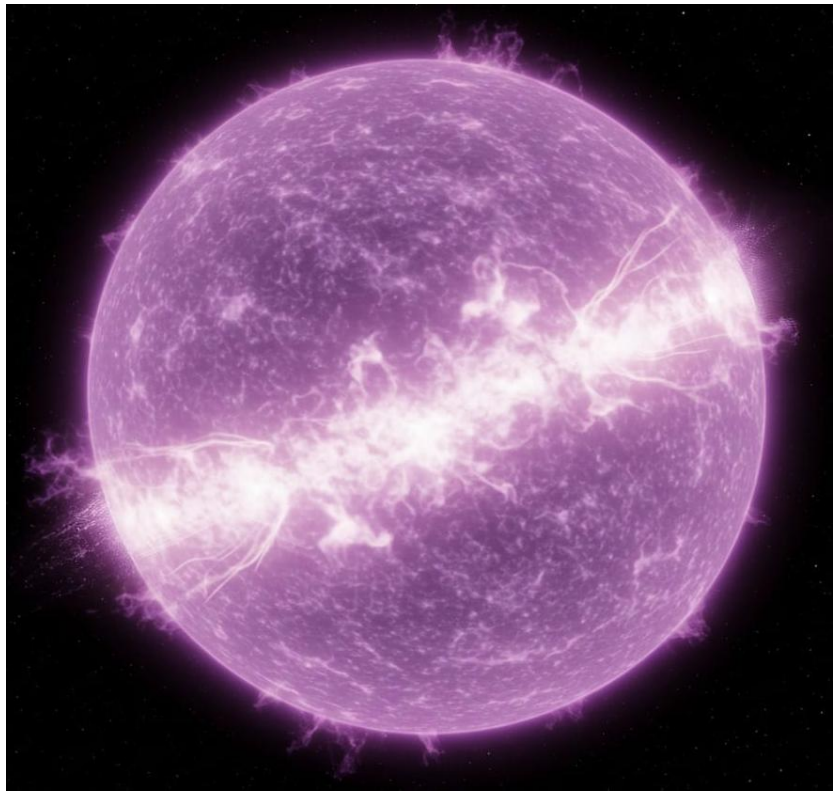

AXP 4U 0142+61 – Phase-dependent pattern

- Phase-dependent PD coherent with the LC (double-peaked and in-phase)
  → determined at the surface

- Phase-dependent PA uncorrelated with the LC (single-peaked, quasi-sinusoidal – RVM)
  → determined far from the surface

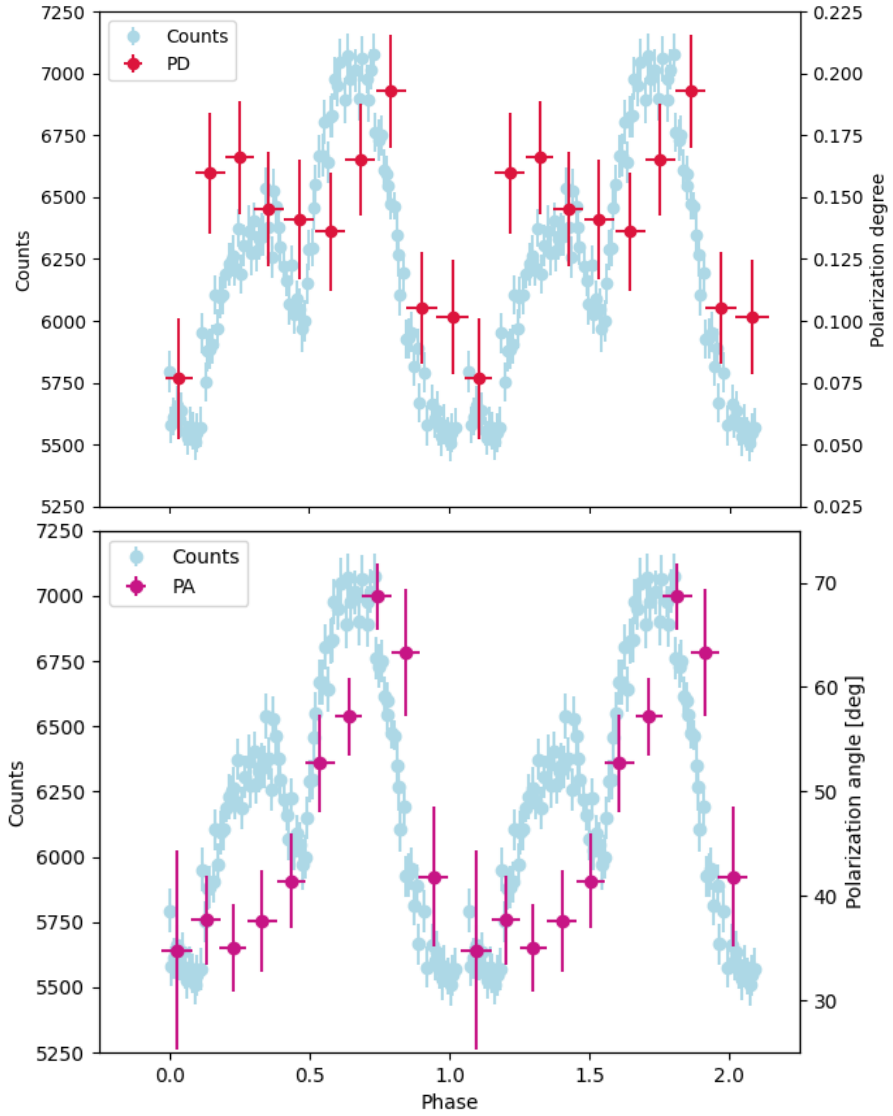

According to the RVM, the polarization angle for radiation emitted from polar spots in a dipolar field follows the projection of the magnetic axis in the plane of the sky

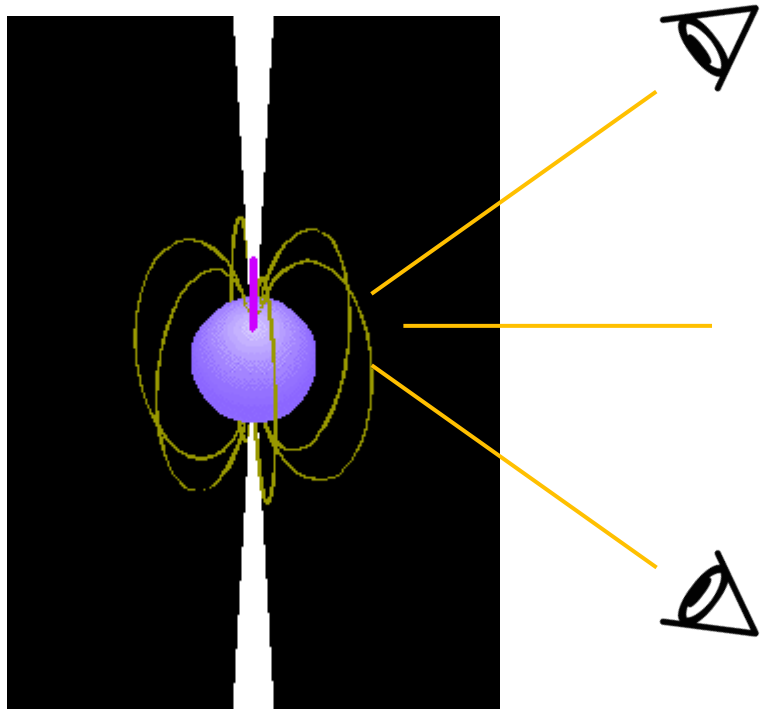

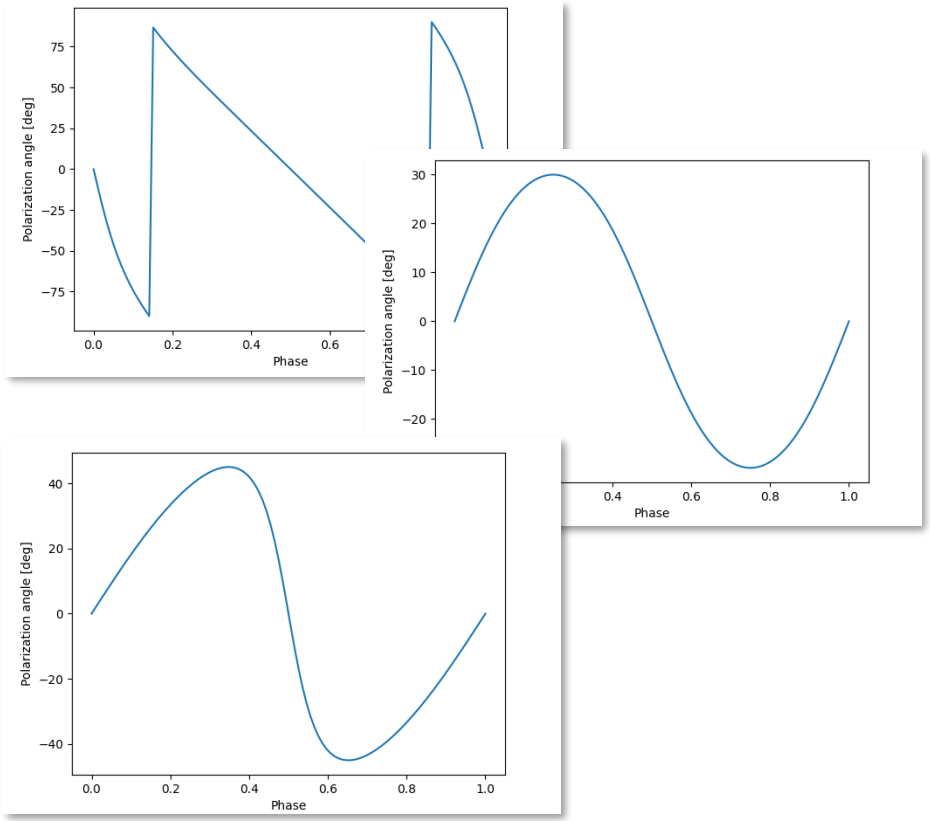

Magnetic field topology on the surface of magnetars is expected to be far from dipolar (and emission region extended)…

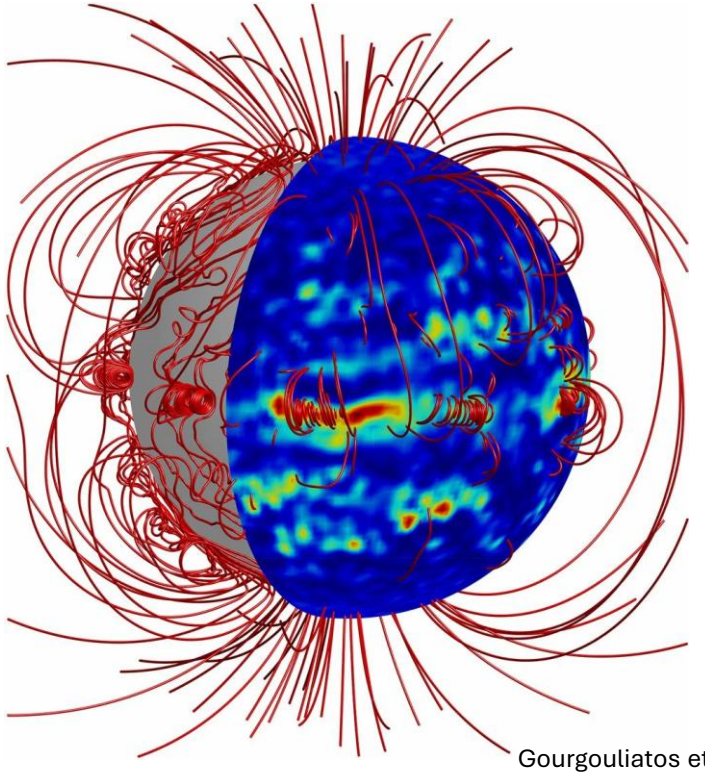

Gourgouliatos et al. (2016)

…but it recovers the dipolar shape far enough from the surface

AXP 4U 0142+61 – Phase-dependent pattern

- Phase-dependent PD coherent with the LC (double-peaked and in-phase)
  → determined at the surface
- Phase-dependent PA uncorrelated with the LC (single-peaked, quasi-sinusoidal – RVM)
  → determined far from the surface
- Vacuum birefringence naturally explains PD fixed at the surface and PA determined outside (at r_{pl} polarization vectors freeze)

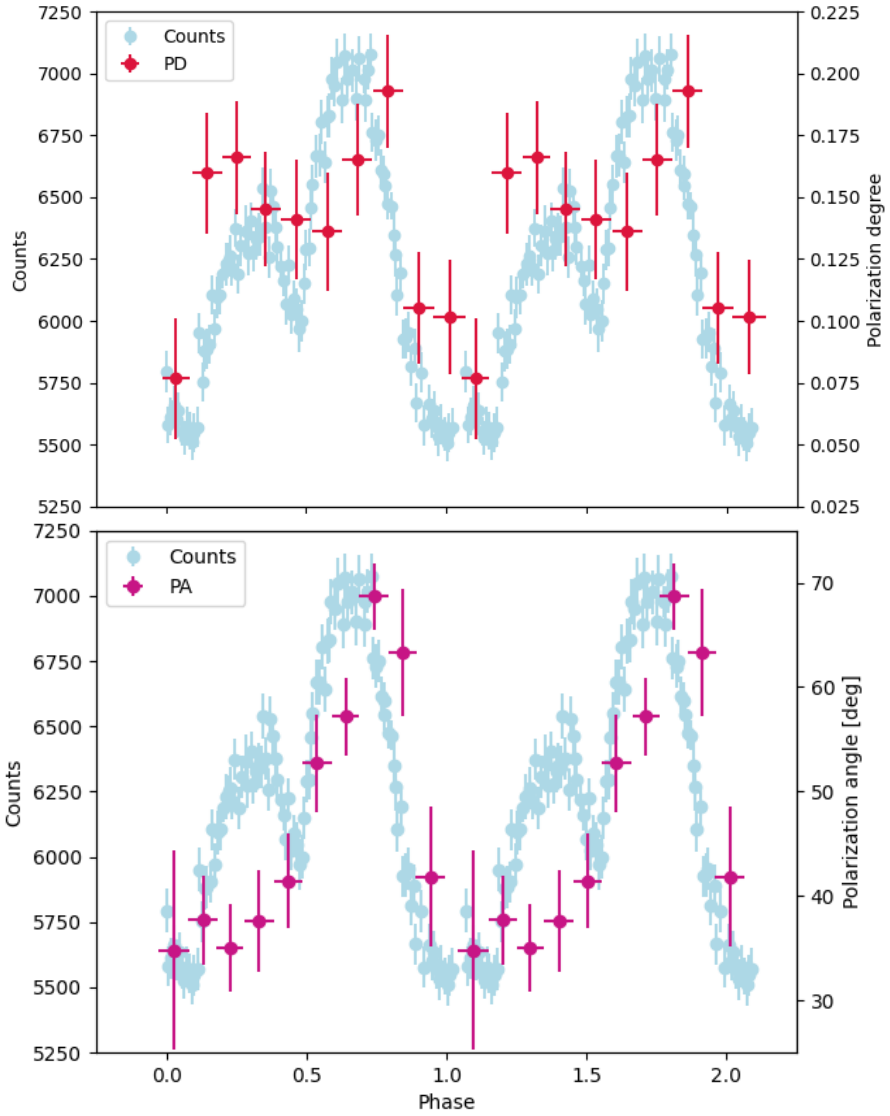

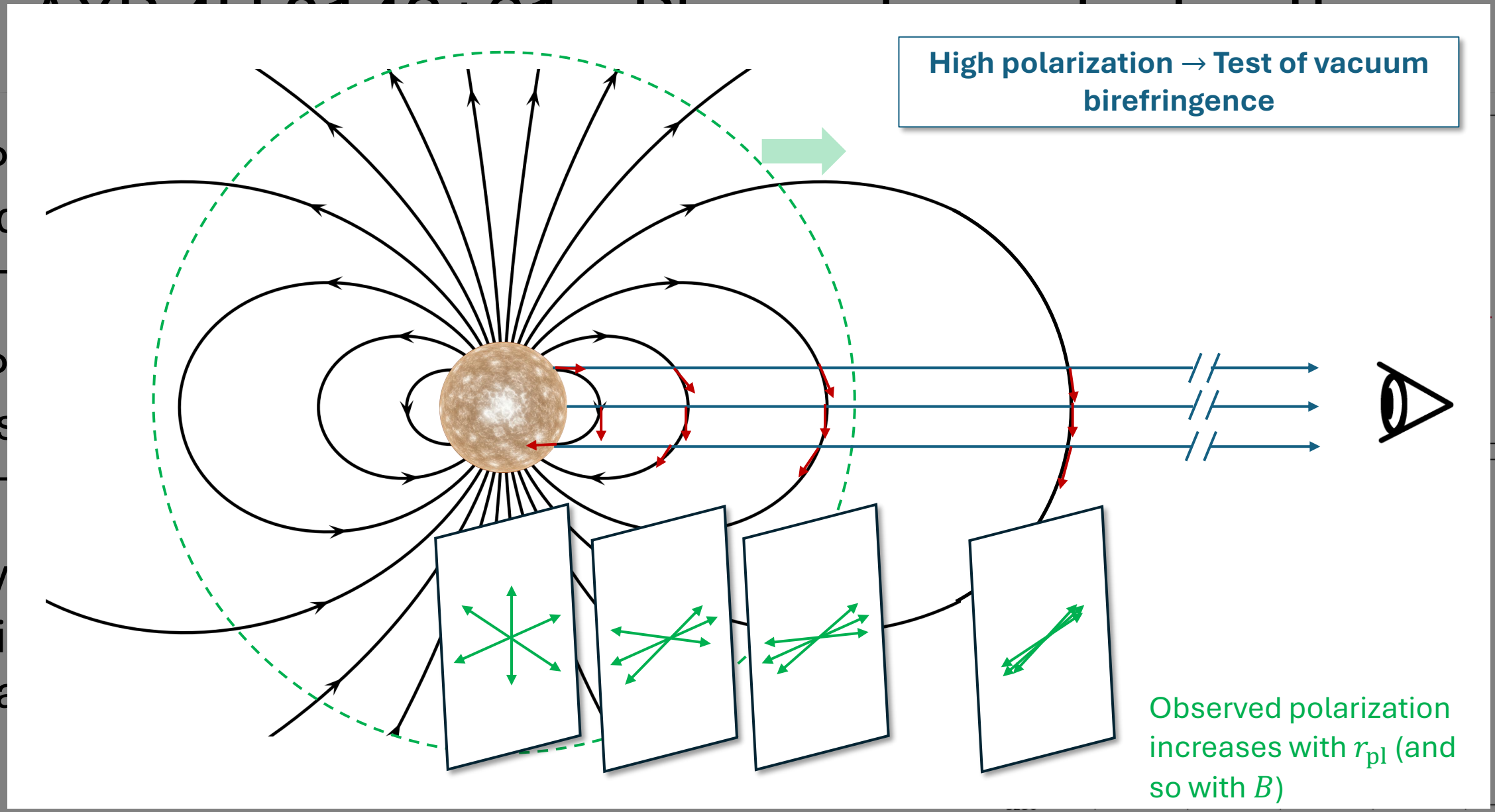
High polarization → Test of vacuum birefringence
Observed polarization increases with $r_{\rm pl}$ (and so with B)

AXP 1RXS J1708 – Phase-integrated results

- IXPE + NICER observations not clear enough to disentangle between BB+BB and BB+PL decompositions

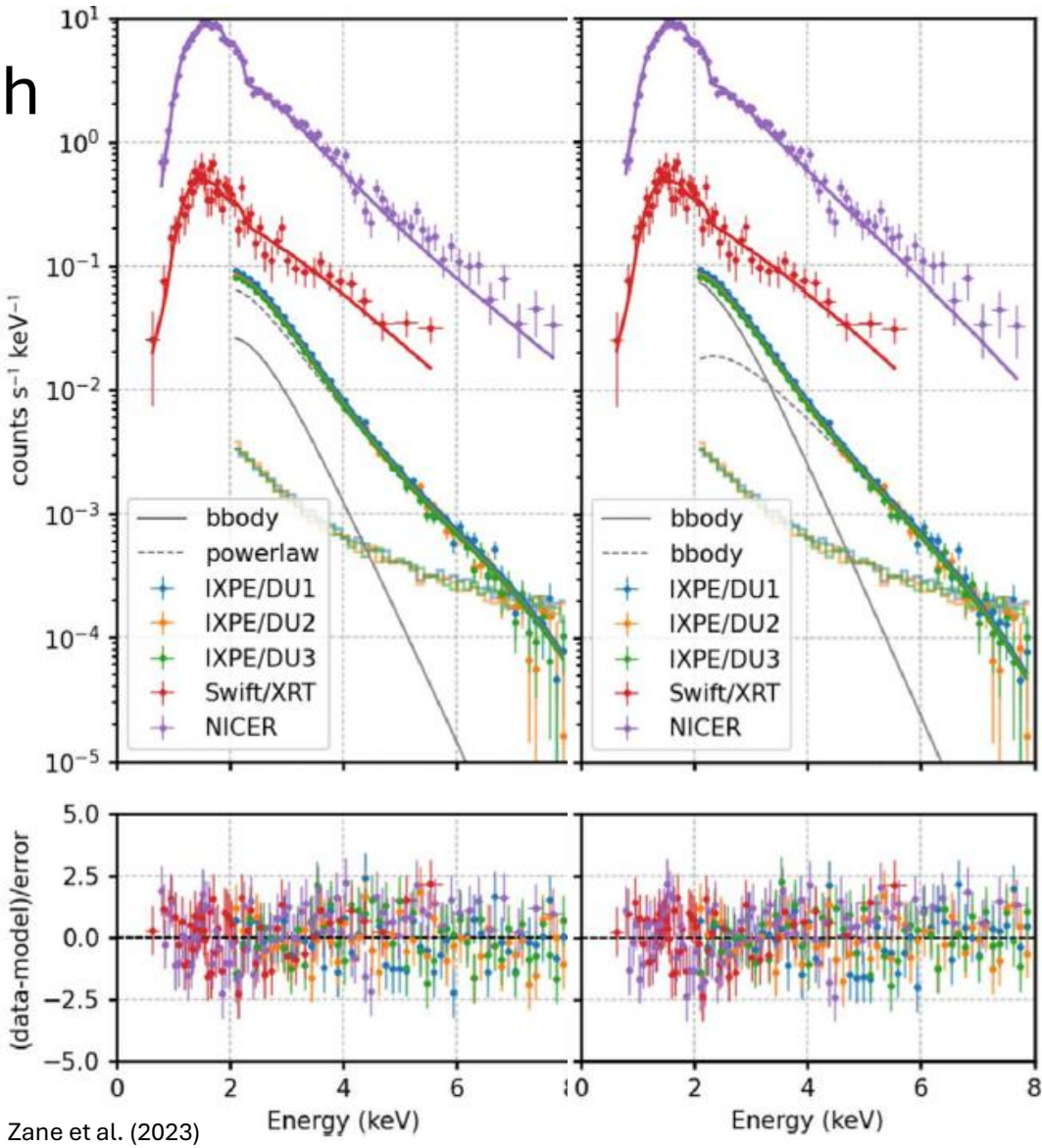

Zane et al. (2023)

AXP 1RXS J1708 – Phase-integrated results

- IXPE + NICER observations not clear enough to disentangle between BB+BB and BB+PL decompositions

- Polarization measurement
  - $\mathrm{PD}_{2-4} \approx 35\% \; - \mathrm{PA}_{2-4} \approx 60^\circ$ W
  - $\mathrm{PD}_{6-8} \approx 80\%$
  - PA constant with energy in the $2 - 8$ keV band

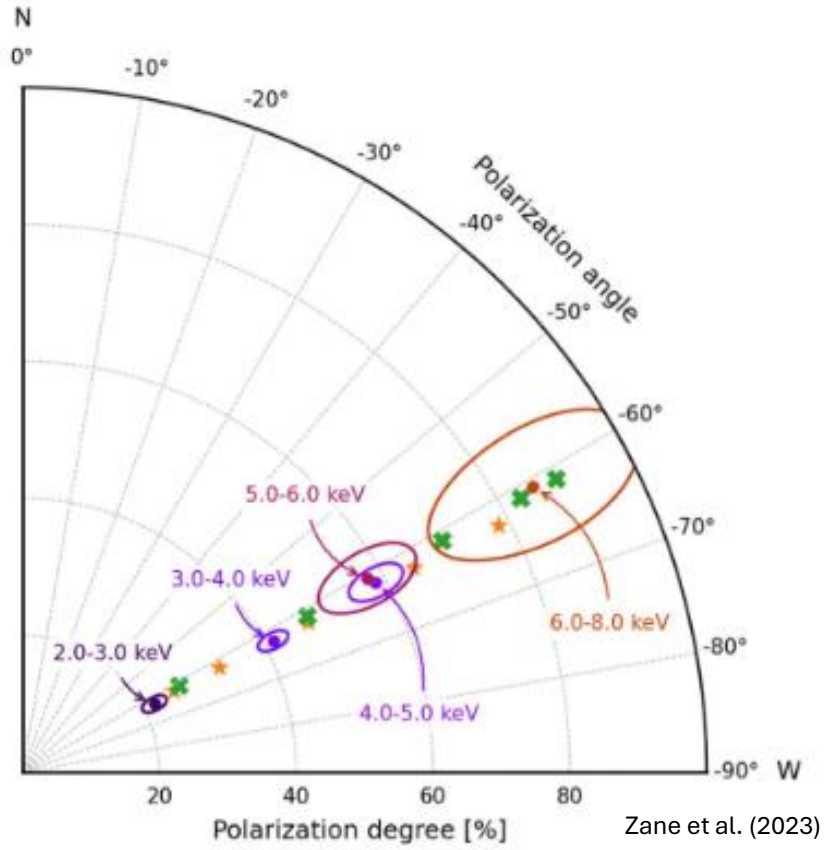

Zane et al. (2023)

AXP 1RXS J1708 – Interpretation

- High polarization at high energy → NS atmosphere
- RCS not effective ($\mathrm{PD} \gg 33\%$) → No PL tail

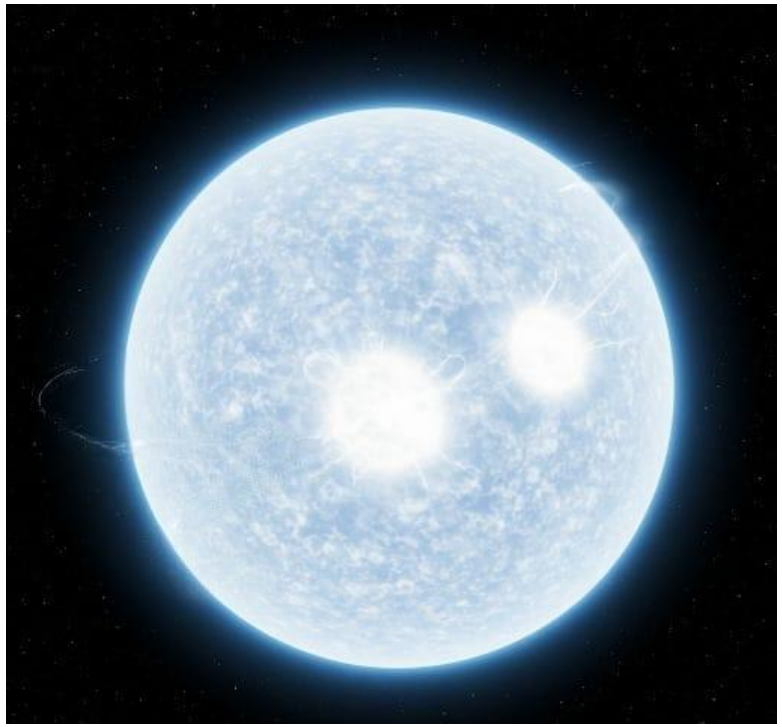

AXP 1RXS J1708 – Interpretation

- High polarization at high energy → NS atmosphere
- RCS not effective ($\mathrm{PD} \gg 33\%$) → No PL tail
- Low polarization at low energies → condensed surface
- Phase transition across the surface

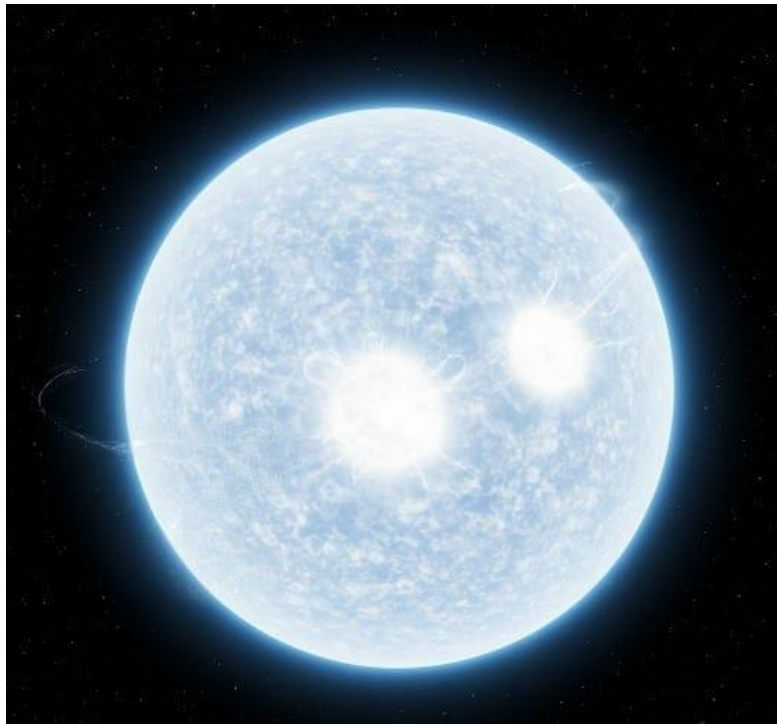

AXP 1RXS J1708 – Phase-dependent pattern

- Phase-dependent PD and PA coherent with the given explanation

Flux and PD
in counter-phase

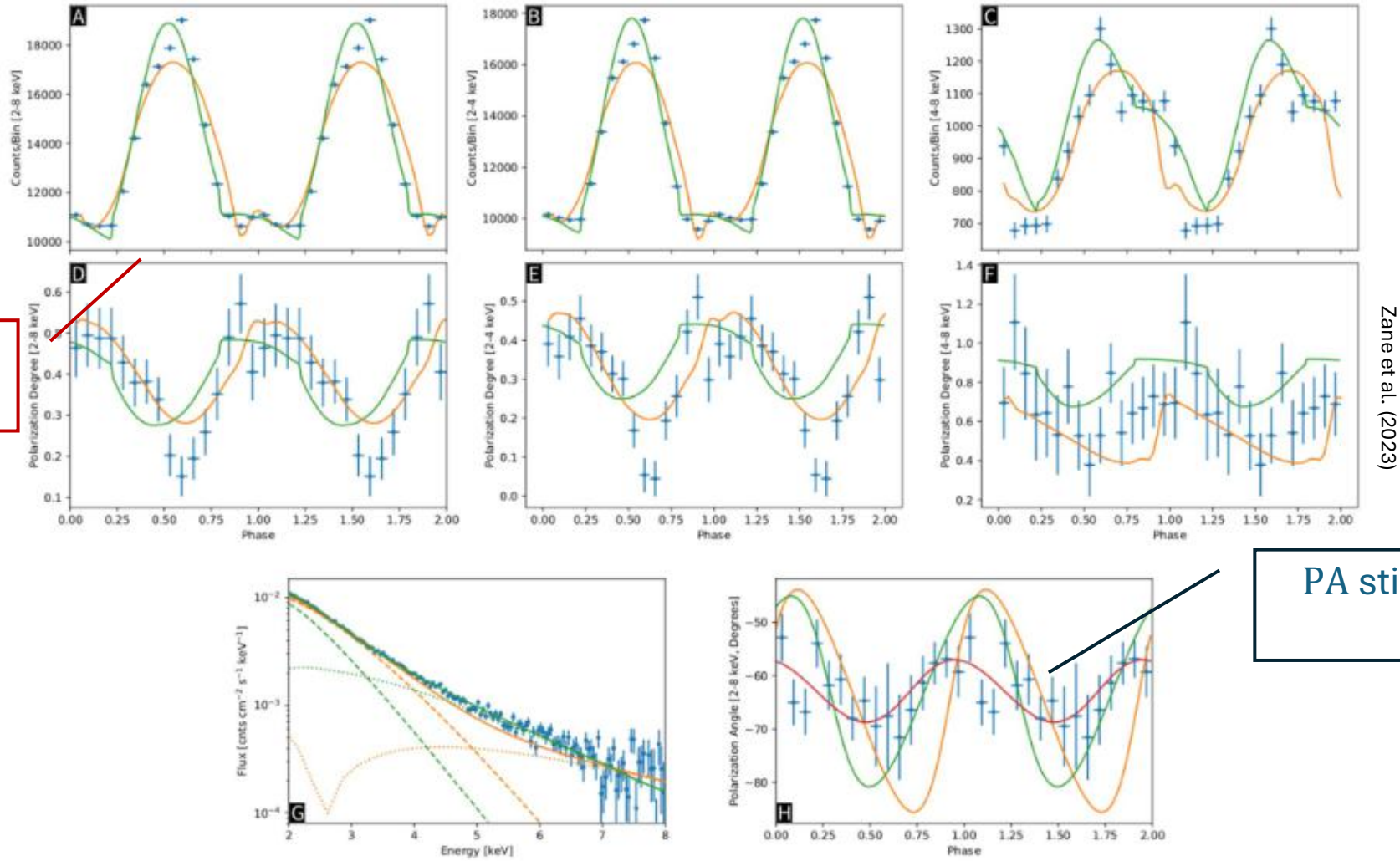

Zane et al. (2023)

PA still fitted by the
RVM

SGR 1806–20

- Emitted the strongest giant flare ever detected (December 2004, $L_{\mathrm{peak}} \approx 10^{47}\ \mathrm{erg/s}$)
- Observed contemporary by XMM-Newton

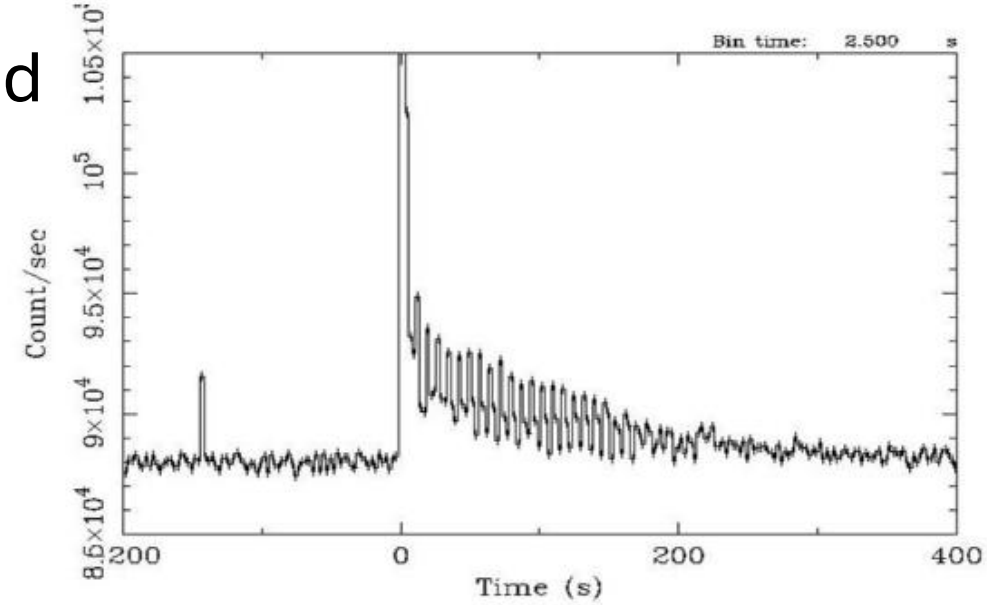

Mereghetti et al. (2005)

SGR 1806–20

- Emitted the strongest giant flare ever detected (December 2004, $L_{\rm peak} \approx 10^{47}$ erg/s)
- Observed contemporary by XMM-Newton
- IXPE measurement was only marginally significant
  - Unexpectedly low flux (4×10^{-12} cgs, $\approx 1/10$ historical)
  - Occurrence of solar flares during the observation
  - PD $\approx 32\%$ ($4-5$ keV, 99% c.l.)
- Not enough to confirm/exclude any model

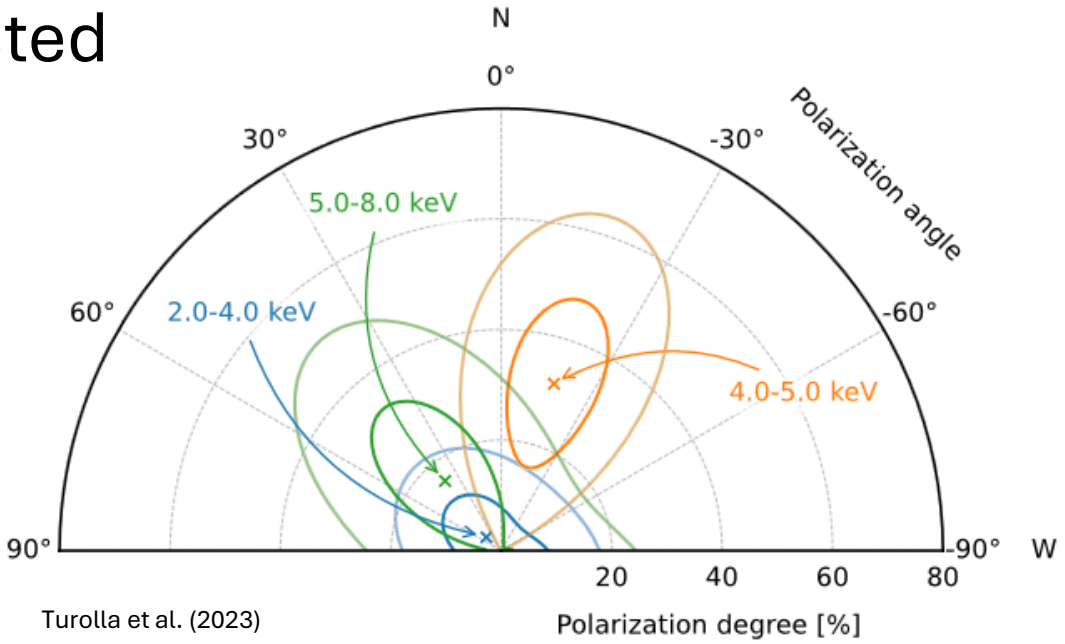

Turolla et al. (2023)

AXP 1E 2259+586 – Spectral properties

- IXPE+XMM spectral fit pinpoints the presence of a spectral line at $\approx 1\ \mathrm{keV}$, confirming previous studies (Pizzoccaro et al. 2019)

- Interpreted as produced by RCS of thermal surface photons intercepted by a bundle of twisted field lines

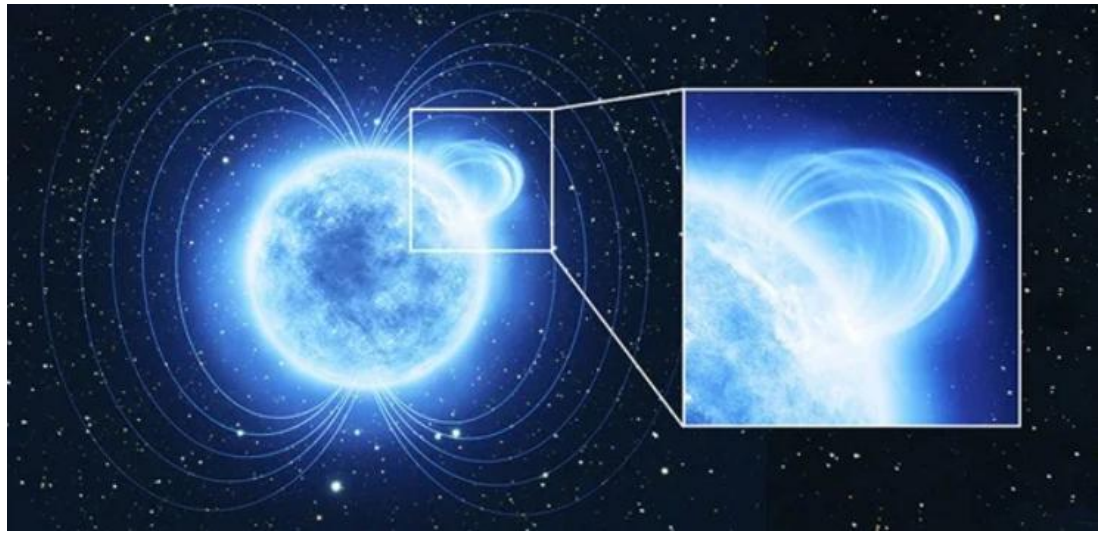

Credits: ESA

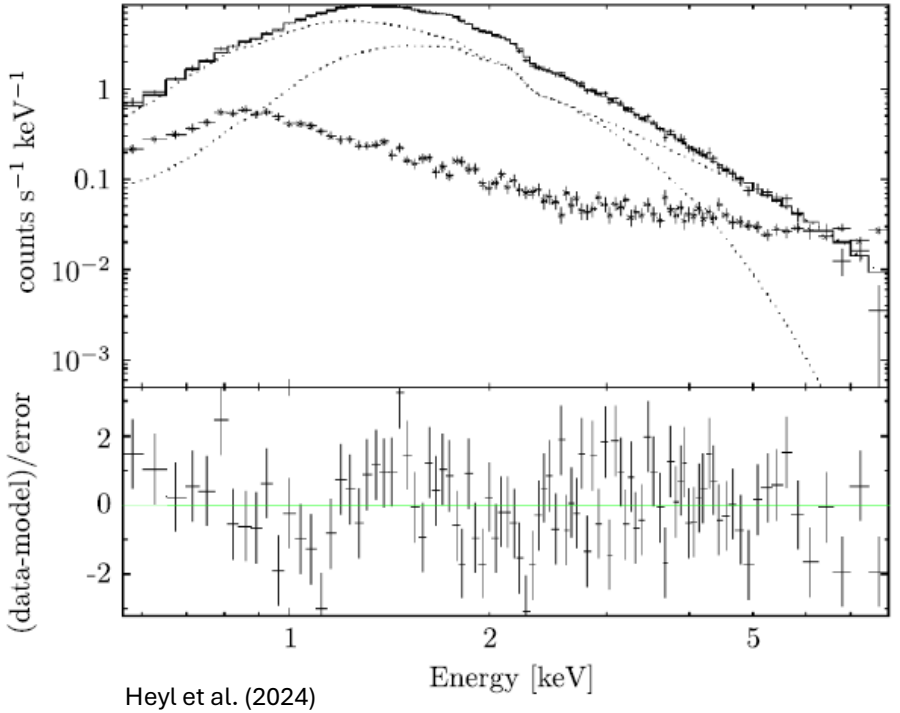

Heyl et al. (2024)

AXP 1E 2259+586 – Polarization

- Low phase- and energy-integrated polarization ($\mathrm{PD} \approx 5.6\%$) only significant at low energies
- Peculiar phase-dependent behavior
  - Double-peaked pulse profile
  - $\mathrm{PD} \approx 25\text{-}30\%$ (well above MDP_{99}) only at particular phases (minimum and rise of the primary peak)
  - PA still well fitted by a RVM (photons are assumed to swing by $90°$ from the 1st to the 2nd peak)

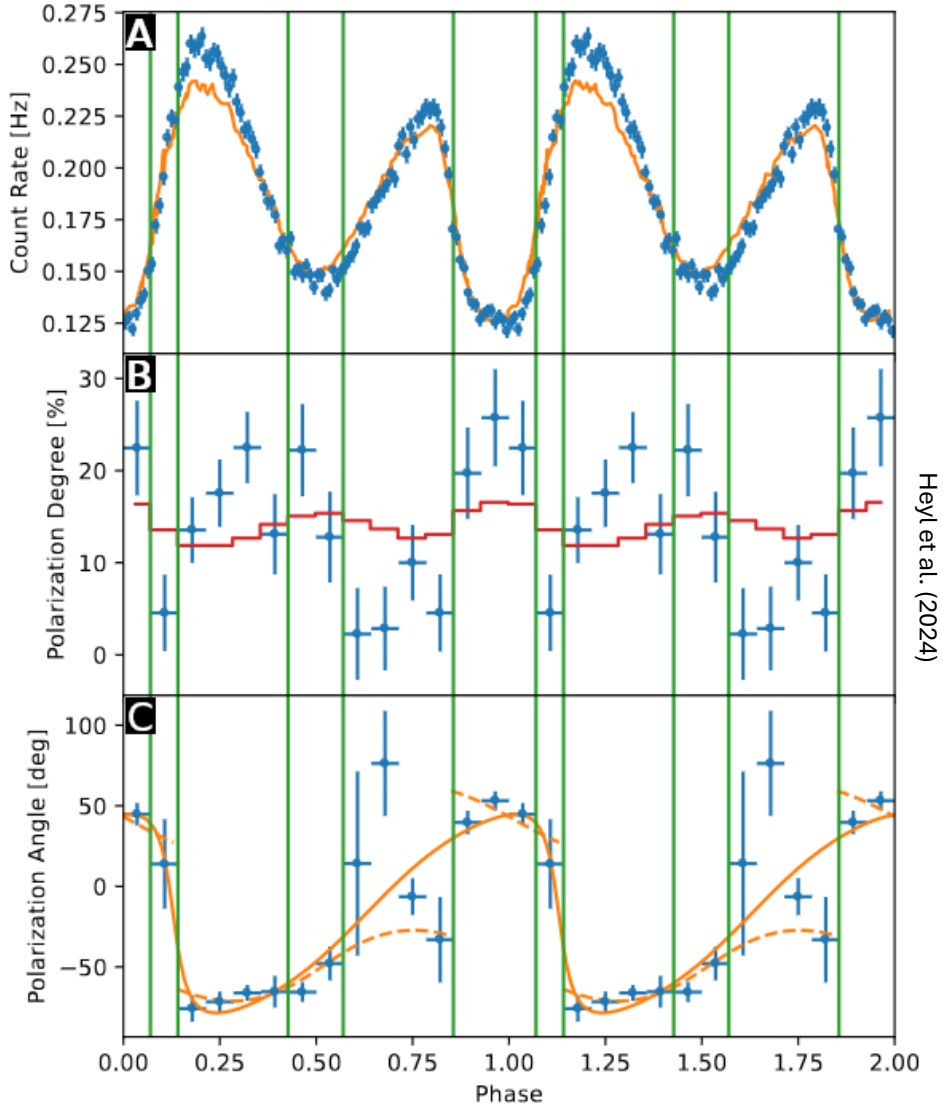

Heyl et al. (2024)

AXP 1E 2259+586 – Interpretation

- Condensed surface with two hot-spots, the primary covered by a magnetic loop

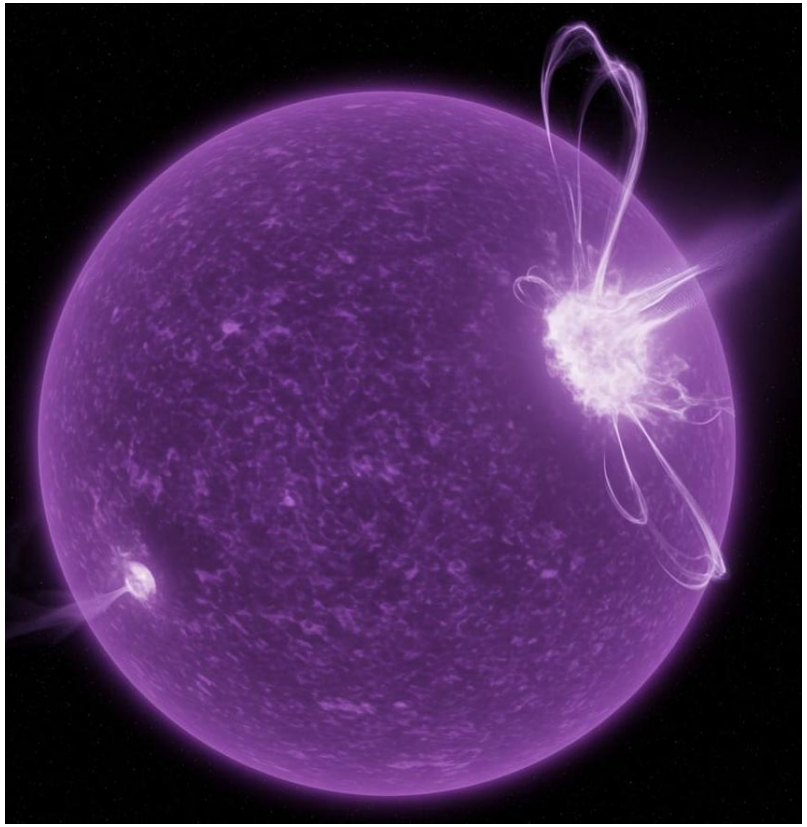

AXP 1E 2259+586 – Interpretation

- Condensed surface with two hot-spots, the primary covered by a magnetic loop

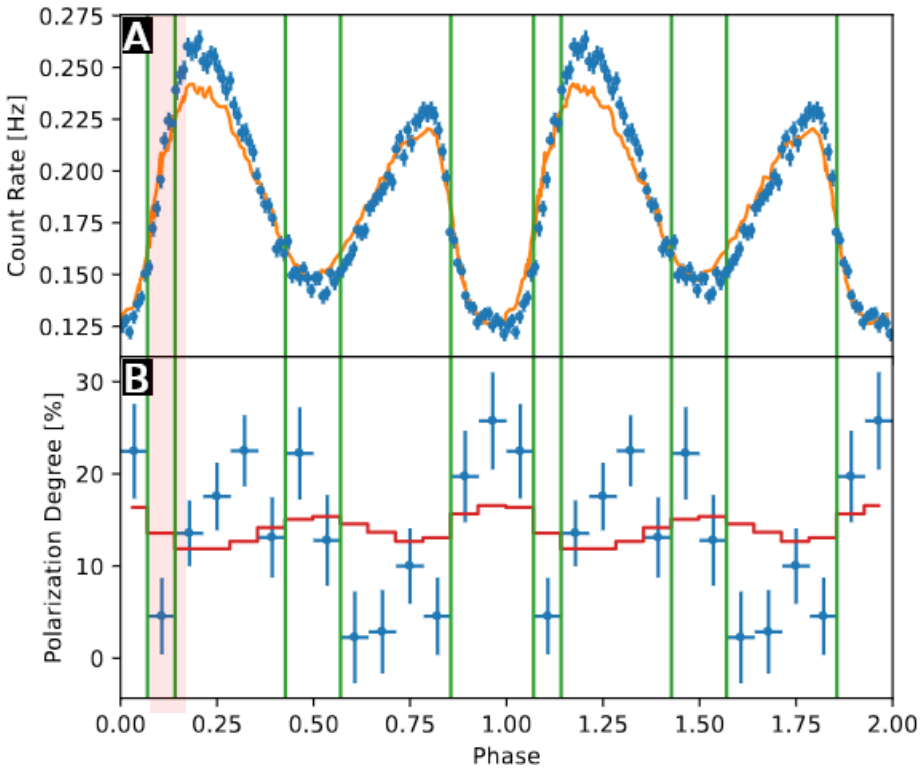

Heyl et al. (2024)

- **1st rise: primary spot face-on**
  - Thermal photons (low PD in O-mode) mostly scattered away from the LOS by RCS onto p^+

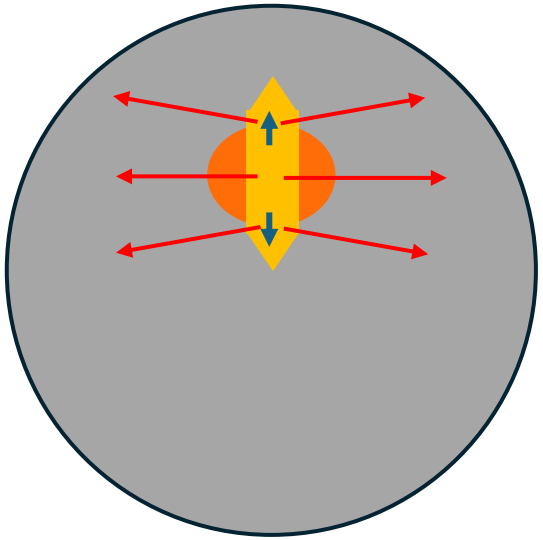

AXP 1E 2259+586 – Interpretation

- Condensed surface with two hot-spots, the primary covered by a magnetic loop

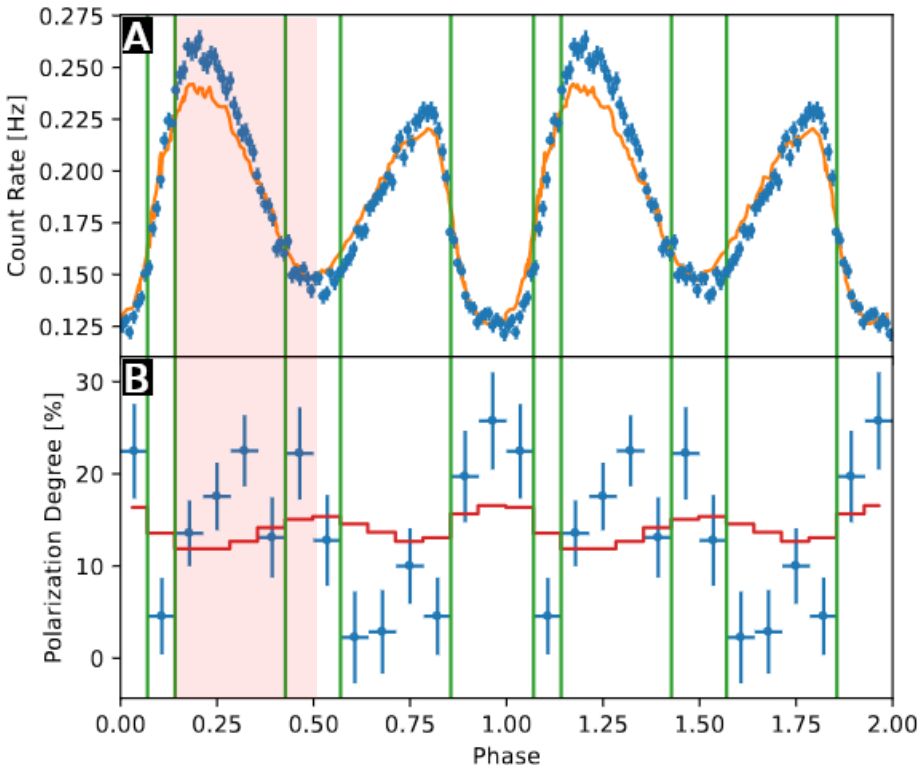

Heyl et al. (2024)

- **1st rise: primary spot face-on**
- **1st peak: primary spot off-axis**
  - Scattered photons enter in view (PD → 33%, mostly in X-mode)

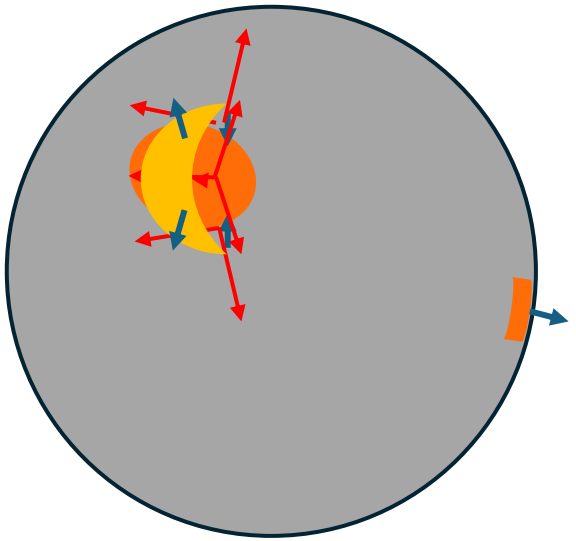

AXP 1E 2259+586 – Interpretation

- Condensed surface with two hot-spots, the primary covered by a magnetic loop

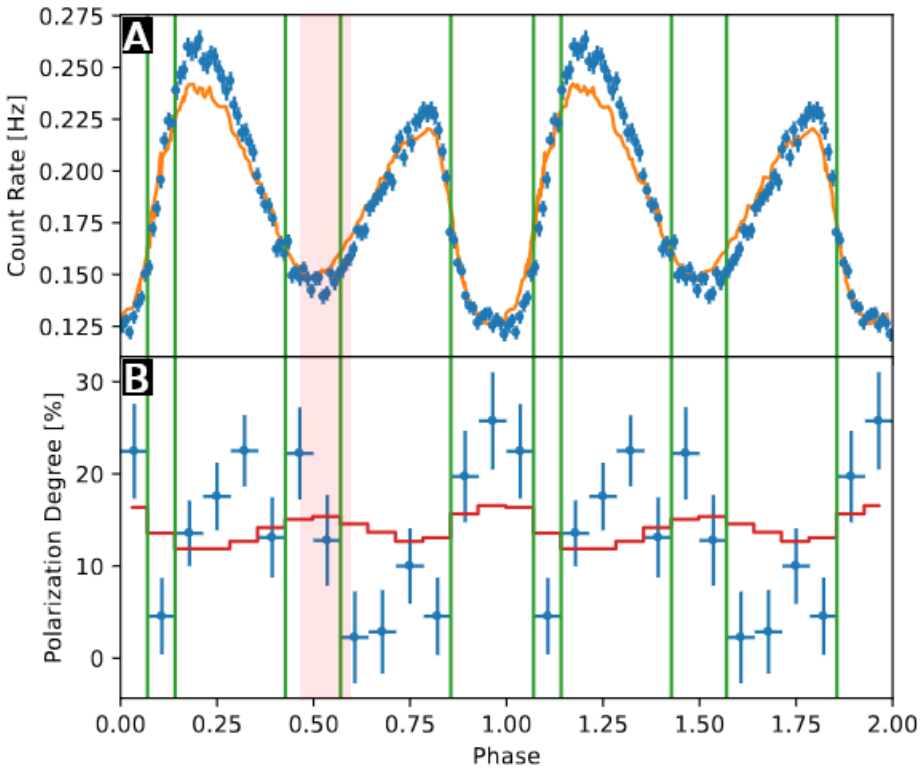

Heyl et al. (2024)

- **1st rise: primary spot face-on**
- **1st peak: primary spot off-axis**
- **1st min: two spots are in view**
  - X-mode (mildly polarized) photons from the primary spot sum with O-mode (lowly polarized) photons from the secondary spot

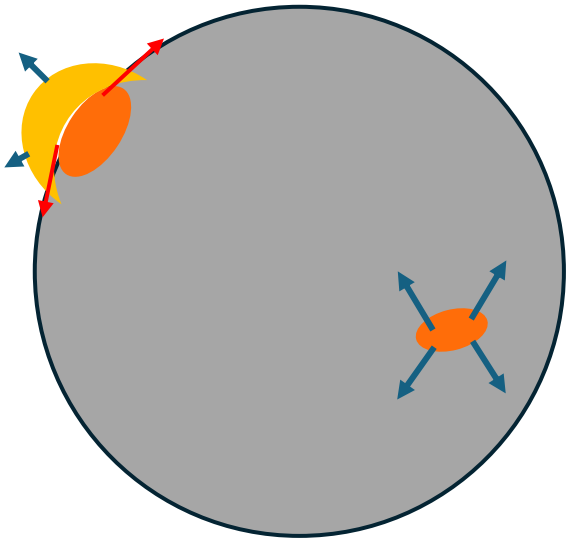

AXP 1E 2259+586 – Interpretation

- Condensed surface with two hot-spots, the primary covered by a magnetic loop

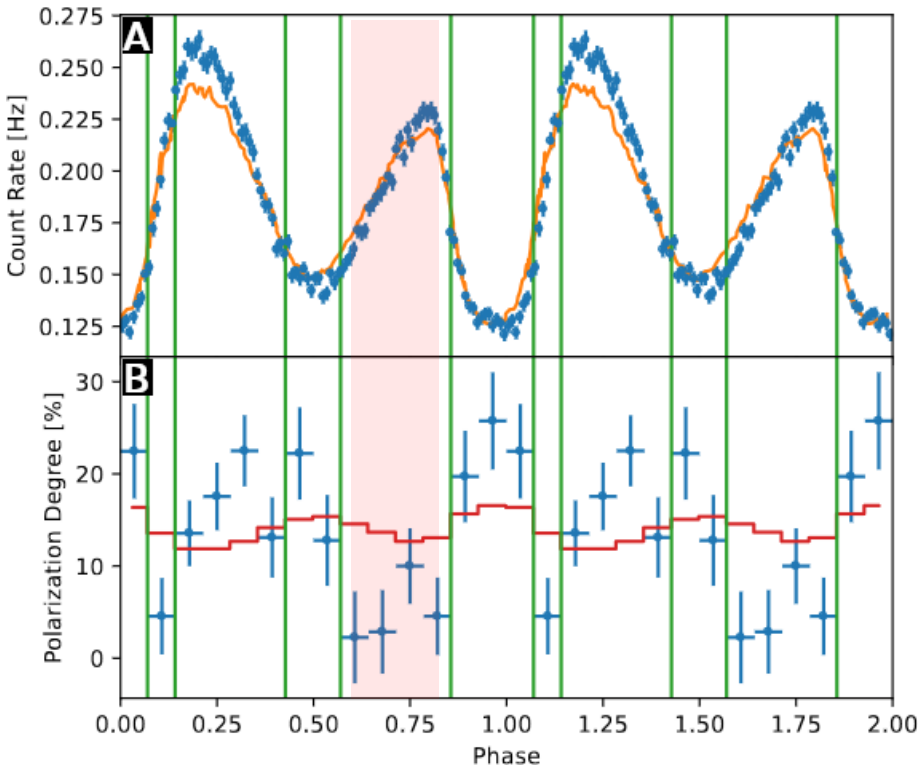

Heyl et al. (2024)

- **1st rise: primary spot face-on**
- **1st peak: primary spot off-axis**
- **1st min: two spots are in view**
- **2nd peak: secondary spot only**
  - O-mode (lowly polarized) photons (not scattered) arrive directly to the observer from the condensed surface

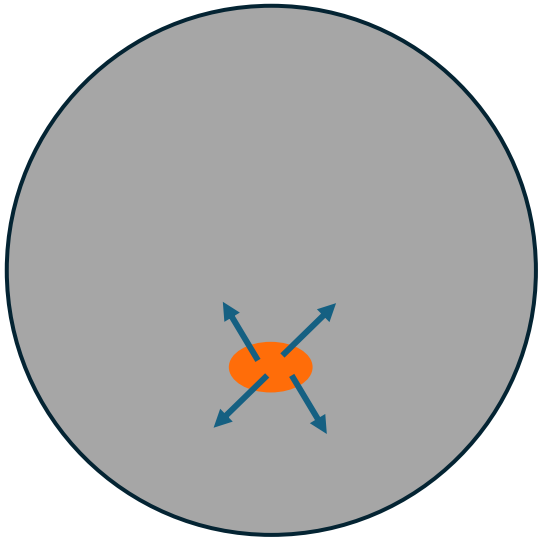

AXP 1E 2259+586 – Interpretation

- Condensed surface with two hot-spots, the primary covered by a magnetic loop

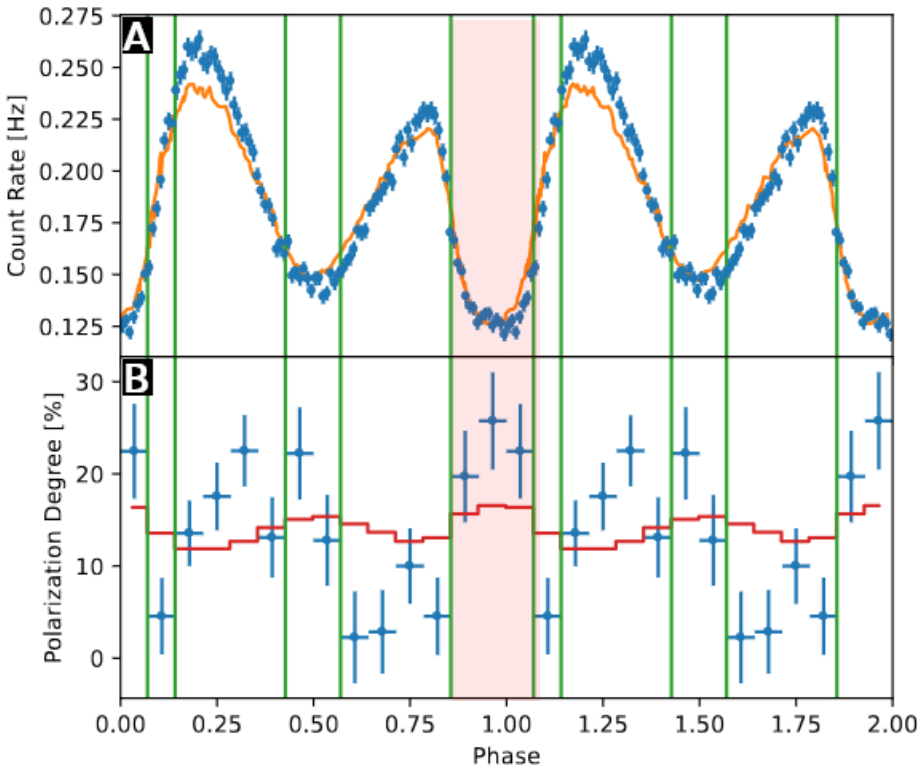

Heyl et al. (2024)

- **1st rise: primary spot face-on**
- **1st peak: primary spot off-axis**
- **1st min: two spots are in view**
- **2nd peak: secondary spot only**
- **2nd min: primary spot returns**
  - Secondary spot photons exit from the FOV, primary spot returns into view, firstly showing scattered photons (PD → 33%, X-mode) from the loop

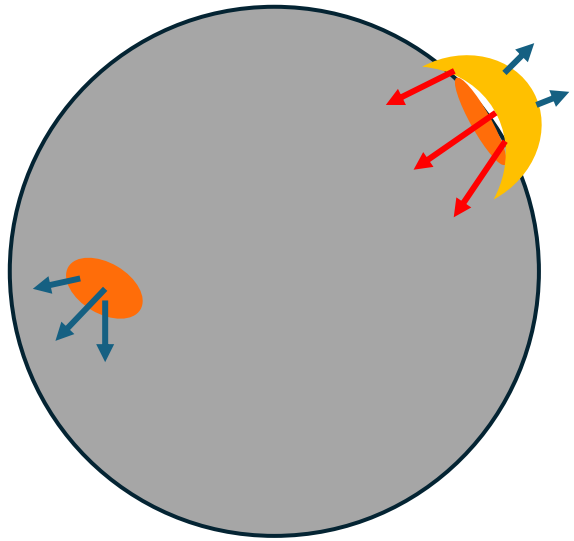

AXP 1E 1841–045 – An IXPE ToO

- At the center of the Kes 73 SNR, observed just after an intense burst-emission phase

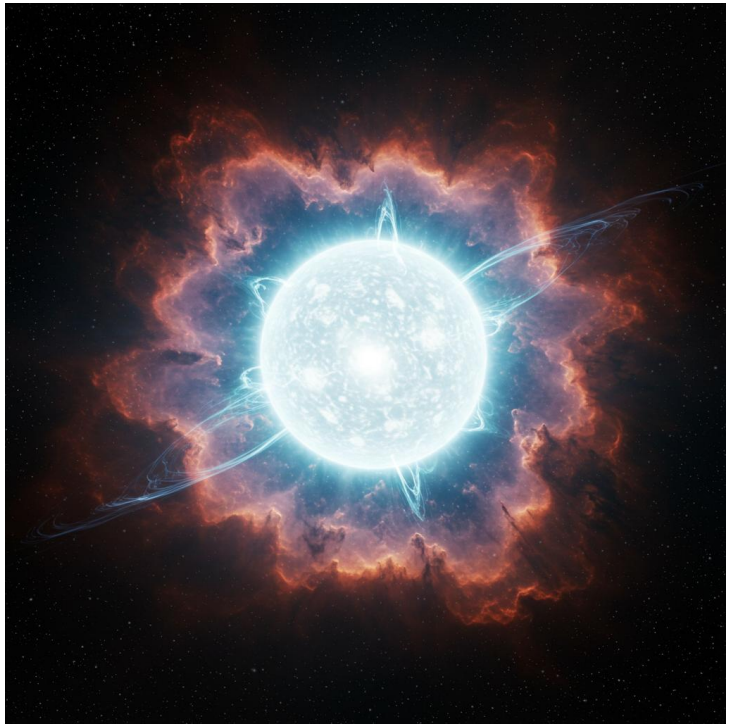

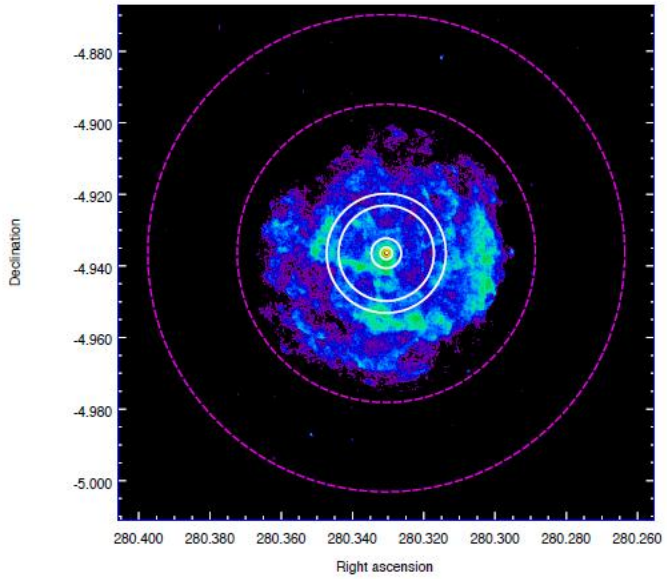

Rigoselli et al. (2025)

AXP 1E 1841–045 – An IXPE ToO

- At the center of the Kes 73 SNR, observed just after an intense burst-emission phase
- Spectral analysis (IXPE+XMM+NuSTAR) reveal the presence of 3 spectral components above 2 keV BB+PL+PL (hard PL already present at ≈ 6 keV)

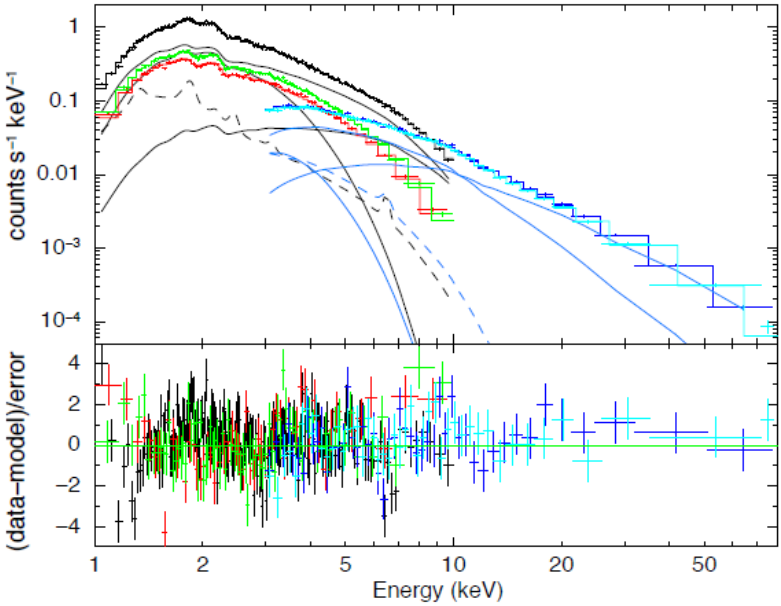

Rigoselli et al. (2025)

AXP 1E 1841–045 – Spectro-polarimetry

- Energy-dependent polarization very similar to 1RXS J1708
  - PD increases with energy from $\approx 15\%$ to $\approx 55\%$ across the 2–8 keV band
  - PA is constant with energy within the errors

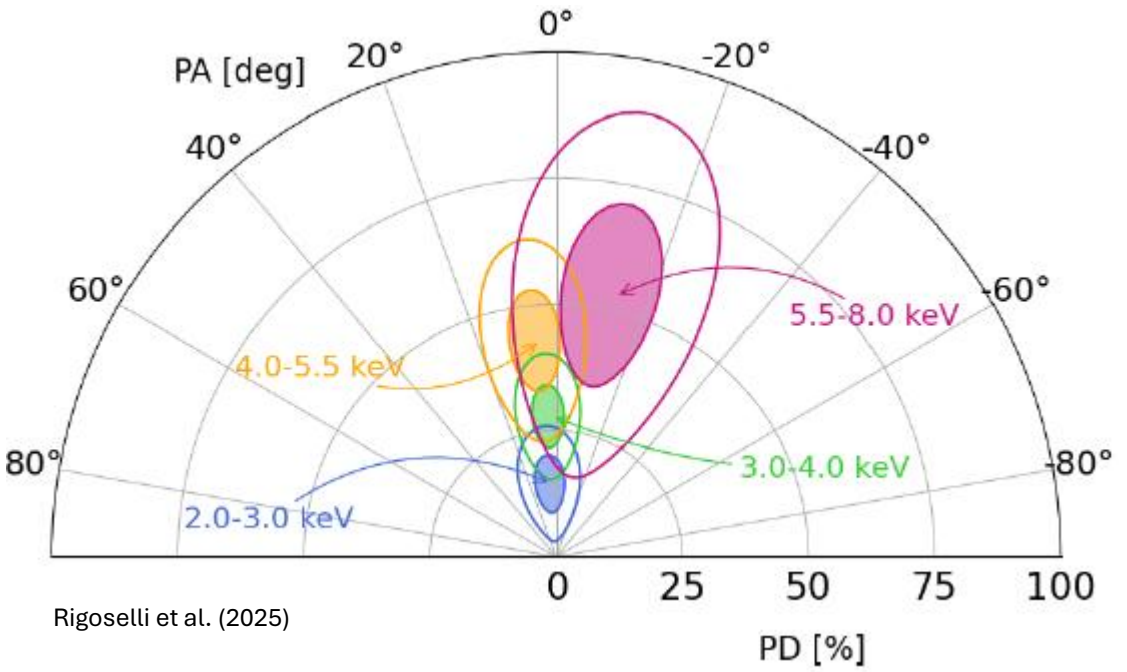

Rigoselli et al. (2025)

AXP 1E 1841–045 – Spectro-polarimetry

- Energy-dependent polarization very similar to 1RXS J1708
- Freezing the soft-PL PD at 33% (RCS) results are compatible with a high PD for the hard PL ($\gtrsim 70\%$)

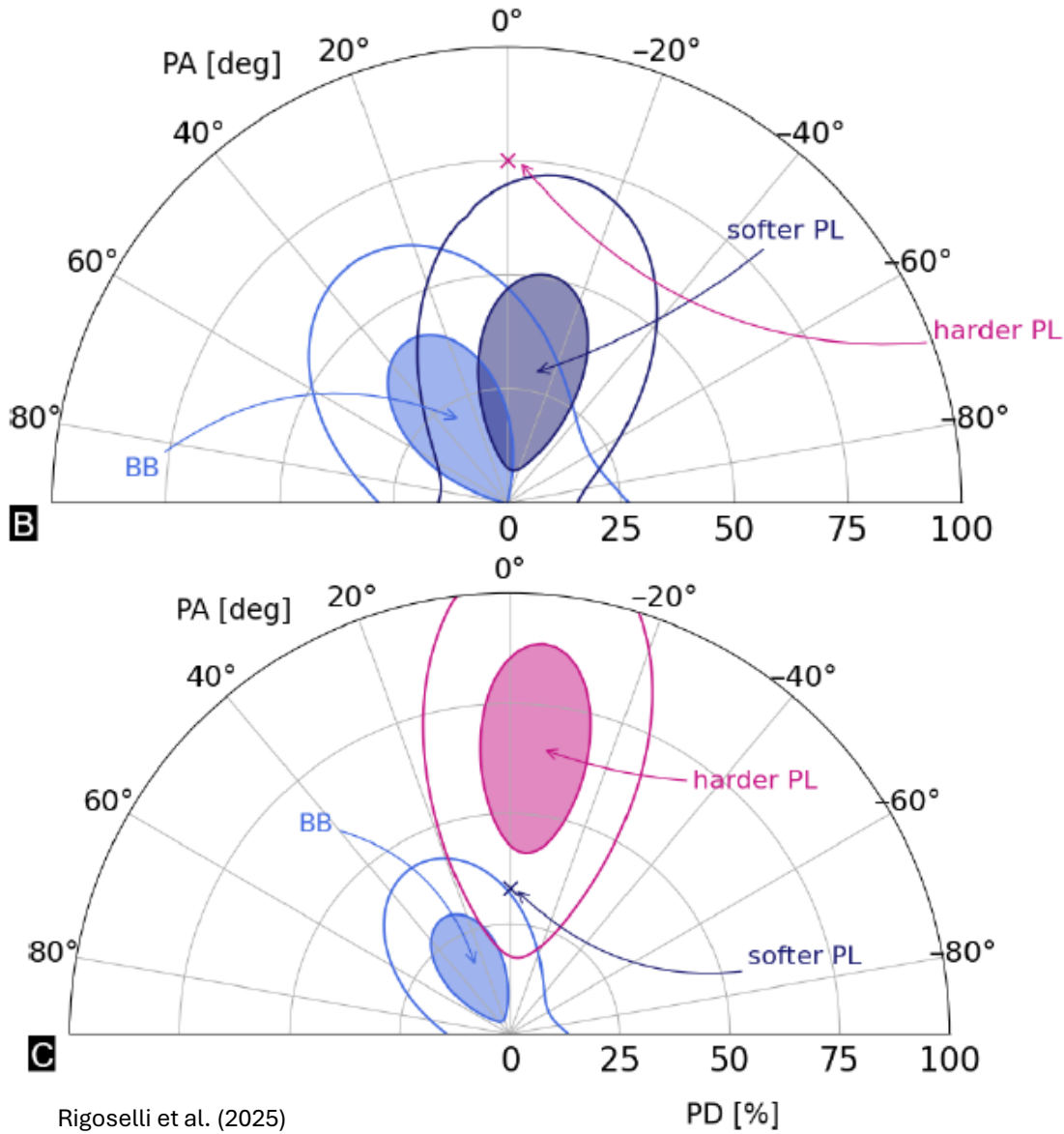

Rigoselli et al. (2025)

AXP 1E 1841–045 – Spectro-polarimetry

- Energy-dependent polarization very similar to 1RXS J1708
- Freezing the soft-PL PD at 33% (RCS) results are compatible with a high PD for the hard PL ($\gtrsim 70\%$)
- Interpretation
  - BB (thermal) photons coming from the condensed surface
  - soft-PL due to RCS in the magnetosphere
  - high-PL compatible with synchrotron emission from relativistic electrons

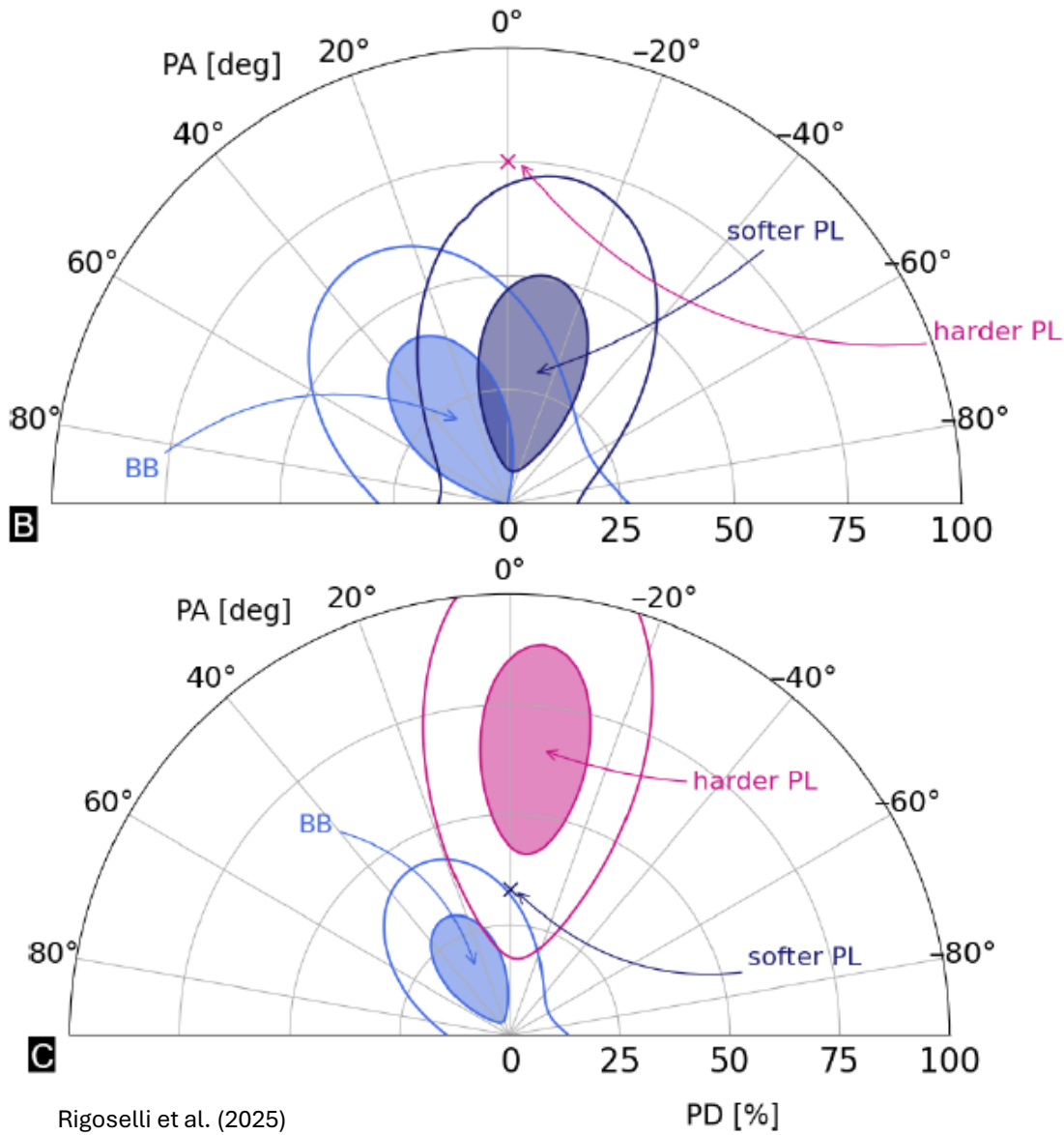

Rigoselli et al. (2025)